

TECHNISCHE UNIVERSITÄT MÜNCHEN
Lehrstuhl für Entwicklungs-genetik

Characterisation of the zebrafish cerebellar efferent system

Andreas N. Babaryka

Vollständiger Abdruck der von der Fakultät Wissenschaftszentrum Weihenstephan für Ernährung, Landnutzung und Umwelt der Technischen Universität München zur Erlangung des akademischen Grades eines

Doktors der Naturwissenschaften

genehmigten Dissertation.

Vorsitzender:	Univ.-Prof. Dr. H. Luksch
Prüfer der Dissertation:	1. Univ.-Prof. Dr. W. Wurst
	2. Univ.-Prof. A. Schnieke, Ph.D.

Die Dissertation wurde am 29.12.2008 bei der Technischen Universität München eingereicht und durch die Fakultät Wissenschaftszentrum Weihenstephan für Ernährung, Landnutzung und Umwelt am 15.05.2009 angenommen.

Table of contents

Table of contents	2
Abbreviations	4
Abstract.....	6
Zusammenfassung.....	7
1. Introduction.....	8
1.1. <i>Morphology of the cerebellum</i>	8
1.1.1. Topology and gross anatomy	8
1.1.2. Histology of the cerebellum	9
1.1.3. Comparison between mammals and fish.....	11
1.2. <i>Development of the cerebellum</i>	13
1.2.1. Establishment of the cerebellar anlage.....	13
The isthmic organiser (IsO).....	13
Rotation of the cerebellar neuroepithelium establishes the cerebellar anlage	14
1.2.2. The two germinal zones of the cerebellar anlage	15
The Rhombic Lip and its associated transcription factor <i>atonal homologue 1</i>	15
The Ventricular Zone and its associated transcription factor <i>ptfla</i>	16
1.2.3. Migration and cerebellum morphogenesis	18
Migration of RL- derived neurons.....	19
Migration of VZ- derived neurons	20
DCN neuron are both VZ- and URL-derived.....	21
1.3. <i>PCs control GPC proliferation and maturation of the cerebellum</i>	22
Modes of MYC action.....	25
1.4. <i>Aim of this study</i>	25
2. Materials and methods	27
2.1. <i>Materials</i>	27
2.1.1. Equipment	27
2.1.2. Consumables	29
2.1.3. Chemicals.....	30
2.1.4. Enzymes and Kits	32
2.1.5. Antibodies	33
2.1.6. Zebrafish strains.....	35
2.1.7. Bacteria	35
2.1.8. Primers	35
2.1.9. Vectors	37
2.1.10. Antisense oligo nucleotides (morpholinos).....	39
2.1.11. Buffers, media, solutions	39
2.2. <i>Methods</i>	41
2.2.1. Molecular biology	41
2.2.1.1. Purification of nucleic acids.....	41
2.2.1.2. Amplification of DNA by PCR (polymerase chain reaction).....	42
2.2.1.3. Restriction digest DNA	43
2.2.1.4. Site-Directed Mutagenesis	43
2.2.1.5. Blunting 5´-ends of DNA	43
2.2.1.6. Dephosphorylation of DNA	43
2.2.1.7. Ligation of DNA	44
2.2.1.8. TA-Cloning, TOPO.....	44

2.2.1.9. Transformation of bacteria	44
2.2.1.10. Preparation of DNA	46
2.2.1.11. Determination of nucleic acid concentration.....	48
2.2.1.12. Separation of nucleic acids using agarose gel electrophoresis	48
2.2.1.13. cDNA synthesis by reverse transcription	49
2.2.1.14. DNA sequencing	50
2.2.1.15. Analysis of DNA sequences.....	51
2.2.1.16. <i>in vitro</i> synthesis of RNA.....	51
2.2.2. Manipulation of zebrafish embryos	53
2.2.2.1. Cytoplasmic injection of nucleic acids.....	53
2.2.2.2. Cytoplasmic injection of morpholinos	54
2.2.2.3. Single cell transplantation	54
2.2.2.4. <i>In vivo</i> retrograde labeling of neurons in the zebrafish larva	55
2.2.2.5. Cyclopamine treatment	55
2.2.3. Histological techniques.....	55
2.2.3.1. Sectioning of embryos, larvae and adult brains.....	55
2.2.3.2. Whole-mount in-situ-hybridisation (ISH)	57
2.2.3.3. Double in-situ-hybridisation.....	59
2.2.3.4. Immuno-histo-chemistry	60
2.2.3.5. Morphological stainings.....	62
2.2.4. Microscopic Analysis.....	62
3. Results	63
3.1. <i>Characterisation of Eurydendroid Cells– the zebrafish 's equivalent of the deep cerebellar nuclei neurons</i>	63
3.1.1. Expression of <i>olig2</i> in the developing cerebellum	63
3.1.2. <i>olig2</i> -expressing precursors differentiate into Eurydendroid Cells.....	65
3.1.3. Development of Eurydendroid Cells.....	77
3.2. <i>Analysis of the protooncogene nmyc in the developing zebrafish cerebellum</i>	87
3.2.1. Cloning of the zebrafish homologue of <i>nmyc</i> and functional variants of <i>zfnmyc</i>	87
3.2.2. Expression of <i>nmyc</i> in the developing cerebellum.....	90
3.2.3. HH-signalling activates <i>nmyc</i> transcription at late cerebellum differentiation stages.....	92
4. Discussion.....	97
4.1. <i>olig2: a potential regulator of neurogenesis in the zebrafish cerebellum</i>	97
4.1.1. A comparative view on ECs and DCN neurons	97
Phylogeny of ECs and DCN neurons	97
Subsets of ECs express <i>olig2</i>	98
Properties of ECs in comparison to DCN neurons.....	99
Is <i>olig2</i> a marker of DCN neurons?.....	101
4.1.2. <i>olig2</i> -expressing VZ-derived cells adopt the fate of glutamatergic projection neurons....	103
4.1.3. Dynamics of EC behaviour	104
4.2. <i>Analysis of nmyc expression and its regulation by HH signalling</i>	107
4.2.1. The proto-oncogene <i>nmyc</i> is expressed in both VZ and URL-derived cells	107
4.2.2. HH signalling regulates <i>nmyc</i> expression at larval stages.....	108
4.3. <i>Future perspective</i>	110
5. References.....	112
6. Appendix.....	124
6.1. <i>Movie legends</i>	124
6.2. <i>Nucleotide sequences</i>	127
<i>Eidesstattliche Erklärung</i>	131
<i>Danksagung</i>	132

Abbreviations

μ	mikro	ECP	eurydendroid cell precursor
AA	amino acids	eg	eminentia granularis
AP	alkaline phosphatase	EGL	external granule cell layer
<i>ascl</i>	<i>ascute complex like</i>	EHH/ <i>ehh</i>	<i>echidna hedgehog</i>
asp	L-aspartate	FBS	fetal bovine serum
<i>ath</i>	<i>atonal homologue</i>	FGF	fibroblast growth factor
BCIP	5-Bromo-4-chloro-3-indolylphosphate	GABA	gamma-aminobutyric acid
bHLH	basic helix-loop-helix	GAD	glutamate decarboxylase
BLBP	brain lipid binding protein	gc	griseum centrale
BMP	bone morphogentic protein	GCL	granule cell layer
bp	base pairs	GCP	granule cell precursor
BSA	bovine serum albumine	GDF/ <i>gdf</i>	<i>growth and development factor</i>
CALB/ calb	<i>calbindin</i>	GFAP	glial fibrillary acidic protein
Calret/ calret	<i>calretinin</i>	GFP	green fluorescent protein
<i>car</i>	<i>carbonic anhydrase</i>	HAT/ <i>hat</i>	<i>histone acetyl transferase</i>
cb	cerbellum	hc	caudal hypothalamus
cce	corpus cerebellaris	HDAC/ <i>hdac</i>	<i>histon de-acetylase</i>
CDK/ cdk	<i>cyclin dependent kinase</i>	HH/hh	<i>hedgehog</i>
cDNA	complementary DNA	hpf	hours post fertilization
CI/ ci	<i>cubitus interruptus</i>	HSE	oligomerized heatshock binding elements
CNS	central nervous system	Hyb-mix	Hybridization mixture
Cy2	cyanine-2 (green)	IGF/ <i>igf</i>	<i>igf receptor</i>
Cy5	cyanine-5 (far red)	IGFR/ <i>igfr</i>	<i>insulin-like growth factor</i>
CYC/ cyc	<i>cyclin</i>	IGL	internal granule cell layer
DAB	diaminobenzidine tetrahydrochloride	IHH/ <i>ihh</i>	<i>indian hedgehog</i>
DAPI	4',6-diamidino-2-phenylindole	INM	interkinetic nuclear movement
DCN	deep cerebellar nuclei	ION	inferior olivary nucleus
DHH/ dhh	<i>desert hedgehog</i>	IPTG	Isopropyl β -D-1-thiogalactopyranoside
DIG	digoxigenin	ISH	<i>in-situ hybridization</i>
DiI	1,1'-dioctadecyl-3,3',3'-tetramethylindocarbocyanine perchlorate	IsO	isthmie organiser
dish	double in-situ hybridisation	KalTA4	kozak gal4 transactivator domain 4
DMF	di-methylformamide	<i>klc3</i>	<i>kinesin light chain 3</i>
DMSO	dimethylsulfoxide	l	litre
DNA	desoxy-ribonucleic acid	lca	lobus caudalis, caudal lobe
DNase	desoxy-ribonuclease	LDTg	laterodorsal tegmental nucleus
dNTP	desoxy-nucleotide-tri-phosphate	LPB	lateral parabrachial nucleus
dpf	days post fertilization	LPB	lateral parabrachial nucleus
E	embryonic day	LRL	lower rhombic lip
EC	eurydendroid cells	M	mol/l
		m	milli
		<i>mash</i>	<i>mouse ascute homologue</i>

MB	medulloblastoma	r1	rhombomere 1
<i>mbp</i>	<i>myelin binding protein</i>	rct	rostral cerebellar thickening
MCS	multiple cloning site	RFP	red fluorescent protein
mes	mesencephalon	rh	rhombencephalon
MHB	midbrain-hindbrain boundary	RL	rhombic lip
MiTg	microcellular tegmental nucleus	RNA	ribonucleic acid
ML	molecular layer	RNase	ribonuclease
mRNA	messenger ribonucleic acid	rpm	rotations per minute
NBT	Nitro blue tetrazolium	RT-PCR	reverse transcription PCR
NGS	normal goat serum	SD	standard deviation
<i>nrgn</i>	<i>neurogranin</i>	SDS	sodium dodecyl sulfate
NSC	neural stem cell	SHH/ <i>shh</i>	<i>sonic hedgehog</i>
NTZ	nuclear transitory zone	SMO/ <i>smo</i>	<i>smoothened</i>
NVPs	nodal vesicular parcels	<i>smu</i>	<i>slow muscle omitted</i>
ot	tectum opticum, optic tectum	TAE	Tris-Acetate-EDTA
P	postnatal day	TBS	Tris-buffered saline
PACAP	pituitary adenylate cyclase-activating polypeptide	tg	transgenic
PBG	parabigeminal nucleus	TWHH/twhh	<i>tiggy-winkle hedgehog</i>
PBS	phosphate buffered saline	URL	upper rhombic lip
PC	Purkinje cell	v	volume
PCL	Purkinje cell layer	val	Lateral division of vc
PCR	polymerase chain reaction	vam	medial division of vc
PDGFR	platelet derived growth factor receptor	vc	valvula cerebelli
PenStrep	Penicillin/Streptavidin	<i>vglut</i>	<i>vesicular glutamate transporter</i>
PFA	Paraformaldehyde	VHB	ventromedial hindbrain bundle
PH3	phospho-histone 3	<i>vim</i>	<i>vimentin</i>
PI3K	Phosphoinositide 3-Kinases	VZ	ventricular zone
PKA	protein kinase a	w	weight
PKB	protein kinase b	WT	wild type
PPTg	pendunculopontine tegmental nucleus	X-Gal	(5-bromo-4-chloro-3-indolyl-beta-D-galactopyranoside)
PTC/ <i>ptc</i>	<i>patched</i>	zf	Zebrafish
<i>ptf1a</i>	<i>pancreas transcription factor 1a</i>	zl	zona limitans
PTU	1-phenyl-2-thiourea		

Abstract

Eurydendroid Cells (ECs) are the teleosts equivalent of the neurons of the deep cerebellar nuclei (DCN) found in tetrapods and cartilaginous fish. While the histomorphological and neurophysiological properties of ECs have been well described, their origin, their development and the molecular features of ECs remain largely unknown. In this study, the EC population of the zebrafish was identified and characterised using expression analysis in combination with retrograde axon tracing and *in vivo* time-lapse imaging. In addition, early development of ECs, their differentiation behaviour and their integration into the layered cerebellar cortex was examined. DiI applied to the ventral mesencephalon was found to label cerebellar neurons that expressed *olig2:GFP*. Despite originating in the ventricular zone (VZ), which is known to give rise to inhibitory GABAergic neurons of the cerebellum, such ECs were found to be glutamatergic as they expressed *vesicular glutamate transporter 2.1*, but not *GAD67*. Development of this neurotransmitter phenotype coincided with the continuous decrease of co-expression of *olig2* and *ptfla*, which is a characteristic gene for specifying VZ-derived neurons. This finding suggests that *olig2* expression may specify the excitatory fate in VZ-derived neurons.

Intriguingly *olig2* expression was found to overlap with the characteristic cerebellar expression domain of the protooncogene *nmyc* of which the zebrafish homologue was cloned by RT-PCR. *nmyc* was found to be expressed in two phases: First expressed in the ventral cerebellar anlage at embryonic stages from 24 to 48 hpf, its transcription reappeared again at larval stages in cerebellar domains that are known germinal zones. Only *nmyc* expression in the caudal lobe was found to be activated by Sonic Hedgehog signalling. Hedgehog-independent expression of *nmyc* in cells other than granule cell precursors may point to precursors of DCN neurons as an additional source of cerebellar malignancies. Taking into account that the cerebellum represents one of the most conserved brain compartments, these results significantly expand our knowledge of cerebellar development in jawed vertebrates in general.

Zusammenfassung

Die Eurydendroiden Zellen (EZ) der Knochenfische sind das Äquivalent der Neuronen der zerebellaren Tiefenkerne der Knorpelfische und Tetrapoden. Während Histomorphologie und Neurophysiologie der EZ detailliert untersucht wurden, sind Ursprung, Entwicklung und molekulare Eigenschaften der EZ weitgehend unerforscht. In Rahmen dieser Arbeit wurden die EZ des Zebrafischkleinhirns mittels Expressionsanalysen in Kombination mit Darstellung ihrer Projektionen und mikroskopischer Zeitrafferanalysen identifiziert und charakterisiert. Zusätzlich wurde ihr Verhalten während ihrer Entstehung, ihrer Differenzierung und ihrer Integration in den Kortex des Kleinhirns untersucht. Wurde der Farbstoff DiI ins ventrale Mittelhirn appliziert, konnte er in solchen Kleinhirnneuronen, die GFP unter Kontrolle regulatorischer Elemente des Genes *olig2* exprimieren, nachgewiesen werden. Obwohl sie in der Ventrikulärzone (VZ) entstehen, von der bekannt ist, dass sie inhibitorische GABAerge Neuronen des Kleinhirns hervorbringt, wurden solche EZ als glutamaterge Neuronen identifiziert, da sie zwar *vesicular glutamate transporter 2.1*, aber nicht *GAD67* exprimierten. Die Ausprägung dieses Neurotransmitterphänotyps ging einher mit dem kontinuierlichen Rückgang an Koexpression von *olig2* und *ptfla*, einem Gen das neuronale Vorläufer der VZ spezifiziert. Dies legt eine mögliche Rolle von *olig2* für die Festlegung des exzitatorischen Phänotyps der EZ nahe.

Interessanterweise wurde eine weitgehende Übereinstimmung der Expressionsdomänen von *olig2* und dem Protoonkogen *nmyc*, welches mittels RT-PCR kloniert wurde, festgestellt. *nmyc* wurde im Kleinhirn in zwei Phasen exprimiert: Während es zwischen 24 und 48 hpf in der ventralen Kleinhirnanlage exprimiert wurde, wurde es im Larvalstadium in solchen Regionen des Kleinhirns, welche bekannte Proliferationszonen sind, exprimiert. Lediglich seine Expression im lobus caudalis war hierbei von einer Aktivierung durch die Sonic-Hedgehog-Signaltransduktionskette abhängig. Hedgehog-unabhängige Expression von *nmyc* in anderen als den Vorläufern der Granulärzellen deutet auf die Vorläuferzellen der Tiefenkerne als einen weiteren möglichen Ursprung bösartiger Kleinhirntumoren hin. Angesichts dessen, dass das Kleinhirn eines der am stärksten konservierten Hirnareale ist, erweitert diese Arbeit unseren Kenntnisstand über die Kleinhirnentwicklung aller Gnathostomata.

1. Introduction

1.1. Morphology of the cerebellum

1.1.1. Topology and gross anatomy

The cerebellum is the most rostral part of the dorsal hindbrain. Occupying approximately 10 % of the brain volume, it contains more than half of the neurons of the entire central nervous system (CNS). In terms of physiology, histology and development, the cerebellum is highly conserved among all gnathostomes (jawed vertebrates), e.g. (Nieuwenhuys, 1967). Agnatha (jawless vertebrates, cyclostomes) such as lampreys do at least possess a cerebellum-like region located posterior to the midbrain-hindbrain boundary (MHB); yet it lacks characteristic properties of the cerebellum on the cellular level as it does not have Purkinje cells, cerebellar nuclei and components of the rhombic lip-derived cerebellar and precerebellar systems (Murakami et al., 2005). The cerebellar organization is relatively simple with only few neuronal subtypes that are arranged in a highly regular manner in only two separate cell layers. Acting subconsciously in humans, the cerebellum controls balance, locomotion and fine motor control by providing precise timing and appropriate patterns of skeletal muscle contraction.

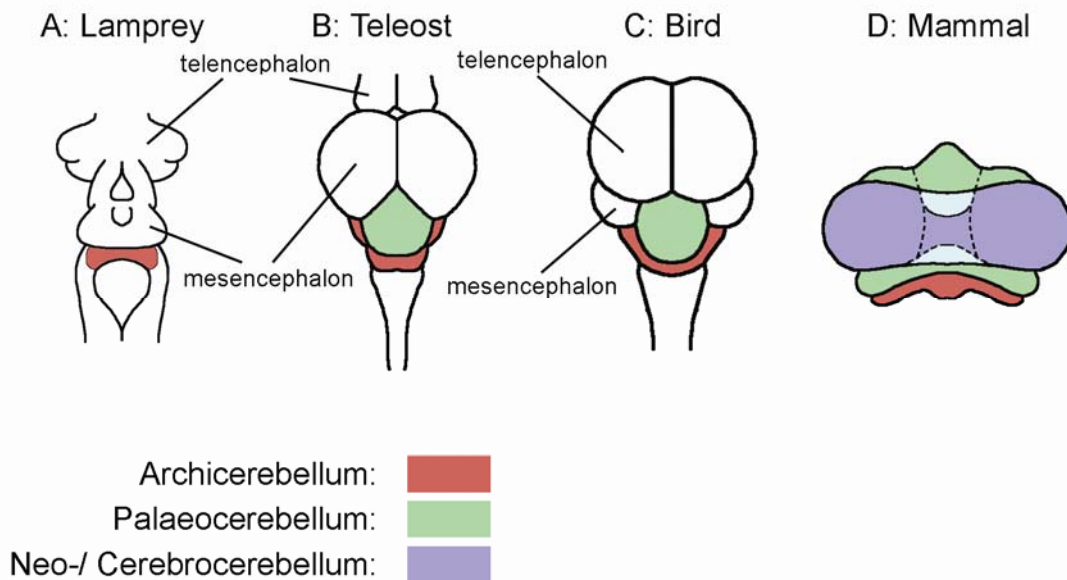


Fig. 1: Evolution of the cerebellum and its subdomains. The archicerebellum is the phylogenetic oldest part of the cerebellum and is associated with the vestibular system and the lateral line system in fishes. The palaeocerebellum as found in the gnathostomes, modulates signals of the descending motor systems. The appearance of a morphological distinct neocerebellum is restricted to mammals. Drawings are not to scale.

The cerebellum can be subdivided based on various criteria. According to its phylogeny, the cerebellum consists of three subunits: the archicerebellum, which is the phylogenetic oldest part of the gnathostomes' cerebellum; the homologous hindbrain territory of the agnathans also is referred to as archicerebellum; the paleocerebellum, as it has evolved in all gnathostomes; and the neocerebellum- also known as cerebrocerebellum- as it solely appears in the mammals' cerebellum (Fig. 1). To a certain extent, this phylogenetic classification also correlates with observable gross anatomic and neurophysiological compartments of the cerebellum. Hence, the archicerebellum resembles the floccunodular lobe (anatomy) and the vestibulocerebellum (functional denomination). The paleocerebellum consists of the vermis and paravermis, which are also delineated as the spinocerebellum. The cerebrocerebellum has its anatomical counterpart in the lateral hemispheres; according to its function and source of innervation it is referred to as the pontocerebellum.

1.1.2. Histology of the cerebellum

Throughout all gross anatomical and functional subdivisions, the cerebellar cortex consists of only few distinct neuronal cell types with essentially two major populations: inhibitory GABAergic Purkinje cells (PCs) and excitatory glutamatergic granule cells (GCs). Additional, less frequent classes of cerebellar neurons are: Golgi cells, stellate cells and basket cells, which are GABAergic and provide an inhibitory feedback to granule neurons (Sotelo, 2004), and the glutamate releasing, excitatory unipolar brush cells (Mugnaini and Floris, 1994). These cells are arranged in a highly coordinated pattern and assemble in the distinct histologic layers of the cerebellum (e.g. (Altman and Bayer, 1997; Jansen and Brodal, 1958; Jansen and Brodal, 1954; Nieuwenhuys, 1967), see Fig. 2). The outer most layer is termed the molecular layer (ML) and consists mainly of the dendrites of the PCs and – oriented perpendicularly to the PC dendrites- the parallel fibres, which are the axons of the GCs. Basket cells and stellate cells are positioned in between the white matter of the molecular layer. The layer underneath the ML is the Purkinje cell layer (PCL). As indicated by the name, the PCL consists of the cell bodies of PCs that are aligned into a single row. The PCs characteristically develop a huge cell soma and widespread, extremely elaborated, two-dimensional dendrites, which are oriented in parallel to the antero-posterior body axis and the sagittal plane. PCs provide the sole output of the

cerebellum, i.e. the PCs are the core unit of cerebellar neuronal circuits, whereas all other neurons of the cerebellar cortex are local circuit interneurons. The innermost cell layer is termed the granule cell layer (GCL, also IGL for inner granule layer). It contains the GCs, the Golgi cells and the unipolar brush cells (Mugnaini and Floris, 1994; Voogd and Glickstein, 1998). GCs are typically T-shaped and by far the most abundant neurons in the entire CNS. The GCL also contains the so-called synaptic glomeruli. These glomeruli are composed by the mossy fibre terminal, the dendrites of several granule cells and the golgi terminal; a coat of glial cells encloses the glomerulus (Jakab and Hamori, 1988). The GCs forward the neuronal input they receive from the synaptic glomerulus via their axon to the ML, where the parallel fibres form plenty of synapses with PC dendrites. Ventral to the GCL follows the “corpus medullare cerebelli” as the innermost layer consisting of afferent and efferent nerve fibres, to simplify matters mostly referred to as “(central) white matter” (WM). As mentioned, the efferent fibres are derived from the sole output neurons of the cerebellum, the PCs. Afferent input to the cerebellum is provided by two different sources, the mossy fibres and the climbing fibres (Apps and Garwicz, 2005; Rollenhagen and Lubke, 2006). Mossy fibres originate from various locations in the brain stem which yet can be placed into three categories: the vestibular tract, which originates from the vestibular nucleus; the spinocerebellar tract, ascending from regions in the medulla; the pontocerebellar tract, which emanates from the pontine nuclei located ventral to the 4th ventricle (Glickstein, 1997; Goldowitz and Hamre, 1998; Voogd and Glickstein, 1998). (This classification of innervating sources is reflected by the functional nomenclature, see above). A single mossy fibre innervates several glomeruli, and one glomerulus is innervated by several mossy fibres, thus providing GCs with neuronal input (Livet et al., 2007). Climbing fibre afferents in several aspects differ from mossy fibres: The only source of climbing fibres is the inferior olive (also inferior olivary nucleus, ION), a prominent, pair wise nucleus located in the ventral medulla oblongata. Instead of innervating the GCL, climbing fibres project to the dendrites of PCs. Furthermore, one individual PC is innervated by only one climbing fibre. Whereas the PCs provide the output of the processed neuronal information, they do not project to structures outside the cerebellum. Rather, in tetrapods and cartilaginous fish, an additional structure, the deep cerebellar nuclei (DCN), accomplish the transmission of the signals towards different regions of the CNS such as the thalamus, the nucleus ruber, the vestibular nucleus or the

reticulospinal tract (De Zeeuw and Berrebi, 1995; Sultan et al., 2003). The DCN are located at the base of the cerebellum and are four in number on either side. From medial to lateral they are termed dentate, emboliform, globose, and fastigial nucleus. (The emboliform and globose nucleus together are often referred to as the interpositus nucleus). Remarkably, the arrangement of the nuclei tightly corresponds with the arrangement of the PCs along the cerebellar cortex which innervate the DCN: PCs that are located in the lateral part of the hemisphere project to the laterally located dentate nucleus; PCs located in the intermediate part of the hemisphere are associated with the interpositus nucleus; PCs of the vermis innervate the fastigial nucleus (Voogd and Glickstein, 1998).

On the cellular and physiological level, the DCN are composed of GABAergic and glutamatergic neurons: large glutamatergic neurons that project to various extracerebellar sites, medium-sized GABAergic neurons that project to the ION and small GABAergic interneurons (Leto et al., 2006; Sultan et al., 2003). The DCN vary in the destinations they innervate, and so vary the role of the DCN and the associated spheres of the cerebellar cortex in neurophysiology. The cerebrocerebellum processes information derived from the sensory cortex. The task of the cerebrocerebellum is the adjustment of movements. The processed information is transmitted via the thalamus to premotor and motor cortical areas of the cortex. The motor areas execute movements via the corticospinal tract. In turn, the spinocerebellum receives sensory input and corrects for errors by comparison of the nominal command and the actual movement. The adjusted signal then finally is forwarded to the cortex and to the nucleus ruber, from where the signals descend towards the effectors via the rubrospinal tract.

1.1.3. Comparison between mammals and fish

The zebrafish *Danio rerio* has become a widely used model organism to study CNS development. On the one hand this is due to its fast development outside the mother's body and the transparency of the embryo and the larva. On the other hand, the use of fluorescent proteins in combination with the use of the accessible genetic tools makes the zebrafish an ideal organism to study cell migration in vivo, because many aspects of the dynamics of neuronal migration can best be resolved by directly observing them in their "natural habitat", the developing neuronal tissue (Köster and Fraser, 2001; Köster and Fraser, 2004; Lichtman and Fraser, 2001).

According to the close evolutionary relation, the cerebellum of the teleosts (bony fishes) resembles that of other gnathostomes to a wide extent, but also exhibits some distinctions. Most obvious are the gross anatomical differences. The cerebellum of fish solely consists of the phylogenetic older parts of the cerebellum, i.e. the archicerebellum and the paleocerebellum (Fig. 1). Otherwise an additional compartment termed valvula or valvula cerebelli (vc) occurs specifically in actinopterygians (ray finned fishes). It extends into the tectal ventricle ventrally to the optic tectum. Histology and innervation of the valvula however clearly indicate that the valvula is part of the cerebellum (Wullimann, 1998). The valvula is merely involved in processing electrosensory input and input derived from the lateral line (Wullimann et al., 1991; Wullimann and Northcutt, 1989). With exception of the gigantocerebellum of mormyrids (Nieuwenhuys et al., 1974), the cerebellum of most teleosts species does not exhibit a roto-caudal subdivision marked by the fissures of the tetrapods' cerebellum. In gross anatomical terms, the fish cerebellum is tripartite: the valvula as the most anterior part with no homologue in tetrapods; the corpus cerebelli (cce) is homologous to the paleocerebellum and constitutes the major functional and anatomical part; the lobus caudalis (lca) and the eminentia granularis (eg), both being the homologue of the archi- and vestibulocerebellum, respectively (Wullimann, 1998).

One major difference anatomy-wise between the cerebellum of teleosts, cartilaginous fish and tetrapods is the absence of structures homologous to DCN in the teleosts' cerebellum. The output of the processed neuronal signal instead is accomplished by a certain type of specialised cells, the Eurydendroid cells (EC) (Finger, 1978; Folgueira et al., 2006; Ikenaga et al., 2005; Meek, 1992; Murakami and Morita, 1987; Nieuwenhuys et al., 1974). Similar as in tetrapods, these efferent cells are innervated by the PCs. In contrast to the situation found in other vertebrate phyla, these ECs are not organised as nuclear clusters at the base of the cerebellum but are located in the PCL intermingled with the PCs. Generally, the EC develop a huge cell body and widely branched dendrites reaching into the molecular layer. Depending on the author and the model organism, morphological variations of ECs have been described, however (Ikenaga et al., 2005; Murakami and Morita, 1987). Such distinctions refer to the number of primary dendrites ("polygonal and monopolar EC") and the spindle like shape of the cell soma ("fusiform EC") (Ikenaga et al., 2005). However, ECs widely innervate the same extracerebellar territories of the CNS as

DCN neurons and function equivalent in terms of their neurophysiology (Wulliman et al., 1996; Wullimann, 1998).

1.2. Development of the cerebellum

1.2.1. Establishment of the cerebellar anlage

The isthmic organiser (IsO)

Originally thought to consist of mesencephalic and metencephalic components (Hallonet et al., 1990; Wang and Zoghbi, 2001), it has been shown that the cerebellum exclusively arises as a derivative of the dorsal part of rhombomere 1 (Wang et al., 2005; Zervas et al., 2004). Its development is orchestrated by a secondary organiser of the neuroepithelium, the isthmic organiser (IsO) or isthmus, which lies at the border between midbrain and hindbrain (Wurst and Bally-Cuif, 2001). Transplantation experiments demonstrated that the IsO is necessary and sufficient to induce development of the tectum and the cerebellum (Millet et al., 1996). Experiments in which beads soaked with Fibroblast Growth Factor 8 (FGF8) deposited in brain regions beyond the IsO revealed similar results (Irving and Mason, 2000). Noteworthy is that the induction of ectopic mes-metencephalic tissue occurs in a polarised manner, i.e. MHB-like structures that are induced artificially reveal rostrocaudal polarity resembling their endogenous counterparts. Such and further studies using loss-of-function and gain-of-function approaches in mice and in chicken further substantiated the key role of FGF8 for inducing cerebellum development. In the mouse, hindbrain expression of *fgf8* is initiated at the 3-5 somite stage in the caudal part of the upcoming hindbrain. In the zebrafish, *fgf8* is activated at 70% epiboly in the anterior hindbrain. This expression domain further becomes restricted to a narrow ring adjacent caudally to the MHB. The gene is expressed in 8 isoforms, from which FGF8 α and FGF8 β are expressed in IsO tissue (Sato et al., 2001). It has been proposed that strong doses of FGF8 β lead to the induction of the cerebellum via the RAS-ERK signalling pathway, whereas low doses of FGF8 β and FGF8 α induce tectum identity via a yet unknown cascade (Basson et al., 2008; Sato and Nakamura, 2004). Positioning of the IsO is controlled by the two homeobox transcription factors *otx2* and *gbx2*. Throughout development, *otx2* is expressed in the anterior CNS; *gbx2* in turn is expressed in the CNS posterior to the later MHB. Because both genes repress the expression of each other, the expression domains of both genes form two

precisely abutting domains with a sharp border at the position of the IsO (Belting et al., 2001; Millet et al., 1996). Experiments, in which the expression domains of either *otx2* or *gbx2* were extended ectopically beyond the normal limit lead to a shift of the MHB and thus of the cerebellum and the mesencephalon along the anterior- posterior axis (Acampora et al., 1997; Broccoli et al., 1999; Millet et al., 1999; Suda et al., 1997). Expression of the markers *otx2*, *gbx2*, *fgf8* and *wnt1* still aligned in a pseudonormal fashion but were shifted in parallel as well.

Rotation of the cerebellar neuroepithelium establishes the cerebellar anlage

Cerebellar patterning eventually results in cerebellar primordium rotation (Distel et al., 2006; Sgaier et al., 2005). During this process the anterior-posterior axis of the two halves of rhombomere1 (r1) is converted into a medial-lateral axis by rotation of this tissue by almost 90°. Subsequently both halves of the cerebellum primordium fuse along the midline to form a continuous brain compartment with newly established anterior-posterior and medio-lateral axes. Direct time-lapse imaging of the rotation of the cerebellum primordium demonstrated that rotation of r1 coincides with the condensation of the ventral hindbrain territory ((Distel et al., 2006), compare supplementary movie 1). Notably, the position of the MHB remains almost unaltered whereas the otic vesicles become positioned closer to the MHB over time when the cerebellar primordium is repositioned. Concomitantly, the cerebellar primordium does not appear to grow significantly. One proposed mechanism that might contribute to this axis transformation is that differential proliferation of cells within r1 may drive the morphogenetic rotation of the axis (Sgaier et al., 2005). It is also feasible that inflation of the ventricle lumen accounts for axis rotation: an osmotic gradient of Na⁺ and K⁺ created by an ATPase is supposed to drive water influx into the ventricle lumen (Lowery and Sive, 2005), suggesting that the neuroepithelial basal borders remain attached to each other at the MHB and caudally to r8, ventricle inflation could lead to the mentioned condensation of the hindbrain tissue. Rotation of the cerebellum primordium is completed at 32hpf in the zebrafish and around E12.5 in mice.

It is important to note that in mammals the epithelium of the cerebellar anlage changes its orientation once more after the rotation and fusion of both cerebellar halves due to the bending of the body axis and growth of the cerebellum, ending up in an ongoing shift of the ventral-dorsal orientation of the cerebellar anlage towards a

rostral-caudal alignment of the rhombic lip (RL) and the ventricular zone (VZ) at late developmental stages. To a lesser extent, such a second axis rotation is also seen in the zebrafish cerebellum. However the ventro-dorsal axis will not be completely distorted, resulting in a tight slope of the posterior border of the cerebellum of adult fish.

1.2.2. The two germinal zones of the cerebellar anlage

The Rhombic Lip and its associated transcription factor *atonal* homologue 1

The rotation of the cerebellar primordium overlaps with and is followed by the formation of the two distinct germinal zones of the hindbrain, the rhombic lip (RL) and the ventricular zone (VZ) (Fig. 2). In both, divergent neurons are generated. The newborn neurons migrate towards their final destination in specific regions of the rhombencephalon. Anatomically, the RL is the dorsal edge of the hindbrain neuroepithelium between alar plate and roof plate. It can be subdivided along the main body axis into the rostral upper rhombic lip (URL) and caudal lower rhombic lip (LRL). The LRL gives rise to various neurons of hindbrain nuclei. Among these are the pontine nucleus and the cochlear nucleus, which both provide mossy fibre input to the neuronal circuits of the cerebellum (Landsberg et al., 2005; Wang et al., 2005). The URL is restricted by the bend of the rotated cerebellar primordium and thus exclusively is a portion of r1. Classically it was assumed to give rise only to cerebellar granule neurons (Alder et al., 1996). More recent fate mapping studies have revealed a much greater impact of the URL as a germinal zone giving rise to different neuron populations in the entire rostral hindbrain (Machold and Fishell, 2005; Wang et al., 2005; Wingate, 2005). Hence, neurons that arise in the URL contribute to the "rostral clusters" outside of the cerebellum (Wingate, 2005), consisting of PBG (parabigeminal nucleus), the PPTg (pendunculopontine tegmental nucleus), the MiTg (microcellular tegmental nucleus), the LDTg (laterodorsal tegmental nucleus), the LPB (lateral parabrachial nucleus), the DCN and the granule cell precursors (GCPs) located in the EGL (Fig. 2). These different RL-derived neuronal populations are generated in a temporally shifted manner. First, neurons that are finally located in the brain stem regions are established. In a second phase, DCN neurons are formed. Finally, neuronal precursors that establish the EGL are generated (Fink et al., 2006; Machold and Fishell, 2005; Wang et al., 2005). Hence, birth date and the distance that

RL-derived precursors migrate towards their destination correlates: the earlier RL-derived neurons are born, the deeper and further away they settle. The precursor pools which accomplish for the generation of the various neurons are temporally restricted, though: In the chicken cerebellum, precursor cells of heterochronically transplanted early grafts from the RL lose their capacity to produce GCPs when implanted into RL of older embryos (Gilthorpe et al., 2002; Wilson and Wingate, 2006).

A molecular refined definition of the RL

On the molecular level, it was shown that the bHLH transcription factor *atoh1* is essential for development of RL-derived neurons (depending on the species from hereon referred to as *zath1* or *math1* for the zebrafish- and the mouse homologue, respectively). Its transcription is activated by BMPs and GDF7 secreted from the roof plate and the choroid plexus and mediated via SMAD (Alder et al., 1999; Chizhikov et al., 2006; Krizhanovsky and Ben-Arie, 2006; Qin et al., 2006). In neuroepithelial cells ventral to the RL (the VZ, see above), BMP signalling is antagonised by Notch signalling (Machold et al., 2007). Experiments in which development of RL-derived cells and their dependence on MATH1-function was studied *in vitro* suggest that *math1* is not necessary for the specification of GCPs. MATH1 is thought to function by regulating various components of the Notch pathway, especially by upregulating *hes5* and downregulation of *notch4* and *dll1* (Gazit et al., 2004). Because RL-derived progenitors are unable to emigrate from the RL, loss of *math1*-function leads to an ablation of RL-derived nuclei and of the EGL (Gazit et al., 2004; Wang et al., 2005).

In the hindbrain, *ath1* is expressed exclusively in the RL from E9 on in mouse embryos and from 20 to 48 hpf in the zebrafish (Ben-Arie et al., 1997; Kim et al., 1997). Its impact on cerebellum development and characteristic expression in the RL has led to “a refined definition of the rhombic lip as consisting of the *Math1*-expressing neuroepithelium along the fourth ventricle” (Wang et al., 2005). It thus also serves as a useful and important molecular marker for the RL and its derived neuron populations.

The Ventricular Zone and its associated transcription factor *ptf1a*

The VZ comprises the alar plate adjacent but ventral to the RL (Fig. 2). The cerebellar part of the VZ generates the inhibitory, GABAergic neurons of the cerebellum. These are the PC, the Golgi cells, the stellate cells and the basket cells.

Furthermore, GABAergic projecting neurons and interneurons of the DCN are generated in the cerebellar VZ (Hoshino et al., 2005; Leto et al., 2006). Similar to the expression of *ath1* in the RL, a specific bHLH factor, *pancreas transcription factor 1a* (*ptfla*) defines the VZ and the birthplace of VZ-derived cerebellar neurons (Glasgow et al., 2005; Hoshino et al., 2005; Obata et al., 2001; Pascual et al., 2007). Consequently, in the cerebellar primordium, the loss of *ptfla* results in the absence of GABAergic neurons (Hoshino et al., 2005; Pascual et al., 2007). Instead, precursors derived from VZ regions in which usually *ptfla* is expressed adopt an EGL –like phenotype in that such neurons allocate ectopically in the EGL and express typical genetic markers of the EGL like *math1*, *zic1/2* and *reelin* (Pascual et al., 2007). Acquisition of an EGL-like fate in turn depends on morphogen signalling secreted from the roof plate and the choroid plexus (Alder et al., 1999; Chizhikov et al., 2006; Krizhanovsky and Ben-Arie, 2006; Qin et al., 2006). This suggests that *ptfla* prevents VZ-derived cells from responding to such dorsalisating cues. The intracellular domain of the Notch receptor has been shown to block transcription mediated by BMP and its intracellular transducer SMAD in the VZ, providing a possible link between *ptfla* and the repression of RL-inducing BMP activity (Machold et al., 2007). How and whether PTF1A and Notch signalling interact remains to be shown.

In various other regions of the CNS like in the dorsal horn of the spinal cord (Glasgow et al., 2005) and in amacrine cells (Dullin et al., 2007; Nakhai et al., 2007), the fate of GABAergic neurons is mediated by *ptfla*. Furthermore, ectopic expression in embryonic telencephalic regions using *in-utero* electroporation is sufficient to induce GABAergic phenotypes (Hoshino et al., 2005). These facts led to the assumption that *ptfla* in general mediates a GABAergic fate of neuronal progenitors. However, in hindbrain regions posterior to the cerebellum, a small *ptfla*-domain generates neurons of the ION. In contrast to neurons derived from the cerebellar VZ, the ION neurons derived from the hindbrain VZ are glutamatergic (Yamada et al., 2007). Hence, similar to *math1*-expressing cholinergic neurons (Machold and Fishell, 2005), there solely appears to be a bias of specification towards GABAergic fates mediated by *ptfla* expression which depends on the environmental context. The molecular mechanisms governing glutamatergic vs. GABAergic neuronal subtype specification appear to be more complex though.

1.2.3. Migration and cerebellum morphogenesis

Neurons arise in the respective germinal zones at a specific developmental time point and reach their final destination by migration (Fig. 2). Obviously, this process relies on tight control over various parameters such as accurate timing, appropriate orientation, path finding and proper cease of migration and terminal differentiation. Migrating cells hence need to select pathways, establish polarity, activate specific adhesion systems and assemble and disassemble cytoskeletal components to finally execute migration. Disturbance of cellular processes enabling migration in turn leads to severe malformations of the brain such as lissencephalies, which are characterised by ectopic positioning of neurons.

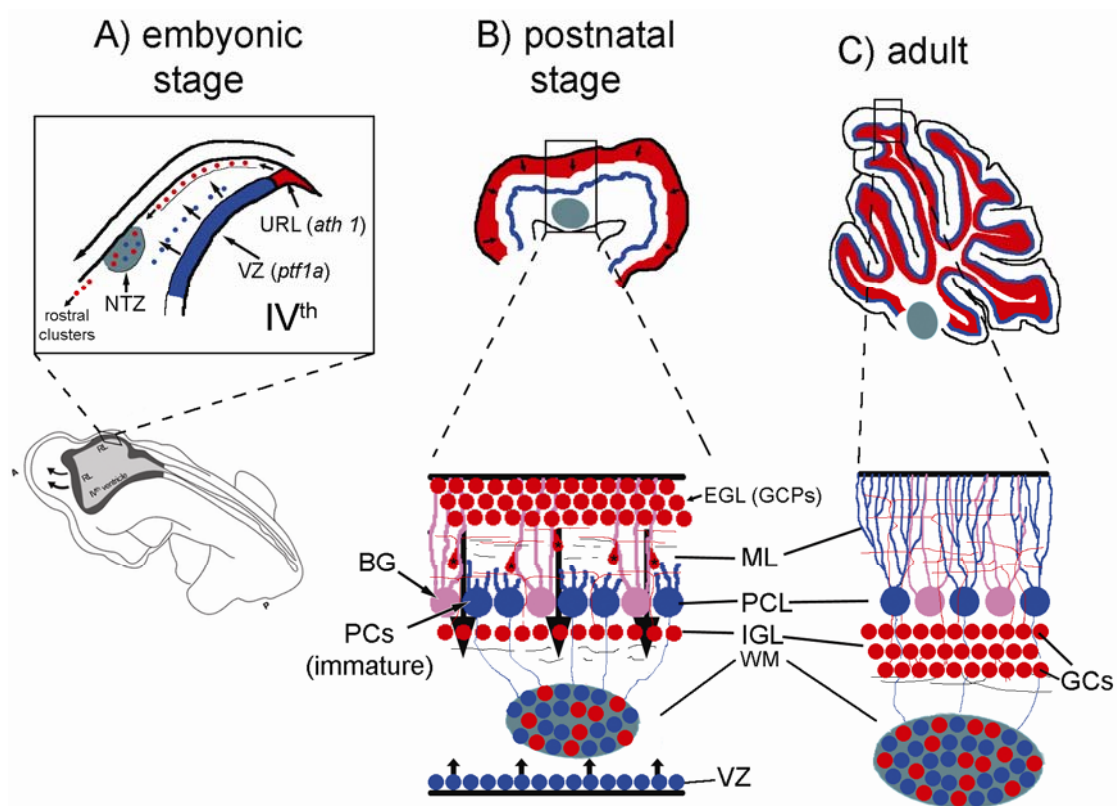


Fig. 2: The two germinal zones of the cerebellar anlage and histogenesis of the cerebellum. The drawing depicts the origin of GABAergic and glutamatergic neurons in the respective germinal zone, their migration towards their destination and their final location in the cerebellar tissue. Where VZ-derived neurons migrate radially, URL-derived cells migrate tangentially to give rise to the rostral clusters, neurons of the NTZ and the secondary germinal layer, the EGL. GCs, which are EGL derived, migrate radially along BG fibres towards the IGL after exiting the cell cycle (arrows in B delineate the directory, arrowheads label migratory GCPs). Note that both precursors of the VZ and the URL contribute to the DCN. Drawings are not to scale. BG: Bergmann glia; EGL: external granule layer; GC: granule cells; GCPs: granule cell precursors; IGL: inner granule layer; IVth: fourth ventricle; ML: molecular layer; NTZ: nuclear transitory zone; PC: Purkinje cell; PCL: Purkinje cell layer; URL: upper rhombic lip; VZ: ventricular zone; WM: white matter.

Dependent on the relative migratory direction, two modes of migration are distinguished. Migration of neurons along the apico-basal direction of the neuroepithelium is termed radial migration. If cells move perpendicularly to this route, they are said to perform tangential migration. In both cases, migration can occur homo- and heterophilic, i.e. neural precursors move by forming chain like structures among themselves or they move along other cells which serve as a scaffold (Rakic, 1990).

Migration of RL- derived neurons

The various RL-derived cell populations are known to migrate over long distances (Köster and Fraser, 2001; Rakic et al., 1994; Volkmann et al., 2008; Wang et al., 2005; Wingate and Hatten, 1999). RL-derived neurons thereby contribute to such diverse neuronal structures like rostral cluster nuclei and the GCPs (Fink et al., 2006; Machold and Fishell, 2005; Wang et al., 2005; Wingate, 2005). As mentioned, commitment of the respective neuronal populations in the RL occurs in a temporally patterned manner. After being generated, the neuronal precursor cells emigrate from the RL along the meninges, i.e. tangentially, towards their respective destination (Fink et al., 2006; Köster and Fraser, 2001; Volkmann et al., 2008; Wang et al., 2005). Migration of GCPs is the best studied episode of RL-precursor migration (Gilthorpe et al., 2002; Komuro and Rakic, 1995; Komuro et al., 2001; Köster and Fraser, 2001; Miale and Sidman, 1961; Rieger et al., 2008; Volkmann et al., 2008). Typically, GCPs undergo migration from the RL towards their destination, the IGL, in three distinct phases (Komuro and Yacubova, 2003). First GCPs migrate tangentially along the pia mater towards ventral, thereby also getting deeper into the EGL towards the forming ML. Importantly the precursors retain their ability to proliferate as long as they are located within the EGL ((Koppel and Lewis, 1983), see 1.3). When having reached the interface of EGL and the forming ML, GCPs remain stationary for a short phase. Cells then extend a single vertical process perpendicularly to the EGL-ML interface and initiate migrating towards ventral regions. This second phase of radial migration of GCPs is known to involve heterotypic interactions with a specialised transient form of astroglial cells, the Bergmann glia (BG) (Edmondson and Hatten, 1987; Rakic, 1971). Migrating neurons further permeate the IGL until they reach the interface between IGL and central white matter. Thus, migrating GCPs terminate radial migration when having reached the innermost IGL. In contrast to the mode by

which GCPs permeate the ML and the PCL, the third phase of GPC-migration again is glia-independent and homophilic. This final step of migration is followed by terminal neuronal differentiation, manifested by expression of i.e. *gabaRa6* (Hatten et al., 1997).

In the developing zebrafish cerebellum, GCPs migrate without interacting with glial cells at least until early larval stages. Instead, it was demonstrated that a tangential homotypic mode of GPC migration is the predominant form. Cell adhesion mediated by Cadherin2 was shown to play a key role in the establishment and maintenance of polarization during chain-like migration of cerebellar GPCs (Rieger, 2008; Volkmann et al., 2008).

Migration of VZ- derived neurons

Although not being the only cells that arise from the VZ, previous studies mostly addressed the migration of precursors of DCN neurons and PC precursors (Altman and Bayer, 1978; Altman and Bayer, 1985a; Altman and Bayer, 1985b; Bourrat and Sotelo, 1986). VZ-derived precursors are supposed to exclusively migrate radially. Whether these movements occur in a hetero- or homophilic manner is under debate (Hatten, 1999; Yamada and Watanabe, 2002). On the one hand, fibres of radial Bergmann glia that could serve as a scaffold are present at the respective stage (Yamada et al., 2000). It was also shown that Bergmann fibres in the adult cerebellum can facilitate migration of transplanted foetal PCs (Sotelo et al., 1994; Tsurushima et al., 1993). Ablation of GFAP-expressing cells, i.e. astro- and Bergmann glia, leads to perturbed positioning of PC somata (Delaney et al., 1996). Noteworthy though the fibres themselves do not provide cues that induce directional migration. At least *in vitro* neurons can migrate into both directions along a glial fibre (Edmondson and Hatten, 1987; Hatten, 1990).. Direct experimental evidence supporting a model in which PCs migrate along the radial fibres of Bergmann glia during cerebellar development is missing though (Yamada and Watanabe, 2002).

Considering the two re-orientation events of the cerebellar neuroepithelium during development (see 1.2.1), radial migration from the VZ occurs from the ventral towards the dorsal side of the cerebellum, being actually executed in a medial-to-lateral and a caudal-to-rostral direction, respectively. Precursors of the VZ giving rise to DCN neurons arise in the rat at E16 and subsequently migrate dorsally to reach the “Nuclear Transitory Zone ” (NTZ) (Altman and Bayer, 1985a) underneath the

cerebellar plate. Later arising PC precursors follow this DCN pathway but pass the NTZ, align at the cerebellar plate and continue to form a layer, the developing PCL. Worth to mention is that the generation of the PCL proceeds in a temporal pattern: early born PC settle in rostral parts of the PCL while precursors born afterwards expand the PCL in caudal direction (Altman and Bayer, 1985b). The somata of radial precursors of Bergmann glia follow successively and align within the PCL. The cells then morphologically transform into their typical shape with the soma allocated in the PCL and shaft fibres constituting a palisade-like glial framework in the ML. The ramified fibres of the Bergmann glia then inter alia provide the scaffold for both the radial inward migration of GCPs (Edmondson and Hatten, 1987) and formation of PC's dendritic tree (Lordkipanidze and Dunaevsky, 2005).

In rats, the precursors of interneurons and glia migrate postnatally from the central white matter towards the cerebellar cortex (Zhang and Goldman, 1996). More recent work implicate that the source of these precursors could be stem cells located within the WM (Lee et al., 2005a). While remaining mitotically active, precursor cells transit the WM and finally end up at their appropriate position. According to Zhang and colleagues, the fates of the various progenitors get increasingly restricted with time, with those precursors generated later giving rise mainly to glial cells.

DCN neuron are both VZ- and URL-derived

The neurons of the DCN are heterogenous in terms of morphology, projections and neurotransmitter phenotype. Both the VZ and the URL generate neurons of the DCN (Fig. 2). Where the classic studies by Altman and Bayer described the migration of VZ-derived precursor towards the NTZ (Altman and Bayer, 1978; Altman and Bayer, 1985a), a more recent study made use of a tamoxifen inducible *in vivo* genetic fate-mapping strategy to identify regions containing neurons that originated from *ascl1* (*ascute-complex like 1*) expressing progenitor cells. *Ascl1* was shown to label undifferentiated neural precursors in the VZ. Depending on the embryonic stage at which progenitors were labelled, *ascl1* defined lineages gave rise to GABAergic neurons in the DCN. Noteworthy, GABAergic DCN neurons were generated in two non-overlapping temporal cohorts at around E10 and E13 (Kim et al., 2008). This finding is consistent with the description of the two differing populations of GABAergic DCN neurons, i.e. the GABAergic neurons that project to the ION and the small GABAergic interneurons (Leto et al., 2006; Sultan et al., 2003).

Furthermore, the cerebellum of *ptfla* mutants is depleted of all kinds of VZ-derived GABAergic neurons including GABAergic DCN neurons (Hoshino et al., 2005).

A study addressing loss-of-function of *math1*, a detailed expression study and the use of a genetic fate-mapping approach revealed that the URL also contributes to the DCN neurons (Fink et al., 2006; Machold and Fishell, 2005; Wang et al., 2005). These URL-derived DCN neurons were identified to correlate to the large glutamatergic projection neurons (Sultan et al., 2003).

However, it was also suggested that a fourth cohort of neuronal precursor might give rise to a yet unrecognised population of DCN neurons. These were found to arise at around E12 in mice and to express *lmx1a*, which is also known as the *dreher* gene. *lmx1a* and Calret, but not *math1* were coexpressed in these cells. In addition, *lmx1a* expression localized to cells with large nuclei which did not bear GABA, suggesting that neuronal precursor expressing *lmx1a* give rise to glutamatergic DCN neurons that are not URL-derived.

A yet unresolved question is where the teleosts' equivalent of the DCN neurons, the ECs are derived from. Most studies that addressed the ECs concentrated on comparative morphology, neurophysiology and electrosensory circuits of mormyrids (e.g. (Murakami and Morita, 1987; Nieuwenhuys et al., 1974; Pouwels, 1978)). As DCN neurons, EC were suggested to form a heterogenous group of neurons in terms of their neurotransmitter phenotype (Ikenaga et al., 2005). A recent study suggested that a subset of ECs might express *olig2*. In this study, the cascades involved in development of ECs were elucidated; it did not address though the origin of ECs, the time course of EC development and the migratory behaviour of ECs (McFarland et al., 2008).

1.3. PCs control GPC proliferation and maturation of the cerebellum

Cell proliferation is the apparent means of growth of an emerging organism. and a key mechanism of morphogenesis. On the cellular level, control over proliferation is managed by intrinsic factors, which in turn are eventually affected by extracellular signals. Dividing cells need to set up the machineries for genome-replication, cell growth, mitosis and –in most cases- the machinery that executes cytokinesis. Given the cell biological requirements of proliferation, intrinsic factors regulating proliferation also need to determine the differentiation status of a cell.

All cells transiently undergo an iterative series of events termed the cell cycle. The cell cycle commonly is subdivided into four stages: G1-phase, S-phase, G2-phase, M-phase, where G is for gap, S for synthesis (of DNA due to replication) and M for mitosis. An additional term, G0, is used for quiescent, senescent, differentiating and fully differentiated cells. With respect to some variation of this scheme, e.g. cleavage in the development of *Drosophila*, this schematic cycle accounts for all proliferating cells.

Proliferation during CNS development is restricted to specialised germinal zones. During cerebellum development, an additional, secondary germinal territory arises besides the RL and the VZ: the external granular layer (EGL) (Gona, 1976; Miale and Sidman, 1961; Rakic and Sidman, 1970). The URL –derived progenitors settle in the EGL to further proliferate. After exiting the cell cycle, the GCPs migrate radially to finally become part of the cerebellar circuit (see 1.2). Studies in which PCs were selectively ablated demonstrated the drastic decrease of GCPs located in the EGL due to a reduced proliferation rate rather than cell death (Smeyne et al., 1995). Loss-of-function of the tumour suppressor and Hedgehog (HH) receptor *patched* (*ptc*) in mice resulted in an increased rate of formation of medulloblastoma-like cerebellar tumours, indicating an involvement of the HH signalling cascade in controlling proliferation of GPCs (Goodrich et al., 1997). Three studies then independently provided evidence that Sonic Hedgehog (SHH) secreted by PCs induces proliferation of GPCs. In detail, these studies demonstrated expression of *shh* in PCs on the one hand and expression of its receptors *ptc* and *smo* in GCPs on the other hand. Furthermore, the proliferative effect of SHH was demonstrated in tissue- and in cell culture assays and *in vivo* (Dahmane and Ruiz i Altaba, 1999; Wallace, 1999; Wechsler-Reya and Scott, 1999). HH-signalling was abolished by injection of hybridoma cells into the cerebellum of postnatal mice that synthesise an anti-HH protein. Besides inducing proliferation in GPCs, one of these studies revealed additional functions mediated by SHH (Dahmane and Ruiz i Altaba, 1999). In the absence of SHH, cerebella developed hypoplastically but also showed abnormal foliation suggesting an additional role of SHH in patterning of the developing cerebellum. Furthermore, not only granule neurons but also Bergmann glia were reduced in number, due to loss of SHH-mediated differentiation of Bergmann glia. It was also demonstrated that SHH is not the exclusive regulator of proliferation and differentiation. Termination of SHH-induced proliferation and induction of differentiation is rather likely the result from reduced responsiveness of

GPCs to SHH or conversion of a proliferative response into a differentiative one. PCs hence play a major role in organising cerebellum development.

Analysis of cultured GPCs that were stimulated with SHH revealed an enhanced proliferation rate due to an upregulation of D-type cyclins (CYCD), which are necessary regulators for cell cycle progression through the G1-phase. This upregulation was dependent on protein synthesis (Kenney and Rowitch, 2000). Further studies showed that the protooncogene *N-myc* is a direct target of the SHH pathway in GPCs. It was demonstrated that transfection of *N-myc* into GPCs stimulates proliferation mimicking the SHH-induced upregulation of CYCD1, CYCD2, E2F1 and E2F2. *N-myc* is expressed in GPCs inside the EGL, suggesting a potential role for *N-myc* in GPC proliferation *in vivo* (Kenney et al., 2003; Oliver et al., 2003). Consistent with *N-myc* promoting GPC proliferation, the conditional knock-out of *N-myc* in the CNS resulted in drastic hypoplasia of the cerebellum of newborn and juvenile mice. The effect on the malformation of the cerebellum appears to be due to a drastic reduction in cell number of RL-cells as well as EGL cells and the reduced proliferation of neuronal precursors. In the absence of *N-myc*, the cerebellum primordium exhibits loss of CYCD2 expression and elevated and ectopic expression of the CDK-Inhibitors (CDKI) p27Kip1 and p18Ink4c (Knoepfler et al., 2002). Therefore, *N-myc* is a cellular key effector of SHH- induced GPC proliferation.

N-myc is tightly regulated by a rapid protein turn-over. Proteasomal degradation of NMYC in mice is facilitated by phosphorylation of two aminoterminal AA-residues, T50 and S54, as revealed by targeted mutagenesis of the respective AA into non-phosphorylatable Alanine (Kenney et al., 2004). Phosphorylation of endogenous NMYC at T50 can be prevented by direct inhibition of GSK3 β by adding Li⁺ ions into the culture medium of GPCs. GSK3 β -activity increases upon blocking phosphorylation of GSK3 β by the addition wortmanin, which is known to block activity of Phosphoinositide 3-Kinases (PI3K). This connection indicates regulation of GSK3 β by a cascade of Insulin-Like Growth Factor (IGF), IGF-Receptor (IGFR), PI3K and Protein Kinase B (PKB/AKT). Consistently, PI3K has been shown to be necessary for the known long-term survival of GPCs (Dudek et al., 1997). Phosphorylation of T50 of NMYC is supposed to require previous phosphorylation of S54 carried out by a “priming kinase” (Kenney et al., 2004). A subsequent study provided evidence that NMYC turn-over is triggered by phosphorylation of S54 by a

complex of CDK1 and CYCA or CYCB (Sjostrom et al., 2005). IGF thus regulates NMYC turn over by preventing its phosphorylation.

The mechanism by which PCs organise cerebellar development explains well the developmental interdependence of the various cells types. It is a known phenomenon from classic mutant studies that ablation of one major cell population in the cerebellum results in hypoplasia of the entire organ (Hatten, 1999; Rakic and Sidman, 1973; Rice and Curran, 2001; Vogel et al., 2007). The SHH-NMYC-network furthermore reveals many properties that are shared during normal development and tumourigenesis. Both genes are known oncogenic factors. The EGL is a proposed source of cells that transform into tumour cells constituting the medulloblastoma (MB), and both the SHH- signalling pathway and N-MYC have been associated with the pathogenesis of MB in 20% of all cases (Corcoran and Scott, 2001).

Modes of MYC action

MYC proteins are known to form heterodimers with another bHLH protein, MAX, by its C-terminal leucine zipper domain (Blackwood and Eisenman, 1991; Prendergast et al., 1991). The MYC–Max heterodimers specifically bind an E-box motive of the DNA and serve as a scaffold for various complexes. These include Histone Acetyl Transferases (HATs) (McMahon et al., 1998; McMahon et al., 2000), the INI1 subunit of the SWI/SNF complex, which mediates chromatin remodelling (Cheng et al., 1999) and the ubiquitin ligase SKP2 as part of the SCFSkp2 E3 ubiquitin ligase complex (von der Lehr et al., 2003).

Recruitment of interaction partners mediated by MYC-MAX is antagonised on the protein level by the formation of homodimers of MAX and by formation of heterodimers formed by MAX and MAD (Ayer et al., 1993) or MNT (Hurlin et al., 1997). MAD-MAX as well as MNT-MAX bind to the same E-box motive as MYC-MAX. Both associate with a Histone Deacetylase (HDAC) complex, thus reverting MYC-MAX induced acetylation (Ayer et al., 1995; Hassig et al., 1997; Hurlin et al., 1997).

1.4. Aim of this study

The zebrafish has become one of the favourite model organisms for studying the dynamic processes of development *in vivo*. The cerebellum is a well suited paradigm for examining cellular and molecular mechanisms that govern CNS development. To obtain deeper insights into the orchestration of migration of the various cerebellar cell

types, I combined time lapse imaging with expression analysis, morphological and histological description, retrograde labelling, micromanipulation and genetic approaches. While recent studies addressed migration of GPCs, its contribution to cerebellum development and molecules governing GPC development (Köster and Fraser, 2001; Köster and Fraser, 2006; Rieger, 2008; Rieger et al., 2008; Volkmann et al., 2008), development of cerebellar neurons other than GPCs such as ECs remains elusive. Hence this study aimed to identify ECs in the zebrafish cerebellum and to characterise them on the histological, cellular and molecular level. Further questions related to the time course of EC development: when are ECs generated? At which stage do they proliferate, differentiate and migrate? From where and how do EC precursors get to their destination? Answers on these questions may help to better understand how various cells types build up a functional brain compartment. Comparison of ECs and DCN neurons also will allow to distinguish between processes of brain development that have been conserved throughout evolution and such that have diverged.

One further aim was to elucidate a possible role of the protooncogene *nmyc* in the developing zebrafish cerebellum in order to establish a novel disease model accessible to *in vivo* imaging approaches. Complementary to classic disease models of the medulloblastoma such a model would allow tracing of tumourigenic cells ab initio. For example, such a model could yield answers on the motility of cancer cells and their potentiality to generate metastases. Furthermore, zebrafish is accessible to high-throughput assays for small molecules. Therefore, the zebrafish homologue of *N-myc* should be cloned; detailed expression analyses should answer in which cell type(s) *nmyc* might be active in the zebrafish cerebellum. Finally, genetic studies should reveal the HH-dependence of *nmyc* expression.

2. Materials and methods

2.1. Materials

2.1.1. Equipment

Autoclave	ASS und Aigner, Typ 667-1ST, München, Germany
Benchtop rocking boards	Heidolph, Schwabach, Germany
Benchtop thermostats	Thermomixer, 5463/Comfort, Eppendorf, Hamburg, Germany
Binocular	Stemi SV11 Zeiss, Oberkochen, Germany
Centrifuges	Kendro Evolution, Kendro Laboratory Products GmbH, München, Germany; Tabletop Centrifuge 5415D and 5415R, Eppendorf, Hamburg, Germany
Confocal laser scanning microscopes	LSM510 equipped with Argon laser (451, 477, 488, 514nm) and Helium-Neon lasers(561, 594, 633nm), Zeiss LSM510 Meta equipped with Argon laser (451, 477, 488, 514nm) and Helium-Neon lasers (543, 633nm), Zeiss, Oberkochen, Germany; TCF SP5, Leica, Wetzlar, Germany
Cryostat	Microm, HM 560, Walldorf, Germany
Electrophoresis power supplies	Electron EC105, Thermo Fisher Scientific, Schwerte, Germany
Electroporator	Gene pulser Xcell, BioRad, München, Germany
Fluorescence light source	LEJ GmbH, Jena, Germany
Fluorescent Stereomicroscope	MZ 16FA equipped with filters for UV, GFP, FITC/Cy-3,YFP, Rhodamine and Texas Red, Leica
Freezers (-20°C)	Liebherr, Biberach, Germany
Freezers (-80°C)	Heraeus GmbH, Karlsruhe, Germany

Gel documentation	Herolab, Wiesloch, Germany
Gel electrophoresis chambers	Shelton Scientific, Amersham/ BD Biosciences, München, Germany
Horizontal needle puller	Narishige, London, UK
Incubators	BK-600 (28°C) and B15 (32°C), Heraeus GmbH, Karlsruhe, Germany
Incubators	Heraeus GmbH, Karlsruhe, Germany
Light sources	KL2500 (Leica), KL1500 (Zeiss)
Magnetic stirrers	RCT basic, IKA Labortechnik, Staufen, Germany
Microinjection needle holder	Narishige, London, UK
Microinjector	FemtoJet Express, Eppendorf, Hamburg, Germany
Microscope cameras	Axiocam HRC digital camera, Zeiss, Oberkochen, Germany; DFC 350 FX camera, Leica, Wetzlar, Germany
Microtome	Microm, HM 355S, Walldorf, Germany
Microwave oven	Clatronic International GmbH, Kempen, Germany
Objectives	C-Apochromat 40x/NA1.20 water immersion corrected C-Apochromat 63x/NA1.20 water immersion corrected Plan-NeoFluar 5x/NA0.15 Plan-NeoFluar 10x/NA0.3 Plan-NeoFluar 20x/NA0.5 Plan-NeoFluar 40x/NA0.75
Paraffin embedding station	Tissue-TEKÒ TEC, Sakura Finetek, Torrance (CA), USA
PCR machine	PTC 100, MJ Research Inc., Waltham, MA 02451 United States
pH indicator	WTW pH 538, Weilheim, Germany

Photometer	Biophotometer, Eppendorf, Hamburg, Germany
Pipettes (10µl - 1ml)	Gilson, Bad Camberg, Germany
Pipetting aids	Pippettboy, Vitartis AG, Baar, Germany; Multistepper, Brand, Wertheim, Germany
Precision balances	PRS 6200-2, Kern und Sohn GmbH, Balingen-Frommern, Germany
Refrigerators	Liebherr, Biberach, Germany
Rotors	F45-24-11: Eppendorf; SS-34, GSA, GS3: Kendro
Test tube rotator	Model LD 79, Labinco, Breda, The Netherlands
Ultra pure water purification system	MilliQ, Millipore, Schwalbach, Germany
Upright microscope	Axioplan 2, Zeiss, Oberkochen, Germany
Vertical needle puller	Narishige, London, UK
Vibratome	Microm HM 650V, Walldorf, Germany
Vortexers	Vortex Genie, Labortechnik Fröbel GmbH, Germany
Waterbaths	Isotemp 205, Lauda Ecoline E100, Memmert, Schwabach, Germany

2.1.2. Consumables

1,5ml/ 2,0ml microreaction tubes	Eppendorf, Hamburg, Germany
10cm petri dish	Nunc, Wiesbaden, Germany
6 to 96 well plates	Nunc, Wiesbaden, Germany
6cm petri dish	Nunc, Wiesbaden, Germany
Cover slips	Menzel, Braunschweig, Germany
Electroporation cuvettes	Molecular Bio Products, San Diego, CA, USA
Glas capillaries, with filament	Harvard Apparatus, March-Hugstetten, Germany
Glasware	Schott, Mainz, Germany; Brand,

	Wertheim, Germany
Microloader tips	Eppendorf, Hamburg, Germany
Nylon membrane	Hybond-N, Amersham Buchler
Object carriers	Super frost, Menzel Glasbearbeitungswerk GmbH & Co. KG, Braunschweig, Germany
Parafilm	Brand, Wertheim, Germany
Pipette tips	Gilson, Bad Camberg, Germany
Pipettes, 2, 5, 10 and 25ml	Greiner, Frickenhausen, Germany; BD Falcon, Heidelberg, Germany
Reaction tubes, 14ml and 50ml	Greiner, Frickenhausen, Germany; BD Falcon, Heidelberg, Germany
Scalpells	Braun, Melsungen, Germany
Sterile syringe filter (0.22µm)	Qualilab, Olivet, France
Transfer pipettes	VWR international, Darmstadt, Germany

2.1.3. Chemicals

Agarose, for routine use	Sigma-Aldrich Chemie GmbH, Deisenhofen, Germany
Agarose, low-melting	Sigma-Aldrich Chemie GmbH, Deisenhofen, Germany
Ampicillin, sodium salt	Sigma-Aldrich Chemie GmbH, Deisenhofen, Germany
Aquamount	Polyscience Inc., Warrington, USA
BCIP (5-Bromo-4-chloro-3-indolyl- phosphate, 50mg/ml in DMF)	Sigma-Aldrich Chemie GmbH, Deisenhofen, Germany
Bodipy Ceramid	Molecular probes, invitrogen GmbH, Karlsruhe, Germany
BSA (bovine serum albumine)	Sigma-Aldrich Chemie GmbH, Deisenhofen, Germany
Chloramphenicol	Sigma-Aldrich Chemie GmbH, Deisenhofen, Germany
Cyclopamine	Biomol, Hamburg, Germany

DAB (3,3'-Diaminobenzidine)	Sigma-Aldrich Chemie GmbH, Deisenhofen, Germany
DAPI (4',6-diamidino-2-phenylindole)	Sigma-Aldrich Chemie GmbH, Deisenhofen, Germany
Digoxigenin RNA labeling, Mix10x	Roche Diagnostics GmbH, Mannheim , Germany
DiI (1,1'-dioctadecyl-3,3,3',3'- tetramethylindocarbocyanine perchlorate)	Molecular probes, Karlsruhe, Germany
DMSO (dimethyl sulfoxide)	Sigma-Aldrich Chemie GmbH, Deisenhofen, Germany
dNTPs	Fermentas, St. Leon-Rot, Germany
Ethidium bromide	Sigma-Aldrich Chemie GmbH, Deisenhofen, Germany
Fluoresceine RNA labeling Mix, 10x	Roche Diagnostics GmbH, Mannheim , Germany
Frozen section medium	Richard Allan Scientific, Kalamazoo, USA
Gel-loading buffer for RNA, 6x	Ambion, Darmstadt, Germany
Heparine	Sigma-Aldrich Chemie GmbH, Deisenhofen, Germany
HEPES	Sigma-Aldrich Chemie GmbH, Deisenhofen, Germany
IPTG (Isopropyl β -D-1- thiogalactopyranoside)	Sigma-Aldrich Chemie GmbH, Deisenhofen, Germany
Kanamycin	Sigma-Aldrich Chemie GmbH, Deisenhofen, Germany
Lichrosolv	E. Merck KGaA, Darmstadt, Germany
Methylen blue	Sigma-Aldrich Chemie GmbH, Deisenhofen, Germany
Mineral oil, embryo culture tested	Sigma-Aldrich Chemie GmbH, Deisenhofen, Germany
Nail polish	Manhattan, Dr Scheller Cosmetics AG, Eislingen, Germany

NBT (Nitro blue tetrazolium chloride, 100mg/ml in 70% DMF)	Sigma-Aldrich Chemie GmbH, Deisenhofen, Germany
NGS (normal goat serum)	Sigma-Aldrich Chemie GmbH, Deisenhofen, Germany
Penicillin (10000U/ml)/ Streptomycin (10000µg/ml)	Gibco, Invitrogen GmbH, Karlsruhe, Germany
Phenole red, 0,5% in DPBS	Sigma-Aldrich Chemie GmbH, Deisenhofen, Germany
PTU (phenylthiourea)	Sigma-Aldrich Chemie GmbH, Deisenhofen, Germany
Tetramethylrhodamine, 3000 MW	Invitrogen GmbH, Karlsruhe, Germany
Silicon grease	Dow Corning Corporation, USA
TissueTek® OCT medium	Sakura Finetek Europe, Zoeterwoude, The Netherlands
Topro, 1mM in DMSO	Invitrogen GmbH, Karlsruhe, Germany
Torula-RNA	Sigma-Aldrich Chemie GmbH, Deisenhofen, Germany
Tricain	Sigma-Aldrich Chemie GmbH, Deisenhofen, Germany
TRITON X100	Sigma-Aldrich Chemie GmbH, Deisenhofen, Germany
Tween ® 20	Sigma-Aldrich Chemie GmbH, Deisenhofen, Germany
X-Gal (5-bromo-4-chloro-3-indolyl-beta-D-galactopyranoside)	Sigma-Aldrich Chemie GmbH, Deisenhofen, Germany

All further standard chemicals were obtained from Sigma-Aldrich Chemie GmbH, Deisenhofen, Germany and E. Merck KGaA, Darmstadt, Germany.

2.1.4. Enzymes and Kits

Alkaline Phosphatase (1U/µl)	Roche Diagnostics, Mannheim, Germany
DIG RNA-Labeling mix	Roche Diagnostics, Mannheim, Germany
DNaseI (RNase-free, 1U/µl)	Roche Diagnostics, Mannheim, Germany
Gel Extraction kit	Eppendorf, Hamburg, Germany
GeneClean Turbo kit	Q-BIOgene, Heidelberg, Germany

GeneRuler™ 1kb DNA Ladder (molecular weight marker)	Invitrogen GmbH, Karlsruhe, Germany
Klenow-Fragment (10U/μl)	MBI Fermentas, St. Leon-Rot, Germany
Message Machine SP6 Kit	Ambion, Darmstadt, Germany
NucleoBond PC100/500	Macherey & Nagel, Düren, Germany
Pfu Ultra II DNA polymerase	Stratagene, La Jolla, CA, USA
Pronase	Roche Diagnostics, Mannheim, Germany
Proteinase K, 20mg/ml	Roche Diagnostics, Mannheim, Germany
QIAGEN Nucleotide Removal kit	Quiagen, Hilden, Germany
QIAquick PCR Purification kit	Quiagen, Hilden, Germany
Quia shredder	Quiagen, Hilden, Germany
Quiaquick Nucleotide Removal Kit	Quiagen, Hilden, Germany
QuikChange site-directed mutagenesis kit	Stratagene, La Jolla, CA, USA
Restriction endonucleases	MBI Fermentas, St. Leon-Rot, Germany; New England Biolabs, Frankfurt/ Main, Germany; Roche Diagnostics, Mannheim, Germany
Rnasin RNase Inhibitor (40U/μl)	Promega, Mannheim, Germany
RNeasy Mini Kit	Quiagen, Hilden, Germany
RNeasy Mini kit	Quiagen, Hilden, Germany
SP6 RNA-Polymerase (20U/μl)	MBI Fermentas, St. Leon-Rot, Germany
Super script II, reverse transcriptase (200U/ml)	Invitrogen GmbH, Karlsruhe, Germany
T3 RNA-Polymerase (20U/μl)	MBI Fermentas, St. Leon-Rot, Germany
T4 DNA-Ligase (5U/μl)	MBI Fermentas, St. Leon-Rot, Germany
T7 RNA-Polymerase (20U/μl)	MBI Fermentas, St. Leon-Rot, Germany
Taq DNA-Polymerase (5U/ml)	MBI Fermentas, St. Leon-Rot, Germany
TOPO TA Cloning	Invitrogen GmbH, Karlsruhe, Germany

2.1.5. Antibodies

Primary antibodies

antigen

α Aspartate

Host, supplier, ordering #, dilution

rabbit, Abcam, ab9439, 1/400

α Brain lipid-binding protein (BLBP)	rabbit, Nathaniel Heintz (Rockefeller Univ.), personal gift, 1/500
α Calbindin (Calb)	rabbit, Swant, CB 38, 1/2000
α Calretinin (Calret)	rabbit, Chemicon, AB149, 1/250
α digoxigenin	sheep, Roche Diagnostics, 1 093 274 910, 1/2000
α Fluoresceine	sheep, Roche Diagnostics, 1 426 338, 1/2000
α Glutamate Decarboxylase 67 (GAD 67)	rabbit, Chemicon, AB 108, 1/50
α green fluorescent protein (GFP)	rabbit, Torey Pines Biolab, TP401, 1/500; chicken, Aves, GFP-1020, 1/500
α HuC	mouse, Molecular probes, 16A11, 1:10, c=0,1mg/ml
α mouse atonal homologue (MATH)	rabbit, Jane Johnson (University of Texas, Southwestern Medical Center at Dallas), personal gift, 1/250
α O4	mouse, Chemicon, MAB345, 1/100
α phospho-histon 3 (PH3)	rabbit, Upstate Biotechnology, cat# 06-570, 1/300
α red fluorescent protein (RFP)	rabbit, Chemicon, AB3216, 1/100
α ZebrinII	mouse, R. Hawkes (University of Calgary), personal gift, 1/100- 1/1000

Secondary antibodies

<u>host, antigen-conjugate</u>	<u>supplier, ordering #, dilution</u>
donkey α chick-FITC	Jackson Laboratories, 703 095 155, 1/250- 1/500
donkey α mouse IgG H+L- Cy5	Jackson Laboratories, 715 175 151
goat α mouse IgG-Alexa546	Molecular Probes, 11003, 1/250- 1/500
goat α rabbit-alexa547	Molecular Probes, A 21244, 1/250- 1/500
goat α rabbit-Cy2	Jackson Laboratories, 111 255 003, 1/250- 1/500
goat α rabbit-Cy3	Jackson Laboratories, 115 165 044, 1/250- 1/500
goat α rabbit-Cy5	Jackson Laboratories, 111 175 003, 1/250- 1/500

2.1.6. Zebrafish strains

Wildtyp-zebrafish

AB-strain inbred strain at the Helmholtz Zentrum München.

Brass inbred strain of pigmentation mutant that is deficient in melanine synthesis at the the Helmholtz Zentrum München.

Transgenic fish

Tg [*olig2*:GFP] and Tg [*olig2*:dsRED], compare (Shin et al., 2003).

Tg [*ptf1a*:GFP], compare (Godinho et al., 2005).

Tg [*gatal*:GFP], compare (Long et al., 1997; Volkmann et al., 2008).

mutant fish lines

slow muscle omitted (*smu*) (Barresi et al., 2000).

2.1.7. Bacteria

E. coli-strains of the following genotypes were used:

XL1-Blue (Bullock, 1987)

GM4 (Bolivar and Backman, 1979)

El250 (Warming et al., 2005)

2.1.8. Primers

<u>stock #</u>	<u>Oligo name</u>	<u>Purpose</u>	<u>Sequence</u>
99	nmyc3' race2	amplify 3' end of zebrafish <i>N-myc</i>	GTGACACA ACTGAGGAGCCAAC AA
102	zfnmycstop	zebrafish nmyc-cDNA, stop codon TAA, behind stop codon is SnaBI-site for further cloning	AATACGTATTAGCGAGTCCTGGC CTGCTCAAGTCTG
142	zf dhh up1	for amplification of a partial cDNA fragment of zebrafish <i>desert hedgehog</i> together with 143	ACTTCAAAGACGAGGAACGCTC CAATGC
143	zf dhh low1	see 142	GCCTTGCATACCAGTAAACCTCC TTTTG
144	zf ihh up	for amplification of a partial cDNA fragment of zebrafish <i>indian hedgehog</i> together with 145	ATGGAAACAGAAGACGTGACGG TTAGAG
145	zf ihh low	see 144	TCAATAAAAATCTTTGTGGGTCAA GAAATATACG
149	ClaI- NmycATG	for amplification of 5-prime end of zf <i>N-myc</i> together with #5 using #584 as template	GAATCGATATGCCAGCTAAAAC CATGAGCTCA
160	N-mycsequ 398for	upper primer for sequencing <i>N-myc</i>	CGCGAGAGAACTGGAGC
161	N-mycsequ rev890	lower primer for sequencing <i>N-myc</i>	GCTGCTGGTAGATGGAGG

186	zfnmycdeltaz iplo	to create dominant-negative <i>N-myc</i> by introducing a Stop codon before leucine zipper together with primer #149	TCTACGTATTATCGGAACTCCTG AGCCTCCAGGGAGC
187	zf N-myc S53A up	for the exchange of Serine 53 to Alanine in <i>zf N-myc</i> using the quickchange kit (stratagene) together with primer #188. Melting temperature estimated to 88°C	GCTGCTGCCACTCCTCCTCTGG CCCCGAGCCGGG
188	zf N-myc S53A low	see 187	CCCGGCTCGGGGCCAGAGGAGG AGTGGGCAGCAGC
189	zf N-myc MB II delete up	for deleting the MB II domain in <i>zf N-myc</i> together with Primer #190 using the quickchange kit (stratagene). melting temperature estimated to 81°C	CCATCATCATTCAGCGAGAGAA ACTGGAGCG
190	zf N-myc MBII delete low	see 189	CGCTCCAGTTTCTCTCGCTGAAT GATGATGG
358	Ecodhhup	for amplification of zebrafish <i>desert hedgehog</i> homolog by RT-PCR together with #359, clone as EcoRI/XhoI into pBS, Akimenko sequence	TTTGAATTCGGTACTTCTCTTTCT TCATCTGGACA
359	dhhloXhoI	see 358	TTTCTCGAGTTAGTGCTGATGT GTTTTGAGTTTA
360	EcoIhhup	to amplify zebrafish <i>indian hedgehog</i> homolog by RT-PCR together with #361, clone as EcoRI/XhoI into pBS, Akimenko sequence	GCGGAATTCAGAGCTCACGCCG AACTACAACCCG
361	IhhloXhoI	see 360	CTGCTCGAGCCGAAAGCCAGT GAGCCAGCCAGTG
372	MB I ST exchange up	to exchange of S53 and T49 to Alanine in <i>zf N-myc</i> using the quickchange kit (stratagene) together with primer nr 373. Melting temperature estimated to 92°C	GCTGCTGCCgCTCCTCCTCTGG CCCCGAGCCGGG
373	MB I ST exchange low	see 372	CCCGGCTCGGGGCCAGAGGAGG AGcGGGCAGCAGC
374	N-myc T49A low	to exchange of Thr 49 to Alanine in <i>zf N-myc</i> using the quickchange kit (stratagene) together with primer nr 375. Melting temperature estimated to 88°C	CCCGGCTCGGGGACAGAGGAGG AGCGGGCAGCAGC
375	N-myc T49A up	see 374	GCTGCTGCCgCTCCTCCTCTGG CCCCGAGCCGGG
403	EcoRI Kozac Nmyc 5'	to add Kozac sequence to <i>zf N-myc</i> and variants together with Primer 102 (186 for delta zip variant) or #3	GAATTCGCCGCCACCATGCCAGC TAAAACCATGAGCTCAGATC
472	EcoRI Kozac Nmyc5`nu	for adding Kozac sequence to <i>zf N-myc</i> and variants together with Primer #3	TGGAATTCGCCGCCACCATGCCA GCTAAAACCATGA
502	zf nrngn up	for amplification of the full length RNA of the annotated <i>zf</i> homologue of <i>neurogranin</i> together with primer 503	AGGTTTACGCTCTGTTGCTCTCA TA
503	zf nrngn up	see 502	GAGGAGCAAACCAAACAAACCA TTC
640	zf calb1 up	to amplify the homologue of calb1 in zebrafish	GGAGACGACATGGCAAACGCGT ACC
641	zf calb1 lo	see 640	GGATGTTACATCTCCTCTGCAC AC
659	EcoRI Koz olig up	for amplification of <i>olig2</i> ORF together with #660 using 1370 as template. cut produkt EcoRI/ XbaI.	GAGGAATTCGCCGCCACCATGG ACTCTGACACGAGCCGAGTGT
660	XbaI olig	for amplification of <i>olig2</i> ORF together	AAGTCTAGATTATTTGAGTCAC

	low	with #659 using 1370 as template. cut produkt EcoRI/ XbaI.	TGGTCAGCCGT
--	-----	--	-------------

Table 1: primers used in this study

2.1.9. Vectors

Stock #	Plasmid name	Purpose and notes	Cloning/ references
2	pBZfshh	ISH template	Ref.: (Hauptmann and Gerster, 1996)
7	pCSGFP	humanised GFP	HindIII (blunt)/XhoI fragment cloned into StuI/XhoI-digested pCS2
29	pBluescriptSK	n.d.	Supplied from Stratagene
100	pCSZath1	ISH probe	cDNA received from Masahiko Hibi
187	pBZfptc1	ISH probe	Ref.: (Concordet et al., 1996)
188	pBZfptc2	ISH probe	Ref.: (Concordet et al., 1996)
237	pDS5Zfvimentin	ISH probe	Ref.: (Cerda et al., 1998).
485	pB-zf-smoh	ISH probe	Ref.: (Varga et al., 2001)
584	pB-zN-myc	ISH probe	Ref.: (Schreiber-Agus et al., 1993)
714	Ptf1a	ISH probe	n. d.
751	P64T/Ehh	ISH probe	Ref.: (Currie and Ingham, 1996)
762	pCRII-zfGluRd2-mid	ISH probe	Ref.: (Mikami et al., 2004)
778	pCRII zfN-Myc3'	Intermediate	PCR using #99/#102, template: 32hpf RT-DNA. TOPOcloning
792	pBS zf-Ehh	ISH probe	Insert: #751EcoRI /Hind III; backbone: pCS#29
793	pCRII zf N-myc 5'	Intermediate	PCR using Primers#5 and #149, template: #584 . TOPO cloning
794	pBS zf N-myc 3'	Cloning of zfNmyc full-length cDNA	Insert: #778 SnaBI/XhoI; backbone: #29 Asp718- blunt- XhoI
807	pBS zf N-myc	zf N-myc, full length cDNA	insert: pCRII zf N-myc5' ClaI/MunI; backbone:zf N-myc 3' ClaI/MunI
985	pCS Nmyc	zf N-myc, full length cDNA	insert: #984 ClaI/ SnaBI ;backbone: #370 ClaI/ SnaBI
1044	pCR II Nmyc Δzip	dominant negative variant of zfNmyc lacking the bHLH	PCR: Primers #149 & #186, template: vector #983 (pCS Nmyc). TOPO cloning
1045	pCS Nmyc Δzip	dominant negative variant of zfNmyc lacking the bHLH	insert: #1044 ClaI/ SnaBI; backbone: #370 ClaI/SnaBI
1046	pCS Nmyc ΔMBII	dominant-negative variant of zfNmyc lacking MBII domain	MBII-domain was deleted using the Quiagene quickchange kit. Primers: #189 & #190, template: #985
1047	pCS Nmyc S53A	constitutive active form of Nmyc. Phosphorylation of Ser53 is required for protein turn over	Ser53 was exchanged to ala using the Quiagene quickchange kit. Primers: #1187 & #188, template: #985
1049	pCRII atoh 1.2	ISH probe	Ref.: (Adolf et al., 2004)
1050	pCS Nmyc-GI	Globin intron added 3' to WT-Nmyc	insert: #985 ClaI/ SnaBI; vector: #978 XbaI-> blunt-> ClaI
1051	pCS Nmyc ΔMBII-GI	Globin intron added 3' to Nmyc ΔMBII	insert: #1046 ClaI/ SnaBI; vector: #978 XbaI- blunt, ClaI
1053	pCS Nmyc S53A-GI	Globin intron added 3' to Nmyc S53A	insert: #1045 ClaI/ SnaBI; vector: #978 XbaI-> blunt-> ClaI
1083	pBSce-her3-KalTA4GIpA	zf her3-enhancer driving KalTA4-globin intron-pA expression	pBSce-KalTA4GI (#987): EcoRV, zip;pB-her3:Gal4 (#944): NotI, blunt, SmaI
1132	pBSK-VGLUT-1	ISH probe	Ref.: (Higashijima et al., 2004)

1142	pBS-VGLUT2.1A	ISH probe	Ref.: (Higashijima et al., 2004)
1146	pBS-VGLUT2.2B	ISH probe	Ref.: (Higashijima et al., 2004)
1159	pB-Glyt2-A	ISH probe	Ref.: (Higashijima et al., 2004)
1160	pBS-Glyt1	ISH probe	Ref.: (Higashijima et al., 2004)
1161	pBS-Glyt1	ISH probe	Ref.: (Higashijima et al., 2004)
1180	pBS-zf ihh Mini3	ISH probe	#29: EcoRI, XhoI; RT-PCR on 32hpf oligodt-cDNA; primers: #360/#361
1181	pBS-zf ihh Mini5	ISH probe	#29: EcoRI, XhoI; RT-PCR on 32hpf oligodt-cDNA; primers: #360/#361
1183	pBS-zf-dhh Mini10	ISH probe	#29: EcoRI, XhoI; RT-PCR on 32hpf oligodT- cDNA; primers: #358/#359
1241	pCS Nmyc T49A	constitutive active form of Nmyc. Phosphorylation of Thr49 is required for protein turn over	Exchange of T49 to Ala using the quickchange kit; template: vector# 985; primers: #374 & #375
1242	pCS Nmyc T49AS53A	constitutive active form of Nmyc. Phosphorylation of Ser53 and Thr49 is required for protein turn over	exchange of T49 and S53 to A using the quickchange kit; template: vector# 985; primers: #372 & #373
1248	pCS Nmyc T49A-GI	globin intron added 3' to Nmyc T49A	insert: #1241 ClaI/ SnaBI; vector: #978 XbaI-> blunt-> ClaI
1249	pCS Nmyc T49AS53A-GI	globin intron added 3' to Nmyc T49AS53A	insert: #1242 ClaI/ SnaBI; vector: #978 XbaI-> blunt-> ClaI
1374*	pCS Kozac Nmyc WT GI	zf <i>N-myc</i> WT GI containing Kozac sequence	PCR using primers #472 and #5; template: vector1051. Cut reaction product EcoRI/ NotI. backbone: #982 EcoRI/ NotI.
1375*	pCS Kozac Nmyc ΔMBII GI	<i>N-myc</i> Δzip-GI containing Kozac sequence	PCR using primers #472 and #5; template: vector1051. Cut reaction product EcoRI/ NotI. backbone: #982 EcoRI/ NotI.
1376*	pCS Nmyc Koz Δzip-GI	<i>N-myc</i> ΔMBII-GI containing Kozac sequence	PCR using primers #472 and #5; template: vector1052. Cut reaction product EcoRI/ NotI. backbone: #982 EcoRI/ NotI.
1377*	pCS Koz NmycT49AS53A GI	zf <i>N-myc</i> T49AS53A-GI containing Kozac	PCR using primers #472 and #5; template: vector1249. Cut reaction product EcoRI/ NotI. backbone: #982 EcoRI/ NotI.
1378*	pCS Koz Nmyc T49A GI	zf <i>N-myc</i> T49A-GI containing Kozac sequence	PCR on vector # 1248 using primers #472 and #5. Cut reaction product EcoRI/ NotI. backbone: #982 EcoRI/ NotI.
1379*	pCS Koz NmycS53A GI	zf <i>N-myc</i> S53A-GI containing Kozac sequence	PCR on vector # 1053 using primers #472 and #5. Cut reaction product EcoRI/ NotI. backbone: #982 EcoRI/ NotI.
1461	pMECar8	zebrafish carbonic anhydrase 8, ISH probe	received from ZIRC, zgc:110118, BC092740 (IRBOP991F0359D2)
1484	pSC-zf gabaRa6-0.4	ISH probe	PCR using primers #538/#539, 0.4kb fragment TOPO-cloned
1738	PCR II zf olig2	genomic region of zfolig2 containig a PstI- fragment suitable for generating ISH probes; no cDNA, ISH probe	PCR:#423 and #426; template:1370 , TOPO cloning
1739*	PCR II nrgn var.1	transcriptional variant II of zf	PCR: #502/#503, T= 56C; template:

		neurogranin	adult RT DNA; TOPO cloning
1740*	PCR II nrgn var. 2	transcriptional variant I of zf neurogranin	see 1739
1743*	PCR II zf calb1	zf Calb1, full length cDNA	PCR: # 640/# 641, T= 57°C, template: adult brain RT DNA, T=57C.
1744	pZL1 zfMBP	ISH template	Ref.:(Brösamle and Halpern, 2002)
1811	pCS calb1	zf Calb1, full length cDNA, transcription vector	insert: 1743 BamHI/ EcoRV; backbone: #1 HindIII-blunt/ BamHI

Table 2: vectors used in this study; the nucleotide sequences of clones labelled by an asterisk can be found in the appendix

2.1.10. Antisense oligo nucleotides (morpholinos)

morpholino name	tag	Purpose, Ref.	sequence
MO1-olig2	5 UTR of zf olig2	knock down of endogenous olig2 plus reporters, (Park et al., 2002)	CGTTCAGTGCCTCTCAGC TTCTCG
MO-olig2ORF	ORF of olig2 beyond start ATG	knock down of endogenous olig2 only	CACTCGGCTCGTGTCAGA GTCCATG

Table 3: morpholino oligonucleotides vectors used in this study

2.1.11. Buffers, media, solutions

Standard buffers were prepared according to Sambrook and Fritsch (Sambrook, 2001).

Embryo solutions and standard zebrafish protocols were derived from M. Westerfield (Westerfield, 2000) and Kimmel et al. (Kimmel et al., 1995).

Ampicillin- stock solution: 100mg/ml Ampicillin-sodium salt in water. The solution was sterilized by filtering (0.22µm, qualilab), aliquoted and stored at -20°C.

Kanamycin- stock solution: 30mg/ml Kanamycin A in water. The solution was sterilized by filtering (0.22µm), aliquoted and stored at -20°C.

Chloramphenicol: 12,5mg/ml in Ethanol, p.a.. The solution was aliquoted and stored at -20°C

LB-medium

Bacto-Trypton	10g
Yeast extract	5g
NaCl	10g
Water	add 1l

The pH value was set to 7.4. The solution was autoclaved and stored at 4°C. If necessary, Ampicillin, Kanamycin and Chloramphenicol, respectively, was/were

added for selection purposes to a final concentration of 100µg/ml, 30µg/ml and 12,5 µg/ml respectively.

LB-agar

Bacto-Trypton	10g
Yeast extract	5g
NaCl	10g
Agar	15g/l
Water	add 1l

The medium was autoclaved and stored at 4°C. For preparing agar plates, the agar was melted by boiling in a microwave oven and subsequent cooling to 60°C. Ampicillin (100µg/ml), Kanamycin (30µg/ml) or Chloramphenicol 12,5 µg/ml were added from 1000x stock solutions. The agar was casted into Petri dishes (10 cm).

1x PBS:

NaCl	137mM
KCl	2.7mM
Na ₂ HPO ₄	10mM
KH ₂ PO ₄	2mM
pH 7.4	

The pH value was set to 7,4 by titrating with 1M NaOH or 1M H₃PO₄, respectively. Afterwards, the solution was autoclaved.

PTW

0.1% Tween in PBS

16% PFA (w/v) in H₂O

PFA powder was dissolved in water by heating to approximately 60°C. To initiate depolymerization, a few drops of 1M NaOH were added. After cooling to room temperature, the pH was controlled to be in a range between 8-9 using pH test stripes. The solution was stored at 4°C.

20x SSC

Tris-Acetate	3M
--------------	----

NaCitrate 300mM

The pH value was set to 7,0 by titrating with 1M NaOH or 1M AcOH, respectively. Afterwards, the solution was autoclaved

Danieau-solution, 300%

NaCl (58mM)	60ml
KCl (0.7mM)	30ml
MgSO ₄ (0.4mM)	30ml
Ca(NO ₃) ₂ (0.6mM)	30ml
HEPES (5.0mM, pH 7.2)	30ml
H ₂ O	820ml

All additional buffers or used solutions are stated in the respective method description.

2.2. Methods

2.2.1. Molecular biology

2.2.1.1. Purification of nucleic acids

For purifying nucleic acids different reaction kits were used (Nucleotide removal, Qiagen; Gene clean, q-biogene). The purification procedure was carried out as described in the manufacturer's manual. DNA was eluted from the column with water, typically in a volume of 30 µl.

Alternatively, DNA was purified by precipitation in alcohol. For this purpose, half of the volume of the DNA solution, 5 M NH₄OAc and either three volumes of ethanol or two volumes of isopropanol were added. The reaction mix was cooled to -20oC for 20 min. The DNA was then precipitated in a centrifuge at 4°C, 13000rpm, for at least ten minutes. The supernatant was removed using a pipette and the precipitate was washed in 70% ethanol. After another five minutes of centrifugation the supernatant was removed again and the DNA was dried from ethanol residues and resolved in water.

RNA from in vitro transcription was purified using the Rneasy kit (Qiagen) according to the manufacturer's manual.

2.2.1.2. Amplification of DNA by PCR (polymerase chain reaction)

PCR is the standard method for amplifying DNA with known flanking sequences. Oligonucleotides with a length between 20-45bp, which were complementary to the 5'-end of the sense and antisense strand of the template were synthesized by the internal service of the Helmholtz Zentrum München, MWG (Ebersberg, Germany) and Sigma-Aldrich (München, Germany).

PCR-reaction batch:

Template –DNA (c= 10ng/μl)	0.5-5μl
10x Taq-buffer	5μl
MgCl ₂ , 25 mM	5μl
dNTP mix, 2mM	5-10μl
Oligonucleotide 1	2μl
Oligonucleotide 2	2μl
DNA-Polymerase, (c=5U/μl)	0,5-1μl
water	add. 50μl

The PCR reactions were run in PTC 100- PCR machines (MJ Research Inc.). First, the samples were heated to 94°C for 5min to separate the complementary DNA strands of the template. Then a defined number of cycles were run dependent on the template from which the fragments were amplified. In a routinely used PCR program cycles consisted of strand separation at 94°C for 30s, annealing of the primers for 15-60s (annealing temperature depends on the primers, ~5°C below melting temperature of the primers) and elongation of the primed DNA strands at 72°C for 30s to several minutes (dependent on the length of the fragments). A final elongation step at 72°C for 5-10min followed the cycles. At the end of the program samples were kept at 8°C. For cloning of amplified PCR fragments, the amplified DNA was separated from remaining oligonucleotides on an agarose gel. The respective DNA fragment was excised from the gel and isolated using the gel clean kit (Eppendorf). The fragment was ligated into the TOPO vector (Invitrogen) by TA-cloning or –if the respective restriction sites were designed to the oligonucleotides- by conventional cloning.

2.2.1.3. Restriction digest of DNA

For the purposes of cloning, creating DNA templates for in vitro transcription and for analysing plasmid DNA, DNA was digested using restriction endonucleases. Such enzymes recognize specific target sequences on the DNA strand to cut DNA double strands by catalysing the hydrolysis of phosphodiesterbonds.

The reaction mixes usually contained between 2 and 30 U of restriction endonuclease in a total volume of 20-40 μ l, depending on the amount of DNA to be cut. Solutions were buffered by adding the supplied reaction buffer in a 1:10 dilution prior to addition of the enzyme. For diagnostic digests, between 0,5 and 4 μ g DNA were used. In preparative digests, the amount of DNA ranged between 5 and 10 μ g. Subsequent purification of the DNA by precipitating or the use of a purification kit stopped the reaction (see 2.2.1.1). Alternatively, gel-loading dye was added (1/5 of the reaction volume) prior to separation of DNA fragments by electrophoresis (see 2.2.1.12).

2.2.1.4. Site-Directed Mutagenesis

To generate point mutations and to delete or insert single or multiple nucleotides, the QuikChange site-directed mutagenesis kit (Stratagene) was used as described in the manufacturer's handbook. The sequences of the primers used are specified in 2.1.8. Successful modification of plasmids was verified by sequencing.

2.2.1.5. Blunting 5'-ends of DNA

If needed, 5'-DNA overhangs were blunted after restriction digest using the Klenow fragment of the DNA polymerase (Fermentas). 10x buffer, dNTPs (final concentration: 200 μ M), enzyme (final amount: 2U) and purified DNA were mixed (total volume was usually 40 μ l). Typically, such batches contained approximately 5 to 10 μ g of DNA. The reaction mix was incubated at 37°C for 45 to 60 minutes. Subsequently the DNA was purified for further processing. The reaction was stopped by heating the reaction mix to 65°C for 5min.

2.2.1.6. Dephosphorylation of DNA

In order to avoid unwanted religation of a vector backbone, the 5'-terminal phosphate residues of a DNA fragment were removed. For this purpose, 1/10 of the volume of the reaction of dephosphorylation buffer and 2U of alkaline phosphatase were added to the DNA solution. The reaction mix was incubated for 20-30min at

37°C. The reaction was stopped by heating to 65°C for 5min. The DNA was either purified using the Nucleotide Removal kit (Qiagen) or by precipitation (2.2.1.1).

2.2.1.7. Ligation of DNA

In order to covalently bind linear DNA fragments with compatible ends, 1.5µl of ligase buffer and 7.5 U of T4-DNA-Ligase were added to a reaction mix of 12µl. The reaction batch was either incubated for 30 minutes at room temperature or over night at 16°C. Depending on the size, vector backbone DNA and insert were applied from equimolar ratios up to 5fold excess of insert DNA. The molar ratio of insert to vector backbone was estimated by agarose gel electrophoresis (2.2.1.12). The reaction was stopped by heating to 65°C for 5min. Between 5 and 15µl of such a reaction were then used for transformation of bacteria.

2.2.1.8. TA-Cloning, TOPO

In order to facilitate further cloning of PCR-products, DNA fragments were ligated into PCR®II-TOPO®-vector using the TOPO TA-Cloning Kit (Invitrogen) according to the manufacturer's instruction manual. The cloning strategy is based on the sequence-independent addition of an adenosine residue by the Taq DNA polymerase at the 3'-end of the synthesized DNA-strand. These residues allow covalent binding to a vector which carries a tyrosine overhang at the 5'-end. The integration of an insert into the PCR®II-TOPO®-vector leads to the disruption of the β-galactosidase gene flanking the vectors TA cloning site. Thus, blue-white selection was used to identify positive clones. Therefore, Amp plates were supplemented with the chromogenic dye X-Gal (40µl each plate, 40mg/ml in 70% DMF) and the inductor IPTG (also 40µl, 200mM). Bacteria carrying a plasmid without insert possess a functional β-galactosidase gene and appear blue due to the X-Gal reaction. In contrast, bacteria containing a plasmid with insert and disrupted β-galactosidase gene remain colourless.

2.2.1.9. Transformation of bacteria

Chemical transformation of bacteria

Positively charged Ca²⁺-ions bind to the negatively charged membranes of the bacteria and by this facilitate the uptake of negatively charged DNA upon heat shock. For this purpose the classical CaCl₂ method was used (Cohen et al., 1972).

Preparing CaCl₂ competent cells

250ml LB-medium were inoculated with 0,5ml of a stationary overnight culture of the respective E. coli strain and incubated at 37°C until the culture reached an OD600 of 0,5. The culture was then centrifuged at 5000rpm at 4°C for 10min (Sorvall evolution, GSA rotor). The sedimented cells were resuspended in 40ml of a 100mM MgCl₂-solution and incubated on ice for 30min. This suspension was again centrifuged as described above. The obtained cell pellet was resuspended in 20ml of a 50mM CaCl₂-solution and subsequently incubated on ice for 30min. After another round of centrifugation at 5000rpm and 4°C for 10min, the cells were resuspended in 2ml 50mM CaCl₂/ 15% (v/v) glycerol and aliquoted in batches of 200µl. After quickfreezing in liquid nitrogen, the bacteria were stored at -80 °C and subsequently used for transformation. All mentioned solutions were sterilized and precooled in ice water before application.

Heat shock induced transformation/ chemical transformation

To obtain transgenic bacteria, cloned DNA plasmids were transformed into CaCl₂-competent E. coli cells by heat shock induced chemical transformation. Competent cells were slowly thawed on ice or used immediately after preparing the competent cells. Between 5 and 15µl of a ligation reaction were added and the mixture was transferred into a 14ml single use culture tube (“snap cap”, BD falcon). The mixture was incubated on ice for approximately 20 min. The suspension was then heated to 42°C for 45’’ to enable the uptake of DNA into the bacteria. Subsequently the suspension was put on ice for 2 min. 500ml LB- medium were added and the cells were incubated at 37°C for 20 to 60 min on a shaker to allow expression of the antibiotic resistance encoded on the transformed plasmid. 100µl and 400µl of the culture were subsequently plated on LB-plates supplemented with the respective antibiotic. The plates were incubated at 37°C overnight up to 24h. Single colonies/clones from such plates were then used to inoculate 5ml cultures for DNA preparations.

Electroporation of bacteria

Sudden exposure of a bacterial suspension to a square pulse of electricity results in an inversion of the membrane potential of the cells causing an uptake of charged molecules such as DNA. Electroporation was used especially for transferring large DNA constructs such as BACs or to transfer targeting constructs for BAC recombineering into bacteria.

Preparing electro competent cells

0,5 ml of an overnight culture of bacteria were used to inoculate 250 ml LB medium free of any antibiotic. When the cell density reached an OD600 of 0,5, the culture was centrifuged at 4°C and 5000 rpm for 5 min (Sorvall evolution, GSA Rotor). The supernatant was discarded, the sediment was resuspended in 50 ml ice cold 10% sterile Glycerol (v/v) and the suspension was then transferred to a 50ml falcon tube. This suspension was again centrifuged for 5 min at 4°C and 4000rpm (Heraeus multifuge 3L-R). This washing step was repeated twice. The washed cells were resuspended in 1 ml 10% Glycerol (v/v). The suspension was divided in 50µl aliquots, which were either immediately used for electroporation or stored at -80°C.

When electrocompetent cells were needed for recombineering approaches, the procedure was the same unless that the volume of the initial bacterial culture was 25 ml and that the cells were resuspended after the last washing step in 50µl.

For homologous recombination, specific bacterial strains (EL 250) harbouring recombination-inducing enzymes under control of a heat shock promoter were used. Expression of these enzymes was induced before the washing procedure by incubating the bacteria at 42°C for 15 min (Warming et al., 2005).

Procedure

Electrocompetent cells were used directly after preparing the electrocompetent cells or thawed on ice. The cells were transferred into an electroporation cuvette (Molecular Bio Product, d= 1mm). 20 to 100 ng of linearised DNA were added and the mixture was incubated on ice for ten to 15 minutes. To introduce the DNA into bacterial cells, one square pulses was given (BioRad Gene pulser Xcell; Voltage: 1700V, capacitance: 25µF, resistance: 200 Ω, cuvette: 1mm). Subsequently 0,5 ml LB medium were added. The suspension was transferred to a single use culture tube ("snap cap", BD falcon) and incubated on a shaker for 20 to 60 minutes at 32°C and 200rpm to allow expression of the antibiotic resistance encoded on the transferred DNA. The cells were then separated from the medium by centrifugation at 13000 rpm (Eppendorf) for one minute and resuspended in 100µl LB medium. This suspension was plated on LB agar supplemented with the respective antibiotic. The plates were incubated at 32°C overnight up to 24h.

2.2.1.10. Preparation of DNA

Mini-preparation

In order to identify bacterial clones that carry a desired vector, plasmids or BAC DNA was isolated by preparing “mini-preps” and then further characterized by restriction digest or sequencing. For this purpose, a number of single cell colonies were cultured in small amounts of LB-medium (usually 5ml) supplemented with the antibiotic according to the resistance encoded on the desired plasmid. Such cultures were incubated overnight on a shaker (200rpm) at 37°C or –in case of BAC DNA at 32°C. The bacteria were separated from the medium by centrifugation of 2ml each of the culture in 2ml eppendorf reaction tubes at 13200rpm for 5min (Centrifuge 5415D, Eppendorf). If high amounts of DNA were needed, this cell harvesting step was repeated. The supernatant was discarded and the pellet resuspended in 200µl of cold buffer S1. Afterwards, 200µl S2 buffer were added to disrupt the bacterial cell wall, resulting in lysis of the cells and denaturing of proteins and DNA. Extrachromosomal elements usually are existent in a supercoiled conformation within the cell which leads to a delay of denaturing and hence keeps them in a solvent state. After incubation for 2-5min, 200µl of buffer S3 were added to neutralize buffer S2 and to coagulate protein. To separate protein aggregates and bacterial debris from the floating plasmid, the mixture was centrifuged for 8min at 13200rpm (Centrifuge 5415D, Eppendorf). The supernatant containing the plasmid DNA was transferred to a fresh 1,5 ml reaction tube. 400µl isopropanol were added and the mixture was centrifugated at 4°C and 13200rpm for 20min to precipitate the nucleic acids. The supernatant was discarded, the sedimented DNA was washed in 500µl of 70% EtOH and again sedimented by centrifuging at 4°C, 13200rpm for 10min. The supernatant was again discarded and the DNA dried to let residual Ethanol evaporate. The DNA was resuspended in 30-50µl water and now available for further analysis.

buffers:

S1

TrisHCl	50mM
EDTA	10mM
RNase A	100µg/ml
buffer storage at 4°C	

S2

NaOH	200mM
------	-------

SDS 1%
buffer storage at room temperature

S3

KOAc 2,8M
buffer storage at 4°C

Maxi-preparation

To obtain larger quantities of plasmid DNA, maxi preparation was performed using the Nucleobond Kit (Macherey & Nagel). An individual *E. coli* colony containing the desired plasmid was cultured in 200ml LB-medium supplemented with the respective antibiotic in a 1000ml Erlenmeyer flask on a shaker (200rpm) overnight at 37°C or 32°C in case of BACs. The bacteria were then sedimented by centrifugation at 5000rpm for 5min at 4°C (Sorvall Evolution, GSA-rotor). All further steps were carried out as described in the guidelines of the manufacturer. After preparing the DNA, the concentration was determined photometrically. Commonly, the concentration of plasmid DNA was adjusted to 1µg/µl.

2.2.1.11. Determination of nucleic acid concentration

The aromatic bases of the nucleic acids absorb UV radiation proportional to their concentration as described by Lambert-Beers' law. Hence, photometric measurements can be used to determine nucleic acid concentrations. This method also allows to distinguish between DNA, RNA or double and single stranded DNA as primers. The maximum absorbance occurs at 260nm. At 260nm, an extinction coefficient of 1 corresponds to a concentration of 50µg/µl of double stranded DNA or 40µg/µl of RNA. As the absorption maximum of aromatic amino acids occurs around 280nm, it is possible to determine the grade of protein contamination of a DNA sample by measuring the extinction at 260nm and that at 280nm. A sufficient purity of DNA or RNA is given by the ratio of $(\text{extinction}_{260}/\text{extinction}_{280})(\epsilon_{260}/\epsilon_{280})$ which should be above 1,8.

2.2.1.12. Separation of nucleic acids using agarose gel electrophoresis

Nucleic acid fragments can be separated by electrophoresis according to their molecular mass. As nucleic acids carry a negative charge (due to their phosphate

backbone) they will migrate to the anode, if a steady electrical field is applied. Larger fragments will migrate more slowly than smaller fragments as they are held back in the jelled agarose. According to the presumed length of the DNA fragments gels between 0,6 and 1,5% (w/v) agarose in 1x TAE buffer were used. For this, agarose was dissolved in 1x TAE-buffer by heating in a microwave oven and casting into a gel chamber fitted with a removable comb to obtain slots for the DNA samples after the jelling of agarose. The gel was put into an electrophoresis chamber and covered with 1x TAE buffer.

1/5 of DNA loading buffer was added to a DNA sample which was subsequently loaded into the slots. Subsequently a voltage of 80-120 V was applied to separate DNA fragments according to their size (power supply: Thermo eltron). Afterwards the gel was immersed in an EtBr/1xTAE solution (200µg/ml EtBr in 1x TAE- Puffer) and incubated for 15min. EtBr intercalates into DNA-strands resulting in enhanced fluorescence, which is used to visualize DNA under short wavelength UV of 320nm. A standard of DNA fragments of known sizes was used to determine the molecular mass of the DNA fragments that were to be analysed.

RNA agarose gelelectrophoresis

To avoid RNase activity, gel chamber and combs were washed with MilliQ water in advance and the gel was pre-run for 10 min at 80V before applying the samples to the slots. RNA-samples of 2µl were mixed with 8µl 5xRNA-loading buffer (Ambion. RNA was melted for 10 min at 95°C to break up secondary structures of the mRNA before applying it to the gel slots.

10x TAE-buffer:

Tris-Acetate	400mM
EDTA	10mM

gel-loading buffer:

Glycerol	30% (v/v)
EDTA	0.25% (v/v)
Xylenecyanol FF or bromphenolblue	0.25% (w/v)

2.2.1.13. cDNA synthesis by reverse transcription

Isolation of total RNA from whole embryos

RNA from embryos, complete adult brains and the cerebella of adult animals was isolated using the RNeasy kit (Qiagen) in combination with QIAshredder columns (Qiagen) according to the manufacturers' instructions for isolating total RNA from animal tissue. Chromosomal DNA was eliminated by DNaseI digest (50µl nucleic acid extract, 6µl 10x transcriptionbuffer (Roche), 2µl RNAsin (Promega), 2µl DNaseI (Roche, 10U/µl), incubation for 30 min at 37°C). Afterwards, the RNA was purified using the RNeasy kit (Qiagen). Quality and quantity of the RNA was controlled by agarose gel electrophoresis and photometry. Integrity of the two major rRNA-bands indicated that RNA degradation did not occur.

Reverse transcription of mRNA

To create a DNA/ RNA hybrid template as it is needed for the reverse transcriptase reaction, 11 µl of the purified total RNA and 1µl of random hexamer primers were mixed and incubated at 65°C for 5 min. After quick chilling on ice, the contents of the tube were collected by brief centrifugation. To this solution the following reaction mix was added:

5x Superscript II Buffer (First Strand)	10µl
RNAsin	1µl
2mM dNTP's	5µl
0,1mM DTT	5µl
RNase free water	18 µl

The mix was incubated at 25°C for 5 min. Then, 1 µl SuperScriptII (invitrogen, 200U/µl) were added. RT reaction was carried out at 42°C for 60 min. To inactivate the reaction, it was heated to 70°C for 10 min. The reaction was diluted with water to 100µl and stored at -20°C. In a PCR setup, 2 to 5µl commonly were used as template.

2.2.1.14. DNA sequencing

DNA sequencing was carried out by the following companies:

Sequiserve
Bahnhofstr. 30
85560 Vaterstetten
Germany

MWG
Anzinger Str. 7a
85560 Ebersberg
Germany

2.2.1.15. Analysis of DNA sequences

To analyse DNA sequences the DNASTar software package was used (Lasergene, GATC Biotech, Konstanz, Germany). For primer design, Oligo4 software was used.

2.2.1.16. *in vitro* synthesis of RNA

Capped mRNA

For the synthesis of capped mRNA for subsequent embryomicroinjection, 10µg of an expression vector containing the gene of interest were linearized (see 2.2.1.3). Expression vectors usually were derivatives of pCS2 + (Rupp et al., 1994), which carries a promoter of the phage RNA polymerase Sp6 upstream of the insertion site of the respective cDNA. The restriction endonuclease used for template digestion was usually NotI (Fermetas). The template was purified using the Nucleotide Removal Kit (QiaQuick, the elution volume was 50µl). To control the integrity of the template DNA, an aliquot of 2µl was analysed on an agarose gel. For in-vitro transcription, the mMessage mMachine SP6 Kit (Ambion) was utilised according to the manufacturer's specifications. A routine reaction mix was composed of the following volumes:

linearized template-DNA	6µl
2x NTP/CAP	10µl
10x SP6-polymerase reaction buffer	2µl
Enzyme mix (SP6)	2µl

The reaction mix was incubated at 37°C for 2 h. Afterwards, 1µl DNaseI (Roche) was added to remove the DNA template and incubated for further 20 minutes at 37°C. The reaction was stopped by immediately purifying the mRNA (RNeasy Mini Kit, Qiagen, procedure according to the specifications of the manufacturer). The RNA was eluted in 50 µl water. For further purification and concentrating, the RNA was precipitated by adding 5µl 3M NaOAc, pH 5,0, and 150µl EtOH. The mixture was then incubated for 20min at -20°C. To precipitate the mRNA, the sample was

centrifuged at maximum speed (Centrifuge 5415D, Eppendorf, 13200rpm) for 20min. The supernatant was discarded and the RNA was washed in 70% EtOH. After centrifuging (15min at 4°C, Centrifuge 5415D, Eppendorf, 13200rpm), the RNA was dried and resuspended in 20µl water. The integrity of the synthesized mRNA was controlled by gel electrophoresis. The concentration of the obtained mRNA solution was determined by measuring the extinction at 260nm. The mRNA was stored at -20°C for several months.

Antisense probe for ISH

10µg of a plasmid carrying the partial or full length cDNA of the gene of interest were linearized 5' to the coding region by restriction digest (2.2.1.3). Afterwards, the DNA was purified using the Qiaquick Nucleotide Removal Kit (Qiagen) and eluted in 50µl water. To confirm the complete linearization of the DNA, an aliquot was analysed by agarose gel electrophoresis (2.2.1.12). The components for subsequent in-vitro transcription were used as follows:

linearized template –DNA (200ng/µl)	10µl
10x transcription buffer	2µl
10x RNA labeling mix (Roche)	2µl
RNasin (promega, 40U/µl)	1µl
Water	3µl
respective RNA-Polymerase (20U/µl)	2µl

The reaction was incubated at 37°C for 2h. Subsequently, the DNA template was digested by DNase1 (Roche, 1U/µl) for 20min at 37°C. The RNA was then purified using the RNeasy Mini Kit (Quiagen) according to the instructions of the manufacturer. The integrity of the RNA was controlled by gel electrophoresis.

Immunological analysis of insertion of digoxigenin label into RNA riboprobes, “dot blot”

Digoxigenin or fluoresceine labelled RNA bound to a nylon membrane can be detected immunologically. Antibodies against digoxigenin and fluoresceine used in this work were conjugated to alkaline phosphatase, which catalyzes a reaction leading to the formation of a blue precipitate insoluble in water. 1µl of the antisense RNA probe and 1 µl of a 10-, 50-, 100- and 500-fold dilution of the RNA probe were

applied to a nylon membrane (Amersham). After drying, the membrane was washed in 15ml buffer PI. Unspecific binding sites for anti-digoxigenin antibodies were blocked by washing in buffer PII while gently shaking for 30min. Subsequently, the membrane was incubated for 30min in a 1:2000 dilution of α -digoxigenin- or α -fluoresceine antibody (Roche) in 15ml buffer PII. Excessive non bound antibody was removed by washing the membrane with buffer PI twice for 15min. To activate the alkaline phosphatase, the membran was incubated with alkaline buffer PIII for 2min. Subsequently, the membrane was covered in freshly made staining solution containing 4,5 μ l/ml NBT and 3,5 μ l/ml BCIP in buffer PIII. The reaction rate was used to estimate the amount of incorporated digoxigenin/fluoresceine and thus the quality of the probe. As a rule of thumb, appearance of the blue reaction product within 60s on the 500 fold diluted sample was taken as an indication for efficient incorporation of the label. The reaction was stopped after 2min by washing in buffer PIII.

buffer PI

TrisHCl, pH7.5	100mM
NaCl	150mM

buffer PII

0.1% TritonX-100 and 10% NGS in 1x PBS

buffer PIII

TrisHCl, pH9,5	100mM
NaCl	100mM
MgCl ₂	50mM

2.2.2. Manipulation of zebrafish embryos

2.2.2.1. Cytoplasmic injection of nucleic acids

In order to manipulate embryos by injecting nucleic acids, zebrafish eggs were lined up in petri dishes filled with agarose (1.5% agarose/ 30% Danieau's solution) in which a mold was embedded to obtain grooves. Plasmid DNA was additionally purified using the GENE CLEAN ® Turbo Kit (QBIogene) according to the specifications of the manufacturer. Capped mRNA and DNA were diluted in water to

the desired final concentration (typically 50-250 ng/μl for RNA and 30-50 ng/μl for DNA). Phenol red was added to the solution to facilitate the injection (1/10 of a 0,5% stock solution, Sigma). The mix was injected into the cytoplasm of the zygote using a micromanipulator (Eppendorf) supported by the use of a binocular (Zeiss). After injection, the embryos were removed from the grooves and transferred into a conventional petri dish. The embryos were incubated at 28°C until they reached the desired developmental stage for further investigations.

2.2.2.2. Cytoplasmic injection of morpholinos

The injection of morpholino antisense oligonucleotides was performed in analogy to the injection of RNA and DNA. The nucleotides were diluted from a 2mM stock to the desired concentration and phenol red was added to a final amount of 0,05% (sigma). The injection mix was heated to 65 °C for 5 min prior to use in a thermomixer (Eppendorf, thermomixer comfort).

2.2.2.3. Single cell transplantation

For experimental questions of cell-autonomy, single cell tracing and observations, cell transplantations were performed. For this purpose, donor embryos were injected with rhodamine dextran at the single-cell stage for tracing purposes (Tetramethylrhodamine, 6% , 3000 MW, Invitrogen GmbH, Karlsruhe, Germany). Donor and acceptor embryos were subsequently incubated at 28°C. When having reached the 1024 cell stage, the embryos were dechorionated by pronase digest. For this purpose, the embryos were transferred to petri dishes coated with agarose (1,5 % w/v in 30% danieau) to avoid sticking of the embryos on the plastic material. The pronase solution was added (0.05 g/ml in 30% danieau, Roche) and the embryos were incubated at RT for about 20 to 30 min. When pivoting, the embryos fell out of their chorion and were now applicable for transplantation. To stop the pronase-digest, the embryos were washed shortly for three times in 30% Danieau. Note that again petri dishes coated with agarose were used. Subsequently donor and acceptor embryos were embedded in alternating rows of an agar mould designed for micromanipulation purposes and covered with 30% Danieau. About 10 cells of the donor embryos were removed using a micromanipulator (Narishige) by drawing them off into a chamfered glass capillary. The cells then were injected carefully into the tissue of the acceptor embryo. Afterwards, embryos were kept at 28°C in 30% Danieau supplemented with

penicillin/ streptomycin (Gibco, 1/50 dilution) until they reached the desired developmental stage.

2.2.2.4. *In vivo* retrograde labeling of neurons in the zebrafish larva

Retrograde labeling was carried out as described (Volkman and Köster, 2007; Volkman et al., 2008), with the exception that DiI (Invitrogen, 1mg/ml in DMSO) was used instead of Rhodamin. The dye was applied to ventral mesencephalic regions by laterally injecting between the eye and tectum.

2.2.2.5. Cyclopamine treatment

Cyclopamine (Biomol) is an alkaloid that interferes with the Smoothed receptor, impairing the signal transduction of the Hedgehog cascade (Frank-Kamenetsky et al., 2002; King, 2002). Embryos were dechorionated prior to cyclopamine treatment as described. At the respective developmental stage, cyclopamine was added from a 100x stock (10 μ mol/ml in DMSO) to the embryo rearing medium, resulting in a final concentration of 100 nmol/ml. Note that if the embryos were younger than 24 h, petri dishes covered with agarose were used in all steps. As a control, the same volume of the DMSO was added in parallel.

2.2.3. Histological techniques

2.2.3.1. Sectioning of embryos, larvae and adult brains

Vibratome

For vibratome sections fixed embryos were incubated for several hours in gelatine-albumin solution. The medium and the embryos were transferred into plastic molds. An amount of 5 ml of the solution was rapidly mixed with 550 μ l of a mixture of 10 parts 4% PFA and 1 part of a 25% m/v glutaraldehyde solution (Sigma). The embryos were orientated quickly due to the short time of polymerisation of the solution. To obtain complete hardening of the gelatine, preparations were then incubated at 37°C for 1h. The gelatine block was trimmed using a scalpel and sectioned on a vibratome into slices of 25-100 μ m thickness (Microm, HM 650V). The slices were transferred to microscope slides (Superfrost®Plus, Menzel GmbH) and kept at RT for drying. The slides were then sealed using Aquamount (Polysciences).

gelatine-albumin solution

gelatine, pork	45g
albumin, fraction V	270g
sucrose	180g
10xPBS	100ml
aqua dest	ad 1l

heat to 42°C for dissolving the gelatine prior to use, store at –20°C.

Cryostat

For cryostat sections, embryos were washed in PBS for several hours after fixation and transferred into 20% sucrose in PBS. When using embryos stored in methanol, they were first rehydrated in a reverse methanol series (96-, 75-, 50-, and 25% MeOH in PTW) and washed two times in PTW. After incubation for at least over night at 4°C, the embryos were transferred onto the object holder of the cryostat covered with a drop of TissueTek® OCT medium (Sakura). The embryos were oriented in the desired position using a binocular. The object holder was put on dry ice to cause hardening of the embedding medium. Subsequently the specimens were cut into consecutive sections of 10 to 40 µm thickness using a cryostat (microm, HM560). The slices were transferred to prewarmed microscope slides (Superfrost®Plus, Menzel GmbH), placed on a heating plate (37°C) for several minutes to dry and precooled again for the next section. Slides were stored at -20°C.

Microtome

For paraffin sections, fixed embryos, larvae and adult brains were dehydrated in a graded ethanol series (70%, 96% and 100%) and cleared in xylene. Times for each dehydration step varied with embryonic stages. Incubation times in xylene may vary and had to be checked for transparency of the embryos. After clearing, the embryos were transferred into liquid paraffin (65°C), incubated over night at 65°C and then embedded in fresh paraffin using embedding moulds. Paraffin embedded embryos and adult brains were cut on a microtome in sections of 3 to 8µm thickness. The sections were transferred to a water bath (37°C), mounted on microscope slides (Superfrost®Plus, Menzel GmbH) and placed on a heating plate (Leica) at 37-40°C to dry. Slides were incubated over night at 37°C and stored at 4°C.

2.2.3.2. Whole-mount in-situ-hybridisation (ISH)

Antisense riboprobes can be labeled due to a chemical modification of one of the monomeric nucleotides, e.g. a digoxigenin or fluoresceine residue covalently bound to UTP. Such antisense RNAs can be detected in-situ using an antibody against the label. The antibody's Fab- fragment is fused to alkaline phosphatase (AP). Using different labels in combination with different substrates for the AP enables one to simultaneously detect several gene transcripts in different colours in one specimen. In situ hybridization permits localization of mRNA transcripts in an organism up to cellular resolution. The mRNA is detected by the formation of a hybrid-nucleotide strand consisting of the endogenous RNA strand and of a labelled antisense riboprobe. Visualization is accomplished by a chromogenic reaction carried out by the AP.

Fixation and storage of fish embryos

Zebrafish embryos were fixed over night in 4% PFA at 4°C on a shaker. Afterwards the embryos were washed in PTW and dechorionated by using forceps or pronase digest. Subsequently they were dehydrated by washing in increasing amounts of methanol. For this purpose the embryos were incubated on a shaker for 5 min each in 25%, 50%, 75% and 96% MeOH/PTW (v/v) and two more times in 100% MeOH. The embryos were then stored at -20°C. Prior to ISH they were rehydrated in a reverse washing series of MeOH/PTW.

Proteinase K-digest of embryos

To obtain better permeability of the tissue for RNA probes and antibodies, fixed embryos were treated with the proteolytic enzyme proteinase K (Roche). After rehydration and two times washing in PTW, the embryos were incubated in proteinase K/ PTW (10µg/ml) for the respective time span (listed below). The digest was stopped by washing in 2mg/ml Glycin/PTW and subsequent fixing in 4% PFA for 20min. To remove excessive PFA, embryos were washed 5 times in PTW for 5min each. Embryos are sensitive after proteinase K digest and were thus treated with care.

<u>developmental stage:</u>	<u>time of proteinase K digest:</u>
24hpf	12min
36hpf	20min
48hpf	30min

3dpf	25min
4dpf	45min

Hybridisation

After proteinase K treatment the embryos were transferred to 2ml eppendorf tubes and prehybridized in 2ml of hybridisation buffer for 1h in a waterbath preheated to 60°C. Afterwards the buffer was exchanged for the hybridisation probe. To prepare the hybridisation probe, 4µl of the labeled antisense RNA were solved in 196µl hybridisation buffer. The mixture was then incubated at 95°C for 5min before replacing the prehybridization mix. The embryos were hybridised overnight at 60°C. The following day the embryos were washed in 2ml of the following solutions each for 45min at 60°C: 2x 50% Formamide/2x SSCT, 1x 2x SSCT and 2x 0,2x SSCT.

20x SSC

Tris-Acetate	3M
NaCitrate	300mM

The pH value was set to 7,0 by titrating with 1M NaOH or 1M AcOH, respectively. Afterwards, the solution was autoclaved.

Hybridisation buffer

Formamide (100%)	25ml
20x SSC	12,5ml
Heparine (50mg/ml)	150µl
Torula-RNA	250mg
Tween®20	50µl
add H ₂ O to 50ml	

The solution was stored at -20°C.

Immunological detection of the hybridisation probe

After the last wash in 0,2x SSCT, unspecific binding sites for anti digoxigenin Fab-fragment were blocked by incubating the embryos in 10% NGS in PTW for 1h on a rotator at room temperature. The embryos were then incubated over night at 4°C in a 1:2000 solution of the respective antibody (Roche) in 10% NGS in PTW while rotating. The following day, the embryos were transferred to a six-well plate and

rinsed with 5ml of PTW six times for 15min each at room temperature on a shaker to remove excess unbound antibody. The embryos were then equilibrated in alkaline staining solution NTMT two times for 5min each. Afterwards the embryos were incubated in freshly prepared staining solution for up to 24h at RT until the staining revealed the desired intensity. Due to light sensitivity of the dye the reaction was carried out in the dark and monitored every 30min. To stop the chromogenic reaction the embryos were rinsed 2 times for 5min in PTW. For long term storage, the embryos were transferred into 90% glycerol (v/v). Alternatively the specimens were further processed for performing double ISH or IHC or prepared for microscopic investigations.

Solution for alkaline phosphatase staining using BCIP/NBT (NTMT)

NaCl	150mM
TrisHCl (pH 9.5)	100mM
MgCl ₂	50mM
Tween®20	0,1%
BCIP, 50 mg/ml in DMF	3,75µl/ml
NBT, 100 mg/ml in 70% DMF	5µl/ml

The solution was prepared freshly from the respective stock solutions on the day of use. BCIP and NBT were added prior to use.

2.2.3.3. Double in-situ-hybridisation

To simultaneously detect two transcripts in the same embryo, two different antisense probes labelled with digoxigenin and fluoresceine respectively were hybridised at the same time. Detection was performed in two consecutive rounds. The two colours used for double staining were Fast red (fast red tablets, Roche) and BCIP/NBT. The more abundant mRNA was usually depicted with the fluoresceine-labelled probe during the first round using fast red as the substrate for the AP-staining. With respect to some modifications, the procedure was carried out as described for ISH. Instead of only one antisense probe, two probes were added to the hybridisation mix. Washing after hybridisation was carried out as described for conventional ISH. After blocking, the preparations were first incubated with the anti-fluoresceine antibody diluted 1/2000 in 10% NGS in PTW. The embryos were washed 6 times as described and then equilibrated in fast red staining solution by

shortly washing two times. The embryos were incubated in freshly made fast red staining solution for up to 48h at RT until the staining revealed the desired intensity. The reaction was stopped by washing three times in PTW for 5 min each. Subsequently the anti –fluoresceine antibody was stripped by incubating the specimens twice in 100mM Glycine, pH2,2, for 10 min each at RT under rigorous shaking. After equilibrating in PTW, the anti- digoxigenin antibody in 10% NGS in PTW was added to the embryos and incubated over night at 4°C. The further procedure for BCIP/ NBT staining was performed as described for ISH.

Solution for alkaline phosphatase staining using fast red (used in double in-situs)

Tris/ HCl (pH 8,2)	100mM
Tween®20	0,1%
Fast red (Roche)	1 tab/2ml
Sterile filter prior to use	

2.2.3.4. Immuno-histo-chemistry

Standard IHC on whole mount embryos, larval brains and cryosections

To obtain a better penetration of the antibody into the tissue, fixed embryos were treated with acetone if not contradicted by special properties of the antigen or of the antibody. For this purpose, the specimens were transferred directly from the methanol in which they were stored into –20°C- cold acetone. The embryos were then incubated in the solvent at –20°C for 7 min. To disrupt cells, the embryos were briefly rinsed in water and incubated in deionised water for 1h. Subsequently the specimens were equilibrated in PTW by washing for 5 min or alternatively subjected to antigen unmasking. For this purpose, the embryos or slices were transferred into preheated sodium citrate (10mM, pH6,0) or 50mM Tris/HCl, pH8,2, with 0,1%Tween and incubated at 95°C in a 2ml reaction tube or a slice holder respectively for 10 to 30 min. After cooling to RT, the preparations were washed in PTW twice. Unspecific binding of antibodies was prevented by blocking in 10% NGS in PTW for 1h. The embryos were subsequently incubated with the primary antibody or antibodies diluted in blocking reagent (for dilution factors see antibodies, 2.1.5.). Incubation was usually performed overnight at 4°C. The next day, the embryos were washed for at least 4 times in PTW for 15 to 60 min each. Subsequently the samples were incubated with

the secondary antibody diluted in blocking reagent. Incubation conditions were the same as for the primary antibodies.

For peroxidase mediated staining, secondary antibodies conjugated to peroxidase were used. The following day the embryos were washed 4 times for 15 to 60 min in PTW. Afterwards, the specimens were incubated for 5min in 0.1M Tris-HCl, pH 7.4. For the staining reaction, the medium was exchanged to 5ml DAB staining reagent. After a delay of 30 min to allow DAB to penetrate the tissue the reaction was started by addition of 20µl of 0,3% H₂O₂ (Sigma). The specimens were then stained for 1-15 min until the desired intensity was reached. The chromogenic reaction was stopped by washing twice in PTW.

For immunofluorescence, samples were incubated with secondary antibodies conjugated to fluorophores such as Cy3, Cy5 or FITC. After incubation, the embryos were washed as described.

Blocking reagent

NGS (Sigma)	10% v/v
Triton X100	0,3% v/v
DMSO	1% v/v
in 1x PTW	

DAB reagent

DAB, 10mg tablets, Sigma	0,05 mM
Tris-HCl, pH 7.4	0,1 M
Tween	0,1%
add 0.02% H ₂ O ₂ from a 30% stock to start the reaction	

Standard immunohistochemistry on microtome sections

First, paraffin was removed from the tissue sections by washing twice in Xylol for 20 min each. The sections were then re-hydrated by washing in decreasing concentrations of alcohol (100% Isopropanol- 100% EtOH- 90% EtOH- 70% EtOH). After washing twice in TBS for 5 min, the slides were incubated in a microwave oven in 10mM NaCitrate, pH 6,0 , for 40 min at 350W. The sections were then washed in TBS at RT for 15 min prior to blocking in 5% NGS in Dako Antibody Diluent for 1h. The slides were then incubated with the primary antibody in a wet chamber at RT for

1h. For this purpose, slides were covered with hybrid slip hybridisation covers (Invitrogen). Subsequently the slides were washed twice in TBS. Immunoreactivity was detected using the DAKO ChemMate K5005 Kit according to the specifications of the manufacturer. The slides were sealed with a coverslip using aquamount mounting medium (Polyscience).

2.2.3.5. Morphological stainings

In order to depict cell membranes and white matter fluorescent vital staining was performed by soaking specimens in green-fluorescent Bodipy FL C5-ceramide (D-3521, Invitrogen) or red-fluorescent Bodipy 630/650-X (D-10000, Invitrogen), respectively, at 28°C for at least 6h. Before image acquisition, the stained embryos were rinsed twice in 30%Danieau. For nuclear counterstaining, DAPI was used at 0.1µg/ml (Sigma). Alternatively, ToPro3 was used as nuclear label (Invitrogen). Here, 1:500 of the 1mM stock were added. In case of IHC stainings the dyes usually were added together with secondary antibodies.

2.2.4. Microscopic Analysis

The techniques and methods for vital imaging, time lapse recording, microscopy of whole mount preparations and of slide preparations have been described in detail (Distel et al., 2006; Distel and Köster, 2007; Köster and Fraser, 2001; Köster and Fraser, 2004). Digital images were processed for brightness, contrast and size using Adobe Photoshop 7.0D (Adobe) and the NIH open source software ImageJ1.34s. Z-stacks from time-lapse recordings were projected to single images for each time point using the LSM510 software version 4.0. Image projections were assembled into movies using QuickTime Player 7.2. Migrating cells were tracked using the NIH ImageJ software (1.34 S; <http://rsb.info.nih.gov/ij/>) together with the Manual Tracking plug-in. For quantifying cell numbers, confocal stacks were subdivided into slices with a minimum net distance of 6µm to avoid double counts. Cell numbers of the respective single- or doublepositive types of one half cerebellum each were summed and the ratio double positives/ single positives was calculated. Average numbers of such ratios were statistically analysed.

3. Results

3.1. Characterisation of Eurydendroid Cells– the zebrafish´s equivalent of the deep cerebellar nuclei neurons

3.1.1. Expression of *olig2* in the developing cerebellum

During development, the patterning of the neural tube along its dorso-ventral axis by morphogens results in the subdivision of the neuroepithelium into specific germinal zones. On the molecular level, these germinal zones are defined by the expression of specific transcription factors, and are known to give rise to distinct cell populations. The bHLH factor *olig2* has been reported to be one of such prominent factors during neurogenesis expressed in the ventral spinal chord and in the ventral telencephalon. First assumed to be a factor specifying oligodendrocytes (Lu et al., 2000; Zhou et al., 2000), *olig2* proved to be a more global regulator of neurogenesis by preventing the establishment of an alternative fate (Lu et al., 2002; Park et al., 2002; Takebayashi et al., 2002; Zhou and Anderson, 2002). Previous reports also addressed a role for *olig2* in the cerebellum (Park et al., 2002; Takebayashi et al., 2002).

In terms of further investigating the possible function of *olig2* during development of the zebrafish cerebellum, we wanted to know in which cell types and at what time *olig2* is expressed in order to get an idea of how it may function in the cerebellum. As shown in Fig. 3, *olig2* mRNA is expressed in the cerebellum from 36 hpf onwards. First only expressed in ventro-lateral regions of the cerebellar anlage (arrows in Fig. 3 A), the expression domain then broadens to form a sickle-shaped structure in both cerebellar halves (Fig. 3 C, C').

To study the cellular dynamics of cerebellum development laser scanning time lapse microscopy was used. For this purpose, two transgenic lines were used: *olig2*:GFP and *olig2*:dsRED. In both lines the expression of the fluorescent protein reporter is driven under control of *olig2* regulatory elements (Shin et al., 2003). In order to verify the reliability of the reporter lines, expression of the *gfp* mRNA was compared with that of the endogenous *olig2* mRNA by performing double in situ hybridisation (DISH). Since it is known that fluorescent proteins are rather stable while maturation and processing of the fluorophore in the centre of the protein can take up to several hours (Corish and Tyler-Smith, 1999; Verkhusha et al., 2001;

Verkhusha et al., 2003), GFP protein in addition was visualised by IHC to estimate the time span between transcription of the mRNA and detectable fluorescence of the mature protein. At 60 hpf and at 4 dpf (not shown), an obvious complete overlap of endogenous *olig2* mRNA and *gfp* mRNA could be ascertained (Fig. 3 C, C'). When

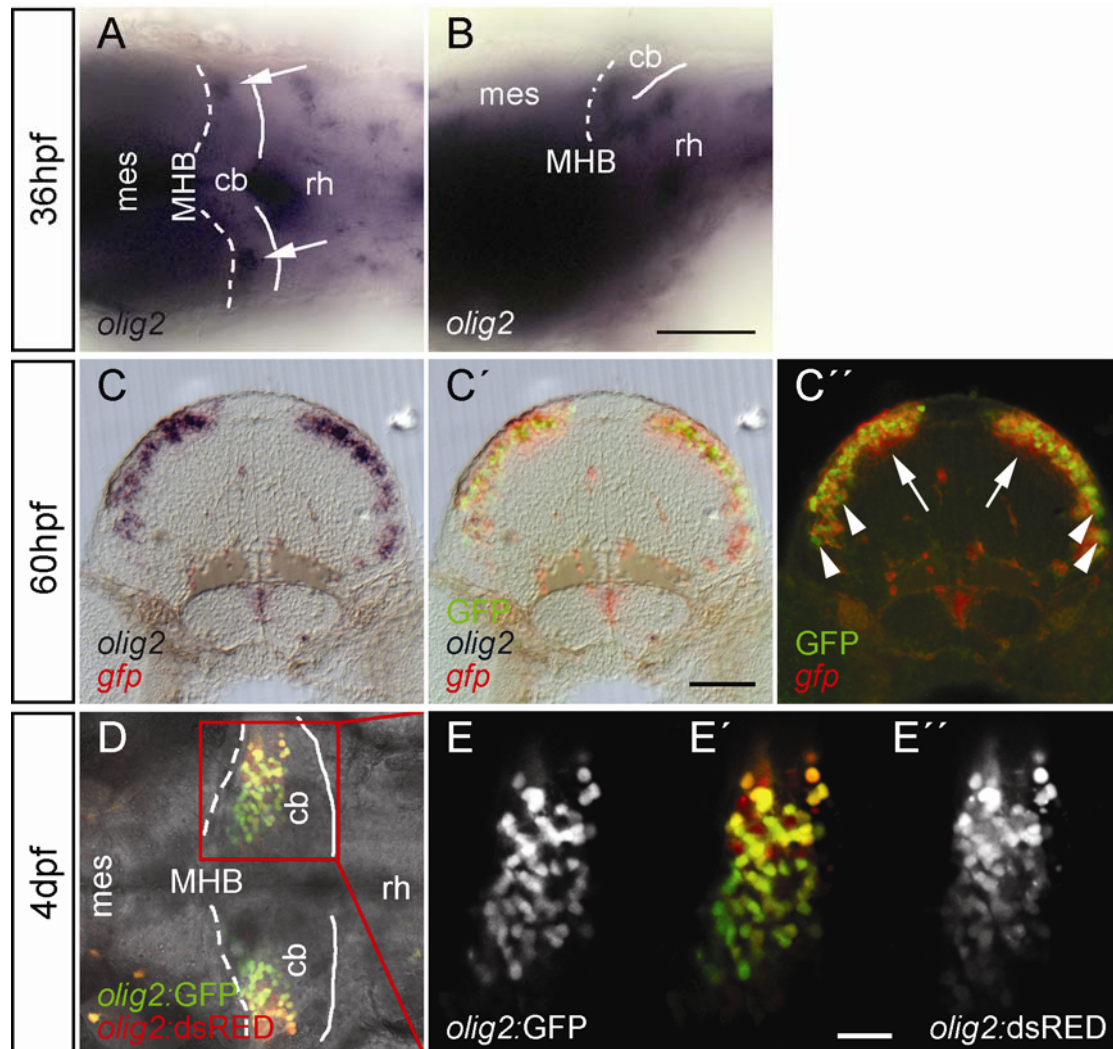


Fig. 3: Expression of *olig2* during cerebellar development in WT and transgenic embryos. (A, B): ISH on whole mount embryos showing the onset of *olig2* expression at 36 hpf from dorsal (A) and from lateral (B) views. Scale bar: 50 μ m; 40 fold magnification. (C-C''): DISH combined with IHC depicting endogenous *olig2* mRNA, *gfp* mRNA and GFP protein in a 60 hpf Tg [*olig2*:GFP] embryo, sagittal vibratome section, 25 μ m thick. Magnification: 40 fold. (D-E''): Confocal section through a double transgenic 4 dpf embryo. (E-E''): zoom into the area labelled by the red frame in D. Magnification: 20 fold. Scale bar in E'': 20 μ m. mes: mesencephalon; cb: cerebellum; rh: rhombencephalon; MHB: mid-hindbrain boundary. cb: cerebellum; mes: mesencephalon; rh: rhombencephalon; MHB: midbrain-hindbrain boundary

comparing *gfp* RNA and GFP protein, a small number of cells revealed a lack of GFP IHC signal though staining positive for *gfp* RNA (arrows in Fig. 3 C''). This gap might be due to the time needed for processing of the protein. In addition, some cells

exhibited GFP IHC signal but lacked GFP mRNA, which may be caused by the prolonged stability of GFP protein in comparison to that of the encoding mRNA.

Likewise, the overlap of GFP and dsRED both driven by the *olig2* enhancer was estimated. Double Tg [*olig2*:dsRED; *olig2*:GFP] embryos were analysed at 98 hpf by confocal microscopy. Although differences in the intensity of the red and green fluorescence signal were detectable, almost all expressing cells exhibited fluorescence of both proteins. Small variations in the strength of the signal may be derived from not yet degraded protein upon downregulation of *olig2* or may be due to a prolonged maturation time of dsRED compared to that of GFP.

The expression analysis revealed the expression of *olig2* mRNA in the cerebellum from 36 hpf until at least 4dpf. Thus, expression coincides with the main period of neural specification in the zebrafish cerebellum. The overlap of mRNA encoding GFP in the reporter line and endogenous *olig2* mRNA demonstrated that GFP expression in the transgenic line reliably reflects endogenous *olig2* expression. An additional transgenic line, *olig2*:dsRED, also proved to be an appropriate reporter for *olig2* expression. Fluorescent dsRED protein however appeared at significantly later developmental stages.

Next the fate of the *olig2* expressing cells in the zebrafish cerebellum ought to be clarified in this study.

3.1.2. *olig2*-expressing precursors differentiate into Eurydendroid Cells

The cerebellar anlage is subdivided into two germinal zones: the dorsally located upper rhombic lip (URL) and the ventrally adjacent ventricular zone (VZ). Throughout neurogenesis, the excitatory glutamatergic neurons of the cerebellum (e.g. GCs) are generated within the URL. Conversely, the GABAergic inhibitory neurons (e.g. PCs and basket interneurons) are generated in the VZ. Both germinal zones express characteristic transcription factors that also have a primary effect on the fate of the generated neurons: *atonal homologue 1a* (*ath1a*) in the URL and *pancreas transcription factor 1a* (*ptf1a*) in the VZ. The phases of expression of the two factors partly overlap: *ath1a* is expressed in the URL from 24 hpf to 48 hpf, while *ptf1a* is expressed from 36 hpf to 48 hpf (Kim et al., 1997; Lin et al., 2004).

To determine from which of these two zones the *olig2*-expressing precursors originate and hence to which fate they are designated, DISH was performed using

either *ath1a* or *ptf1a* in combination with *gfp* as antisense probes on *olig2*:GFP transgenic embryos. First, the expression domains of *ath1a* and *ptf1a* were compared at 36 hpf (Fig. 4 A). In the cerebellum, *ath1a* and *ptf1a* form two non-overlapping, abutting domains, indicating that these two factors define regions homologous to the URL and the VZ in other vertebrate model organisms (Ben-Arie et al., 1997; Ben-Arie et al., 1996; Glasgow et al., 2005; Hoshino et al., 2005). When these two mutually exclusive expression domains were related to *gfp* expression in *olig2*:GFP embryos, the *olig2*-expressing cells were found to be a subset of the *ptf1a* cells within the VZ (Fig. 4 B). In contrast, no overlap of *ath1a* and *gfp* mRNA could be observed (Fig. 4 C).

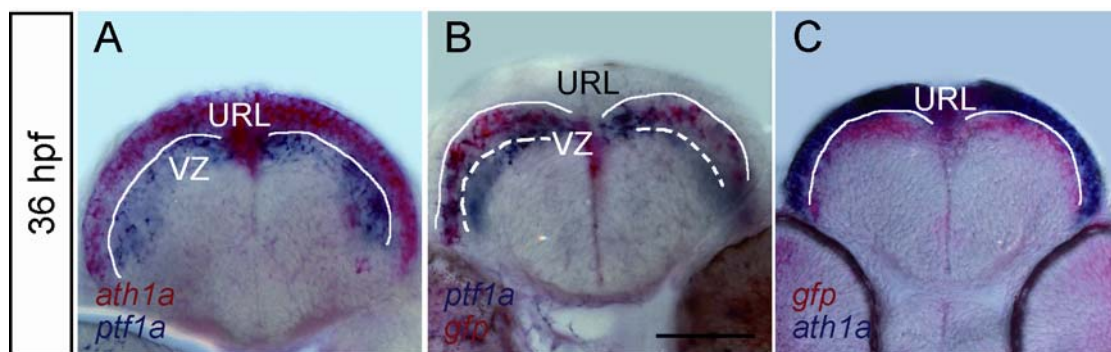


Fig 4: Localisation of *olig2* precursors within the cerebellum primordium. Transverse vibratome sections through the cerebellum of 36 hpf Tg [*olig2*:GFP] embryos after performing DISH using antisense probes as indicated. The illustrations are a montage of the transmitted light picture and the corresponding fluorescent image, making use of the fluorescent properties of the fast red dye. (A): *ath1a* and *ptf1a* form two distinct, bordering domains in the cerebellum primordium. (B): *olig2*-expressing cells form a subdomain within the VZ. (C): *gfp* mRNA does not overlap with *ath1a* RNA. Scale bar: 50µm; magnification: 40 fold. URL: upper rhombic lip; VZ: ventricular zone.

Glia and neurons emanate from the same germinal regions of the neuroepithelium in a temporally ordered manner. Thus, the question arose whether *olig2*-expression is restricted to one of these neural cell types. To examine which fate *olig2*-expressing cells adopt, co-localisation studies of *olig2*:GFP and HuC, which is a prominent marker of postmitotic, differentiating neurons (Wakamatsu and Weston, 1997), were performed at 40 hpf and 56 hpf. In addition, the M-phase marker PH3 (Braunstein et al., 1996) was used to show localisation of proliferating cells in comparison to zones of neuronal differentiation. The localisation of PH3 and HuC revealed a partition of the cerebellar neuroepithelium along its radial axis, i.e. due to the cerebellar rotation, in an anterior-posterior direction (Distel et al., 2006): PH3-positive cells in M-phase were found to be located towards the apical lamina along the IVth ventricle. Conversely, HuC-positive differentiating neurons form a continuous domain in the

anterior part of the cerebellum along the MHB (Fig. 5 A'', B''). At 40 hpf, some of the *olig2*-expressing precursor cells underwent mitosis, as identified by the overlap of GFP and PH3. Consistently, such mitotic *olig2*-expressing cells were localised along the IVth ventricle and were negative for HuC. Most of the *olig2*-expressing cells however were positive neither for HuC nor PH3 and were positioned in middle regions of the neuroepithelium (Fig. 5 A'). Histone 3 is only phosphorylated during mitosis; given that mitosis is a relatively short phase of the cell cycle, it is the absence of HuC protein that suggests that *olig2*-expressing precursors are in a proliferative state at 40 hpf. At 56 hpf, a broad overlap of GFP and HuC was observed (Fig. 5 B). *Olig2*-expressing cells were no longer apparent in M-phase and were localised in anterior parts of the cerebellum. These findings show that *olig2*-expressing precursor cells differentiate into neurons shortly after 2 dpf.

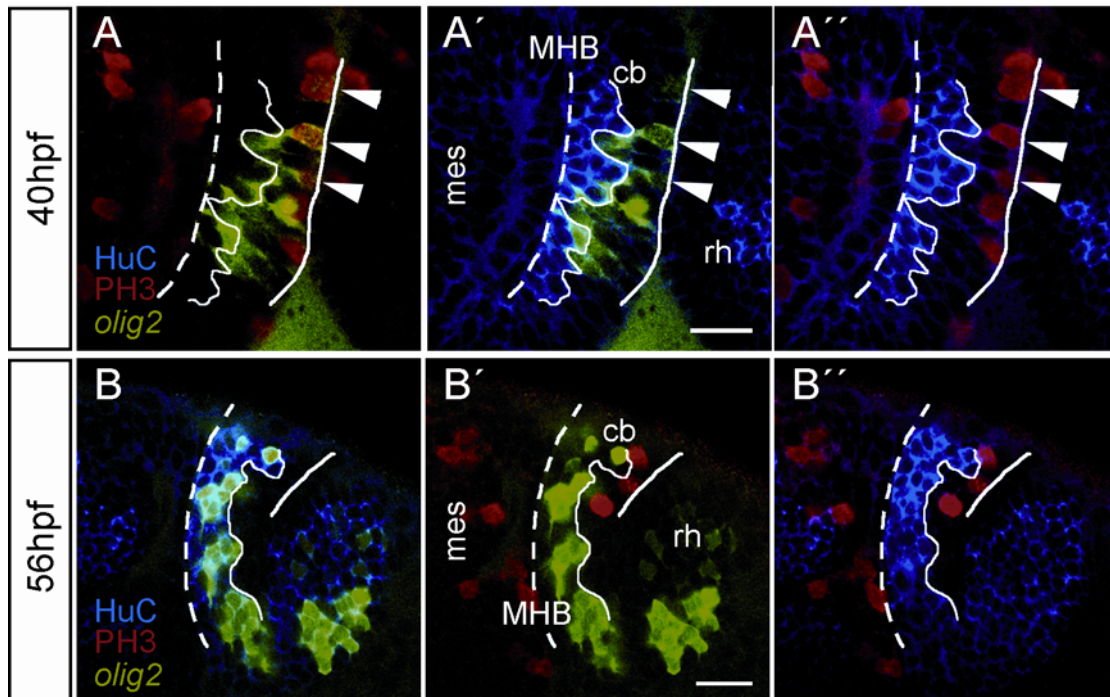


Fig. 5: *Olig2*-expressing precursors are developing neurons. Optical slices recorded by laser scanning microscopy. Whole mount preparations of Tg [*olig2*:GFP] embryos processed by IHC. Anterior to the left, colours of markers as indicated in the figure. The thin line represents the border of the HuC-positive domain. Magnification: 40x, scale bars: 20 μ m. (**A-A''**): dorsal view of one cerebellar half at 40 hpf, with lateral to the top. Arrowheads indicate overlap of *olig2* and PH3, the thin line demarcates the border of the HuC domain. (**B-B''**): lateral view of cerebellum in 56 hpf embryo processed as above. Dorsal to the top. cb: cerebellum; mes: mesencephalon; rh: rhombencephalon; MHB: midbrain-hindbrain boundary

olig2 function is crucial for gliogenesis (Lu et al., 2000; Park et al., 2002; Zhou et al., 2000). Generally, both neurons and glia arise from the same germinal tissues, where neural stem cells first generate neurons and later on produce glia. The temporal

switch results from changes in stem cell properties, which in turn are controlled by

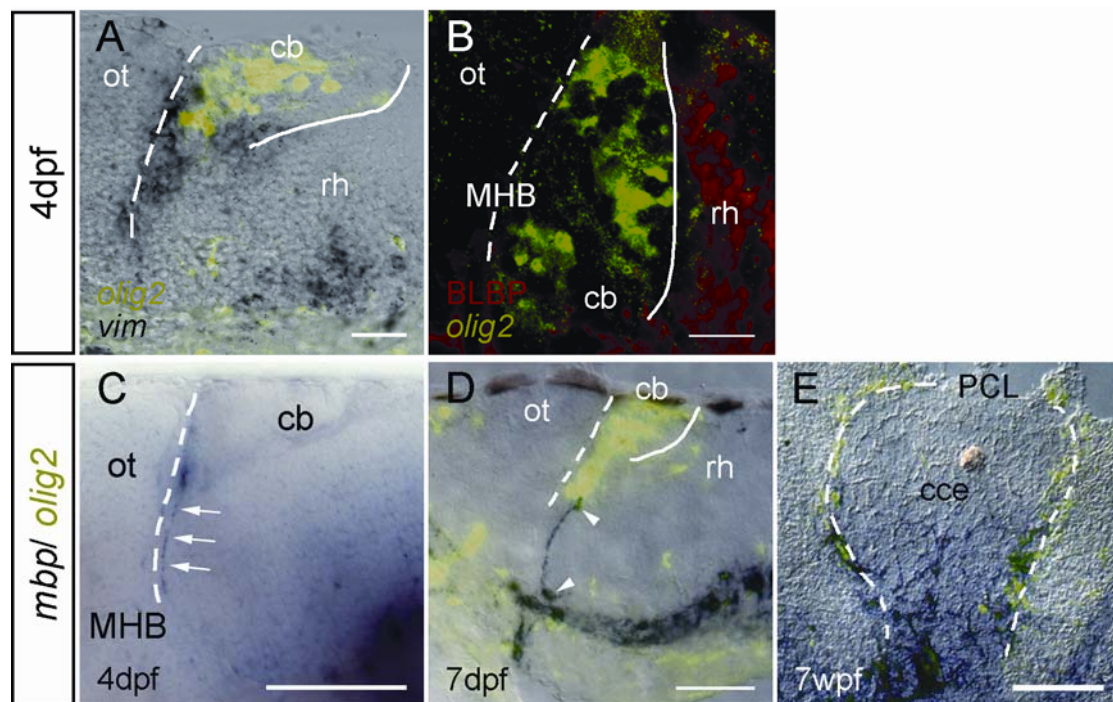


Fig. 6: *Olig2*:GFP-expressing cells in the differentiating cerebellum do not show glial characteristics on the molecular level. Anterior to the left (A): IHC against GFP in Tg [*olig2*:GFP] larva after performing ISH for *vimentin*. The brains were sectioned into 25 μ m slices on a vibratome. *Vimentin* mRNA is found in cranial and caudo-ventral regions of the cerebellum. (B): Optical slice of a whole-mount IHC preparation using α BLBP antibody on Tg [*olig2*:GFP] larva, dorsal view. (C-D): ISH depicting *mbp* expression at the respective stages. (C): lateral view, whole mount preparation. Arrows point to *mbp*-positive myelin structures along the MHB. (D, E): IHC against GFP on Tg [*olig2*:GFP] larva and brains after performing ISH and cryosectioning (18 μ m). Arrowheads in D: structures co-labelled by *mbp* and *olig2*. Magnification: 40x in A, B, C, D, 10x in E. Scalebars: 20 μ m in A, B, 50 μ m in C, D, 100 μ m in E. cb: cerebellum; cce: corpus cerebellaris; lca: lobus caudalis; mes: mesencephalon; ot: optic tectum; rh: rhombencephalon; tel: telencephalon; vc: valvula cerebellaris; MHB: midbrain-hindbrain boundary; PCL: Purkinje cell layer.

both extrinsic and intrinsic cues (Bertrand et al., 2002). An earlier study excluded the presence of glial cells in the fish cerebellum during the stages at which early-born *olig2*-expressing cells develop into ECs (Rieger, 2008). To confirm that *olig2* expression is not confined to glial precursors, expression of various glia marker genes or proteins was investigated. BLBP (Brain lipid-binding protein) and *vimentin* (*vim*) were used as markers for astroglia (Schnitzer et al., 1981) and *myelin basic protein* (*mbp*) was used to identify oligodendroglia (Brösamle and Halpern, 2002; Carnegie, 1971). While α BLBP immunoreactive cells could not be detected in the cerebellum at 4 dpf (Fig. 6 B), some cells located at the base of the cerebellum exhibited *vimentin* expression. These cells, however, did not express GFP driven by the *olig2* enhancer, indicating that *olig2* expression is absent from astroglia (Fig. 6 A). The first

appearance of oligodendrocytes in the cerebellum was observed at 4 dpf, as evidenced by slight expression of *mbp* (Fig. 6 C). *mbp* mRNA, which is known to be located along the myelinating processes of oligodendrocytes (Brösamle and Halpern, 2002), was detected in fibre-like structures projecting from the cerebellum towards the ventromedial hindbrain bundle at 4 and 7 dpf. Though a marginal overlap of GFP and *mbp* could be observed at 7 dpf (Fig. 6 D, arrowheads), the vast majority of cerebellar cells expressing *olig2* clearly did not co-express *mbp*. At adult stages, *mbp* expression was more widespread in the cerebellum, but was still restricted to the ventral half. Still, most of the *olig2*-expressing cells clearly did not co-express *mbp* (Fig. 6 E), indicating that the majority of *olig2*-expressing cells in the adult cerebellum are not oligodendroglia as well. Due to the limited resolution of the ISH/IHC co-labelling method, it is not possible yet to distinguish whether the ventral fibre-like structures in Fig. 6 D and E that are positive for GFP-IHC signal and *mbp*-ISH signal are ensheathed GFP-positive axons or GFP-positive myelinating oligodendroglial processes. It thus cannot be ruled out that *olig2* also is expressed by oligodendrocytes at stages later than 4 dpf, although restricted to ventral regions. The clear absence of expression of glial markers in most *olig2*-expressing cells, however, demonstrated that *olig2* expression is maintained in ECs at juvenile and adult stages.

In order to determine which cerebellar neuronal subtypes arise from *olig2*-expressing precursor cells, expression analyses of *olig2* and established cellular markers were performed. Due to their morphology, Shin *et al* argued that mature *olig2*-expressing cells resemble PCs (Shin *et al.*, 2003). In addition, we found *olig2*-positive cells within the Purkinje cell layer at adult stages (Fig. 16 B, D). 4 day old larvae stay upright, swim, escape and begin to feed. Therefore, essential brain structures are supposed to have differentiated and to be functional. In order to investigate whether the *olig2* expressing cells could give rise to PCs, co-expression of PC markers with either *olig2*:GFP or *olig2*:dsRED was investigated on 4 day old larvae by IHC and ISH. One of the commonly used PC markers is Zebrin II. Though coding for an isoform of aldolase (the encoding gene of Zebrin II is *aldolase C*), which is a housekeeping enzyme in glycolysis, Zebrin II is a useful marker which is restricted to PCs in the nervous system (Ahn *et al.*, 1994). For investigating co-localisation of Zebrin II and *olig2*, double Tg [*olig2*:dsRED; *ptfla*:GFP] larvae were used. This allowed the simultaneous detection of three relevant markers: *olig2*, *ptfla* and Zebrin II. Consistent with the other findings, all Zebrin II-positive cells were

devoid of dsRed in Tg [*olig2:dsRED*; *ptfla:GFP*] larvae (Fig. 7 A-A''). If at all, only few *olig2* expressing cells were co-expressing *ptfla* at 4 dpf (Fig. 7 A', A'', also compare Fig. 14). In contrast, Zebrin II co-localised with GFP driven by the *ptfla* enhancer, demonstrating that PCs in zebrafish, like in higher vertebrates, are VZ-derived. In mammals, IHC against Zebrin II depicts a pattern reflecting a medio-lateral compartmentalisation of the cerebellum and thus only reveals a subset of the PCs (Brochu et al., 1990). Though this compartmentalisation was proposed to be absent in cerebellum of fish (Brochu et al., 1990; Lannoo et al., 1991; Meek et al., 1992), additional PC markers were utilised to rule out the existence of Zebrin II-negative PCs in zebrafish. Carbonic Anhydrase Related Protein 8 (*car 8*) expression has been demonstrated to be restricted to PCs in mouse and human (Kato, 1990; Lakkis et al., 1997). The cDNA of the homologous gene in zebrafish was isolated in our lab and used to generate an antisense probe for ISH (Kazuhiko Namikawa, unpublished results). Expression of *car8* in the zebrafish was investigated by ISH in combination with IHC on transgenic *olig2:GFP* larvae. At 4 dpf, *car8* expression was exclusively found in the cerebellum. Though cells either expressing *car8* or *olig2* closely intermingled, no overlap of *car8* and *olig2* could be detected (note the absence of *car8* expression at the position of *olig2*-expressing cells labelled in Fig. 7 B''). In addition, PCs are known to respond to glutamate as a neurotransmitter and therefore harbour glutamate receptors. The receptor subunit $\delta 2$ is unique to PCs and “neurons with cerebellum-like wiring” in the zebrafish (Mikami et al., 2004). Expression of *GluR $\delta 2$* mRNA did not colocalize with *olig2:GFP* in ISH/IHC experiments (C-C'').

Finally an additional PC marker, *neurogranin* (*nrgn*), has been shown to label the Zebrin II-negative PCs in mouse (Larouche et al., 2006). The cDNA of the homologous zebrafish gene was cloned by RT-PCR. Two different splice variants coding for a protein of 61 and 88 AA length, respectively, could be isolated. On the amino acid level, the short transcriptional variant is 53% identical to that of human and mouse and 65% identical to NRGN of the frog. The extended transcriptional variant shares 48% identity with mouse NRGN, 49% with human NRGN and 61% with frog NRGN (ClustalW method). Performing ISH using antisense probes of both variants and the described ISH protocol (see methods, 2.2.3.2) revealed no expression in the cerebellum at any time point investigated. This confirms that all PCs in the zebrafish express Zebrin II. Taken together, these experiments ruled out that *olig2*-expressing precursors could give rise to PCs.

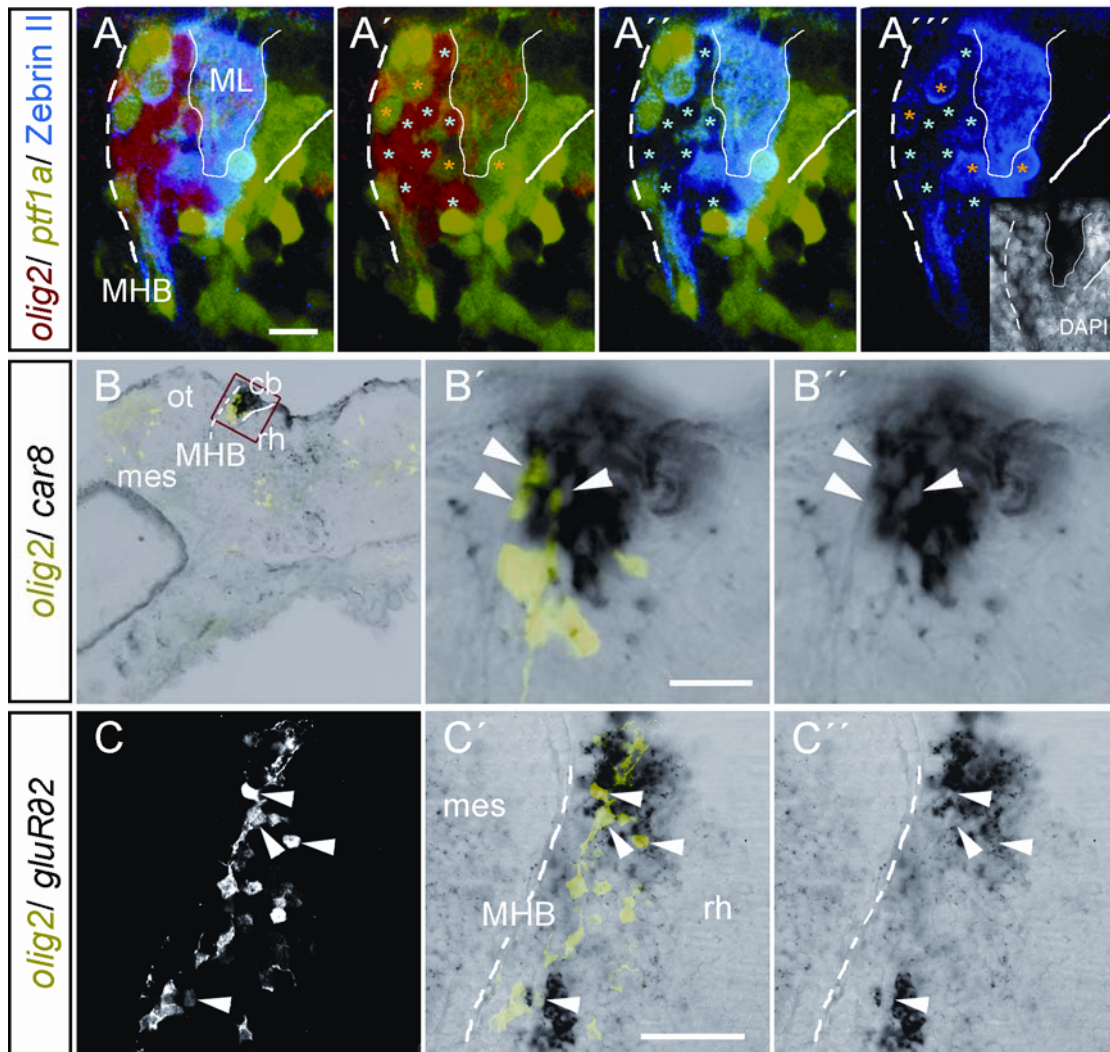


Fig. 7: Lack of co-expression of *olig2* and PC markers at 4 dpf. Anterior to the left, probes and antibodies as indicated on the left. (A-A''): optical slice of a whole mount double transgenic [*olig2:dsRED*; *ptf1a:GFP*] embryo processed for IHC against Zebrin II. Lateral view, dorsal to the top, 40x magnification. DAPI staining (inset in A'') was carried out to delineate white matter areas in which dendrites intermingle (encircled by the thin line). Asterisks in A', A'' and A''' denote the positions of *olig2*-expressing and Zebrin II-positive cells in the complementary colour (turquoise for *olig2*, yellow for Zebrin II). Scale bar: 10 μ m. (B-B''): IHC against GFP on Tg [*olig2:GFP*] larva after performing ISH and laterally cryosectioning into 10 μ m slices. Dorsal to the top. (B): overview (20x magnification) revealing expression of *car8* exclusively in the cerebellum. (B', B''): 40x magnification of the framed region in B. Arrowheads indicate position of *olig2*-expressing cells. Scale bar: 10 μ m. (C-C''): IHC against GFP after performing ISH on Tg [*olig2:GFP*] larvae, 25 μ m vibratome sections, dorsal view, lateral to the top. Arrowheads indicate position of *olig2*-expressing cells. Scale bar: 20 μ m. cb: cerebellum; mes: mesencephalon; ot: optic tectum; rh: rhombencephalon; MHB: midbrain-hindbrain boundary; ML: molecular layer.

VZ-derived neuronal precursors have been shown to generate GABAergic neurons. To unravel whether *olig2*-expressing neuronal precursors of the cerebellum might give rise to GABAergic neurons other than PCs such as inhibitory stellate or basket interneurons, the neurotransmitter utilised by *olig2*-expressing neurons was determined. GAD67 is an enzyme which catalyses the decarboxylation of glutamate

during synthesis of GABA (Kobayashi et al., 1987). To test whether precursors expressing *ptfla* in principal are developing into GABAergic neurons in the zebrafish cerebellum, the co-localisation of GFP in *ptfla*:GFP transgenic embryos and GAD67 was examined. A broad overlap of GAD67 and GFP in the hindbrain of 4 day old

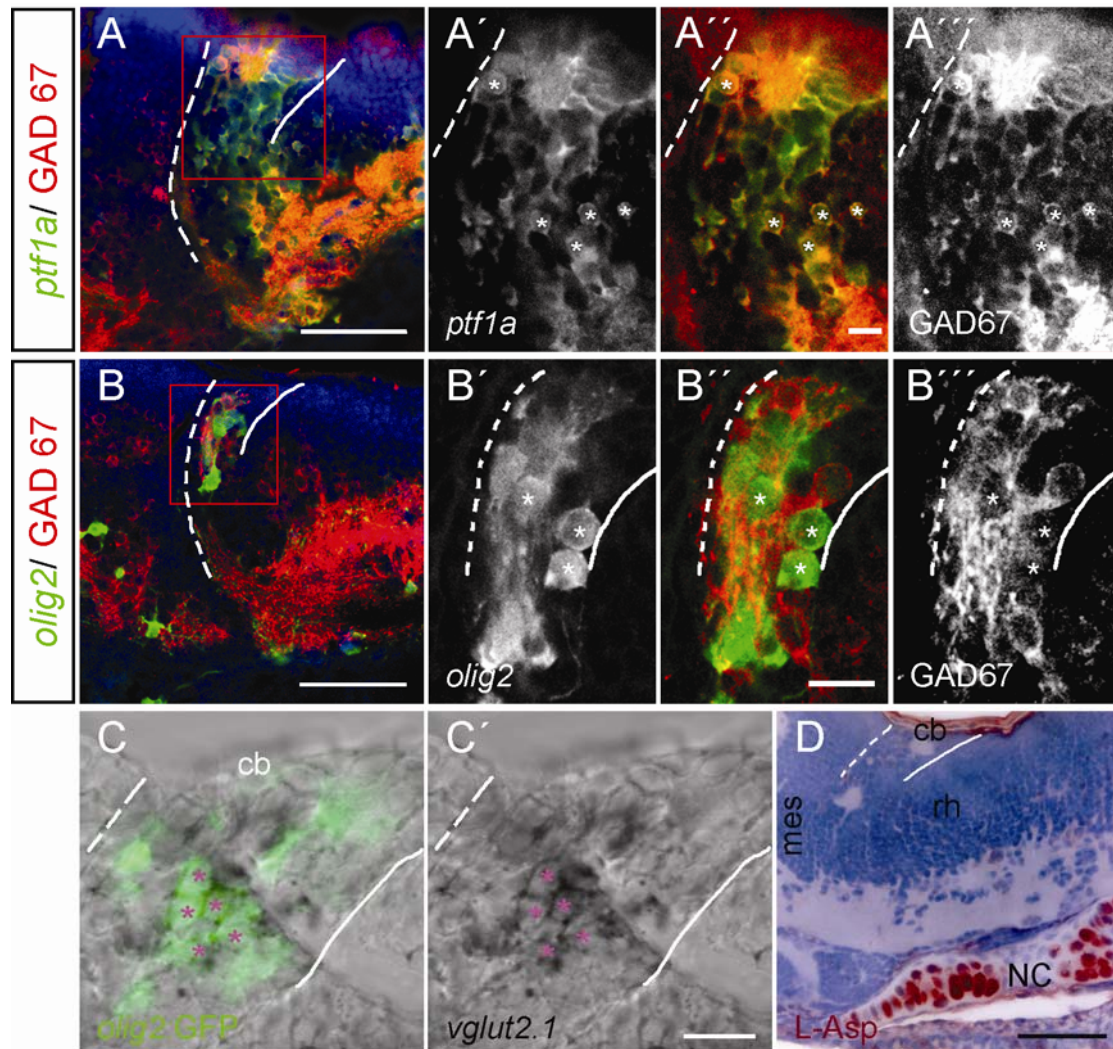


Fig. 8: Neurotransmitter phenotypes of VZ-derived neurons. (A–B''): IHC against GAD67 and GFP on 18 µm sagittal cryosections of 4 dpf Tg [*ptfla*:GFP] and Tg [*olig2*:GFP] larvae, respectively. DAPI nuclear staining is depicted in blue. Anterior to the left, dorsal to the top. (A): high degree of co-localisation between *ptfla* and GAD67 in the white matter of the entire rhombencephalon as indicated by the absence of DAPI and concomitant overlap of GFP and GAD67 as displayed by the orange colour. (A'–A''): Zoom in of framed region in (A). Cerebellar *ptfla*-expressing cells express GAD67 (asterisks). (B–B''): comparable section to A except that GFP reports *olig2* expression. No overlap between *olig2* and GAD67 in the cerebellum or in the residual hindbrain could be observed (B'–B''): Zoom into boxed area in (B). Asterisks indicate the position of *olig2*-expressing cells, which are not co-labelled for GAD67. (C, C'): 25 µm sagittal vibratome section of a Tg [*olig2*:GFP] larva after performing ISH for *vglut2.1* and IHC for GFP. Asterisks label *olig2* expressing cells that co-express *vglut 2.1*. (D). IHC against L-Aspartate revealed no immunoreactivity throughout the entire CNS at 4 dpf, whereas chondrocytes in the notochord (NC) were found to be positive for Asp. Counterstaining: HE. Magnification 40x. Scale bars: 20 µm in A', B', C' and D, 50 µm in A and B. mes: mesencephalon; cb: cerebellum; rh: rhombencephalon

Tg [*ptf1a*:GFP] larvae could be observed, indicating that like in other vertebrates GABAergic hindbrain neurons descend from the VZ in the zebrafish (Fig. 8 A-A''). Consequently, these include the PCs, as confirmed by co-localisation of Zebrin II and GAD67 (not shown). In contrast, *olig2* expression and GAD 67 did not overlap in the cerebellum of 4 dpf Tg [*olig2*:GFP] embryos, nor in other regions of the CNS (Fig. 8 B-B''). Instead the *olig2* expressing precursors differentiated into glutamatergic neurons, as based on the co-expression of *olig2* and *vglut2.1* (Fig. 8 C, C') (Higashijima et al., 2004; Kaneko and Fujiyama, 2002; Takamori et al., 2000; Takamori et al., 2001). It has been described that cerebellar neurons might use L-aspartate (Asp) as a neurotransmitter (Chen and Hillman, 1993; Ikenaga et al., 2006; Kimura et al., 1985). However, at 4 dpf, no immunoreactivity for non-bound Asp was ascertained throughout the entire CNS. These experiments demonstrated that precursors expressing *olig2* develop into excitatory VZ- derived neurons that use glutamate as neurotransmitter.

Another characteristic of cerebellar neurons is the cell type specific presence of Ca²⁺ buffering proteins. Calbindin (*calb*) and Calretinin (*calret*) represent reliable markers for PCs and ECs, respectively (Castro et al., 2006; Celio et al., 1990; Diaz-Regueira and Anadon, 2000; Rogers, 1989). Therefore, IHC using antibodies against both proteins was performed on 4 dpf Tg [*olig2*:GFP] larvae to examine whether *olig2*-expressing cells co-express Calb or Calret. Cells expressing GFP driven by the *olig2* enhancer exhibited no α Calb immunoreactivity. Surprisingly, co-expression of α Calb immunoreactivity and Zebrin II was not observed as well. Instead, cells immunoreactive for α Calb were found to be located at the ventral base of the cerebellum, probably referring to the lateral parabrachial (LPB) neurons, which have been described to express Calb (Wang et al., 2005). By contrast, an apparent co-expression of *olig2* and α Calret immunoreactivity was observed (Fig. 9 C-C''), indicating that *olig2* is expressed by developing ECs.

Calb1 and *calretinin* (alias *calb2*) are homologous genes: the genes share, on the AA level, about 60% of their sequence. The antibodies used in this study were raised against mammalian antigens, which have diverged from their zebrafish homologues. To rule out whether the antibodies recognise their zebrafish homologue and thus do not give a false positive signal, the cDNA of the zebrafish homologue of *calb1* was cloned by RT-PCR and *calb1* expression was examined by ISH (Fig. 9 B). Expression of *calb1* mRNA was found in the same region at the base of the cerebellum that also

was immunoreactive for α Calb. This overlap supports the reliability of the antibody used here (Fig. 9 A, B). These findings show that *olig2*-expressing neurons are likely to be precursors of ECs rather than of PCs.

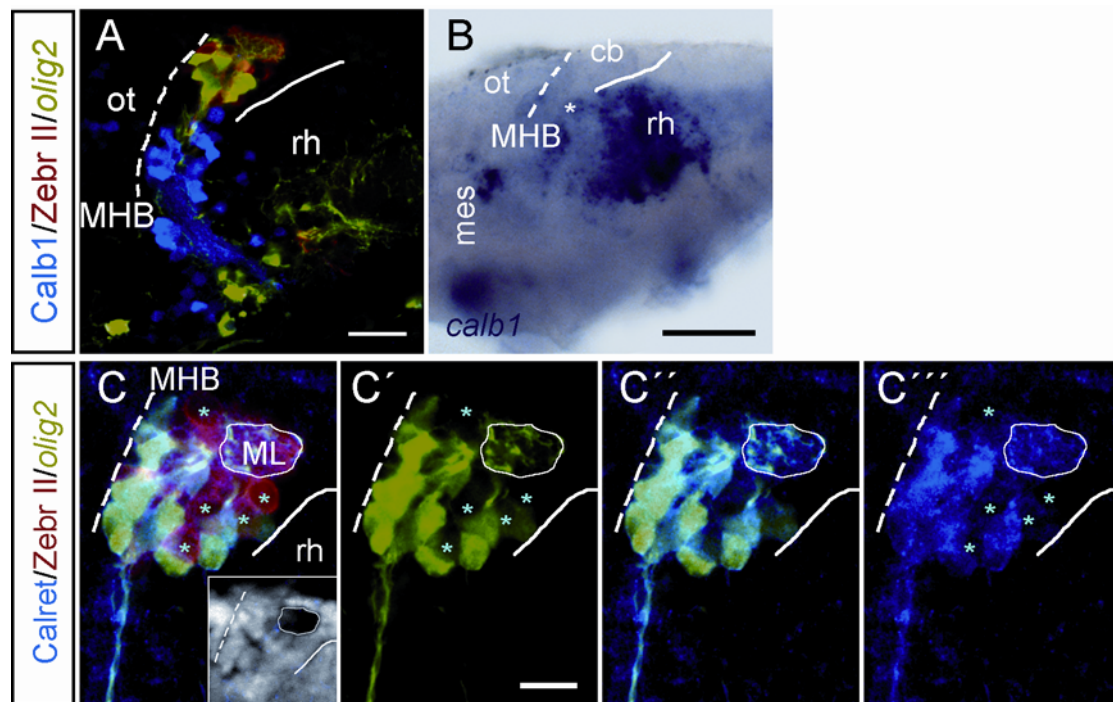


Fig. 9: Calcium buffering proteins in the cerebellum of Tg [*olig2*:GFP] larvae at 4 dpf. Probes and antibodies as indicated on the left of each panel. Sagittal cryosections, 18 μ m, except B (whole mount). Magnification: 40x in A and C-C'', 20x in B. Anterior to the left, dorsal to the top. (A): Calbindin-immunoreactive cells were found in hindbrain regions at the base of the cerebellum. (B): ISH depicting *calb1* mRNA. Areas positive for *calb1* mRNA are positioned ventrally to the areas where *olig2*-expressing cells are usually located (asterisk). (C-C''): *olig2*:GFP, but not ZebrinII, colocalises with Calretinin. Asterisks indicate the position of the PCs as revealed by Zebrin II staining. Inset in C: DAPI staining revealing white matter of the ML, as marked by the encircled area. Scale bar in A, C-C'': 20 μ m; scalebar in B: 50 μ m. mes: mesencephalon; cb: cerebellum; rh: rhombencephalon; ot: optic tectum; MHB: midbrain-hindbrain boundary; ML: molecular layer.

In the cerebellum of teleosts, *calretinin* was shown to be expressed in ECs (Castro et al., 2006; Diaz-Regueira and Anadon, 2000). ECs are the efferents of the cerebellar system towards and project towardsthalamic regions and hence form the physiological equivalent of the DCN in other vertebrates (Meek, 1992; Murakami and Morita, 1987; Nieuwenhuys et al., 1974; Wullmann, 1998). The efferent character of the *olig2*-expressing neurons was observed from early developmental stages on up to adulthood based on axons found to project outside the cerebellum (Fig. 10 A, B). In order to better designate the destination of these projections, a live retrograde labelling approach was performed (Ikenaga et al., 2005; Volkmann et al., 2008). DiI was applied to 6 dpf Tg [*olig2*: GFP] fish into the putative destination of *olig2*-expressing

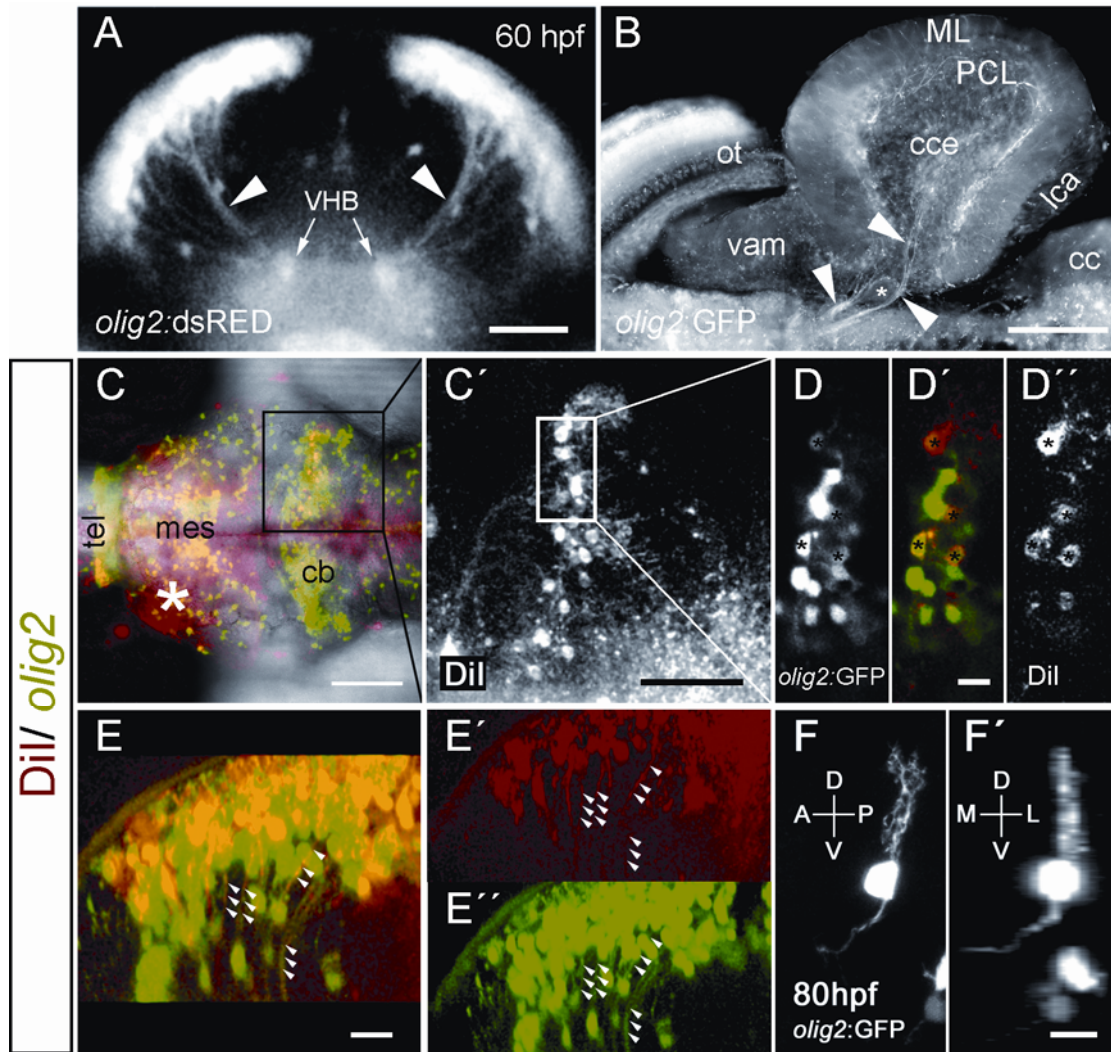


Fig. 10: *Olig2*-expressing neurons are efferents of the cerebellum. (A): An confocal-generated optical section of a 60 hpf Tg [*olig2*:dsRED]embryo at the level of the cerebellum. Axons (arrowheads) of *olig2*-expressing precursors extend ventrally to the ventromedial hindbrain bundle. Scale bar 50 μ m, magnification: 20x. (B): Efferents of the cerebellum express GFP driven by the *olig2* enhancer at adult stage. Sagittal vibratome section, magnification 10x, scale bar: 200 μ m. (C-E): Retrograde labelling of cerebellar efferents in a Tg [*olig2*:GFP] larva at 7 dpf. (C): Maximum projection of a confocal stack showing a whole mount embryo at 7 dpf that has been injected with DiI into the ventral mesencephalon at 6 dpf. The site of DiI application is highlighted (asterisk) and DiI-positive cells are observed within the contralateral half of the cerebellum. Scale bar: 100 μ m, magnification: 20x. (C'): Enlargement of boxed area in C, showing retrogradely-labelled efferents of the cerebellum. The blue box in C' marks the position depicted in D-D''. Scale bar: 50 μ m, magnification: 20x. (D-D''): Retrogradely-labelled efferents co-express *olig2*:GFP (marked by asterisks). Images are an optical slice derived from a confocal stack recording. Magnification 40x, scale bar: 10 μ m. (E-E''): Projection of a confocal stack recording, rotated 90° along the Y-axis, resulting in a transversal view. Note the axons that are positive for GFP and DiI at the same time (small arrowheads). Magnification 40x, scale bar: 20 μ m. (F, F'): Efferent character and morphology of a transplanted cerebellar single cell expressing *olig2*:GFP at 80 hpf. Single cells expressing GFP driven by the *olig2* enhancer were transplanted from a Tg [*olig2*:GFP] donor onto a WT embryo at the 1000 cell stage. Maximum projection of a confocal stack recording. (F): Rotation of the stack depicted in F along the x-axis, resulting in a transversal view of the cell. Note the single axon projection towards antero-ventro-medial and the widely branched dendrites. Magnification 40x, scale bar: 10 μ m. cb: cerebellum; cc: crista cerebellaris; cce: corpus cerebellaris; lca: lobus caudalis; mes: mesencephalon; ot: optic tectum; tel: telencephalon; vam: medial division of the valvula; ML: molecular layer; PCL: Purkinje cell layer; VHB: ventromedial hindbrain bundle.

neurons, the ventral mesencephalon. Such specimens were analysed using confocal laser scanning microscopy to examine the co-localisation between GFP expression and the retrogradely diffusing dye. After incubating for one day, cells labelled by DiI were detectable in the cerebellum, indicating that the dye diffused retrogradely along the projections of the labelled cells. In all specimens, backfilled cells were located on the contralateral side with respect to the DiI injection site. A complete series of a confocal stack recording is shown in supplementary movie 2. The axons can be tracked up to the cell soma both due to the –cytoplasmic- GFP and the injected dye (Fig. 10 C -E'', supplementary movie 2). The ipsilateral ventromedial hindbrain bundle descending towards the trunk revealed DiI staining as well. Unlike the axons ending up in the cerebellum, these axonal tracks did not project commissurally. The morphology of the backfilled cells was typical for that of *olig2*-expressing cells (compare fig 10 C' and F): long protruding axon, huge cell soma, widely dispersed mono- or polygonal dendrites reaching into the parallel fibre white matter (Fig. 10 C', F, F'). Neither all of the GFP-positive cells were traced by DiI, nor were all of the DiI-positive cells positive for GFP. Instead, co-expression of *olig2* was found in about half of the cells that were labelled by DiI (Fig. 10 D-D''). These results additionally support that in the cerebellum *olig2* is expressed by ECs and their precursors.

The results of the present study strongly suggest that cerebellar precursors expressing *olig2* are differentiating ECs, which are the teleost equivalent of the neurons of the DCN in jawed vertebrates other than teleosts. The *olig2*-expressing cells are VZ-derived as indicated by the co-expression of *gfp* and *ptfla* in Tg [*olig2*:GFP] embryos. Immunoreactivity for HuC reveals their neuronal identity. This was also confined by the lack of glial gene expression in the embryonic and the larval cerebellum. These neurons are, though VZ-derived, glutamatergic. Retrograde labelling proved the efferent character of *olig2*-expressing neurons and revealed the ventral mesencephalon as their destination. Such efferents of the cerebellum are referred to as “Eurydendroid cells” (Finger, 1978; Folgueira et al., 2006; Ikenaga et al., 2005; Murakami and Morita, 1987; Nieuwenhuys et al., 1974; Pouwels, 1978). Moreover, none of the PC-characteristic marker genes or proteins investigated could be detected to be expressed in *olig2*-expressing neurons. ECs were found to be immunoreactive for Calretinin, as it has been described for ECs of the cerebellum of adult teleost fish (Castro et al., 2006; Diaz-Regueira and Anadon, 2000).

3.1.3. Development of Eurydendroid Cells

Knowledge about the development of ECs is rather incomplete. Laser scanning confocal microscopy in combination with the use of genetically encoded fluorescent proteins in transgenic embryos offers a powerful tool to directly image neural cells and to reveal their behaviour. Various aspects of EC development such as where they originate, whether they migrate and how development of ECs is timed have not been elucidated yet. Therefore, time-lapse studies using Tg [*olig2*:GFP] embryos were performed (supplementary movies 3, 4, 5 and 6). GFP fluorescence in Tg [*olig2*:GFP] embryos could be detected in the cerebellum from 36 hpf onwards. At this early stage, EC precursors (ECP) are in a proliferative state, as ECPs were observed undergoing cell division (Fig. 11, supplementary movie 3, n= 4). The cell body of proliferating cells periodically moved back and forth while remaining attached to the basal and apical lamina. Cytokinesis was accomplished when cell somata had reached the apical lamina of the neuroepithelium (Fig. 11). This type of movement of proliferating cells in a neuroepithelium is referred to as interkinetic nuclear migration (INM) (Baye and Link, 2008; Götz and Huttner, 2005; Murciano et al., 2002). Prominent INM was observed up to 44 hpf, which is in good agreement with the detected co-localisation of GFP driven by the *olig2* enhancer and PH3 at 40 hpf (compare Fig. 5).

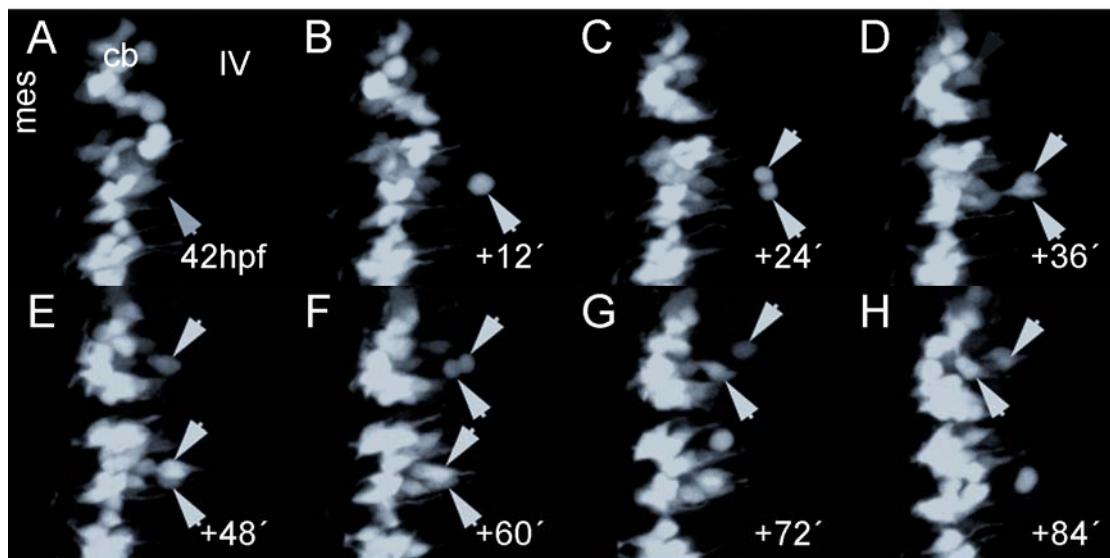


Fig. 11: Time-lapse analysis of proliferating ECPs. (A-H): maximum brightness projections from individual time-points of a confocal laser scanning microscopy study of a Tg [*olig2*:GFP] embryo (compare supplementary movie 3). Anterior to the left, dorsal to the top, lateral view. Arrows point towards mitotic cells. Numbers in the bottom row give the time span between the start and acquisition of respective recordings. Also note the thin cell processes perpendicular to the basal-apical axis. cb: cerebellum; mes; mesencephalon; IV: fourth ventricle.

At 44 hpf, the EC precursor cells started to extend processes anteriorly towards the MHB (Fig. 12. A, B, supplementary movie 4, n=5). As they resemble the axons delineated by retrograde labelling (see Fig. 10), these processes are likely the developing efferent axons. The growing axons further extended ventrally along the MHB, ending up in the ventromedial hindbrain bundle (Fig. 12. C, D). At this time, the cell somata of the ECs remained static in the central area of the dorsal cerebellum, removed from both the URL as well as the MHB. These findings suggest that ECPs initiate differentiation at 44 hpf in central cerebellar positions, which is consistent with the finding that ECPs express the postmitotic marker HuC at this stage.

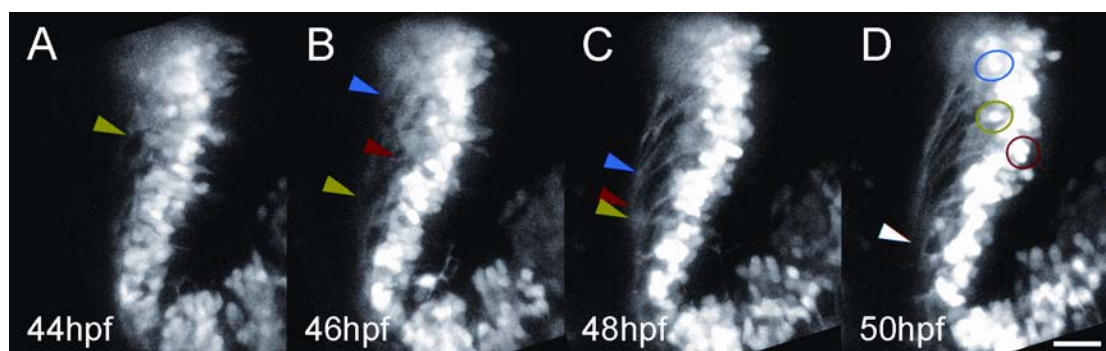


Fig. 12: Formation of cerebellar efferents. (A-D): Maximum brightness projections from individual time-points of a time-lapse confocal microscopy study of a Tg [*olig2*:GFP]embryo (compare supplementary movie 4). Anterior to the left, dorsal to the top, lateral view. The coloured arrowheads indicate the leading process of individual growing axon bundles towards the ventromedial hindbrain bundle, the coloured circles in D indicate the position of the associated cells/cell clusters. Scale bar: 20 μ m.

Once the efferent axonal protrusions were initiated, the somata of the ECPs repositioned within the neuroepithelium as they now moved towards the MHB, following their developing axons (Fig. 13, supplementary movies 5 and 6, n= 4). This mode of migration is termed somal translocation (Baye and Link, 2008; Nadarajah and Parnavelas, 2002). Noteworthy, the temporal sequence of somal translocation of ECPs was strictly orchestrated since all somata that relocated had developed the efferent axon beforehand. These movements lead to a reorganisation of ECP positioning. Cell clusters, which were first located in a more caudal position of the cerebellar primordium now realigned close to the basal lamina (compare encircled area in Fig. 13 B-D). The net distance that cell somata moved was between 3 and 5 cell diameters. After 72 hpf, no significant movements of ECPs were detectable.

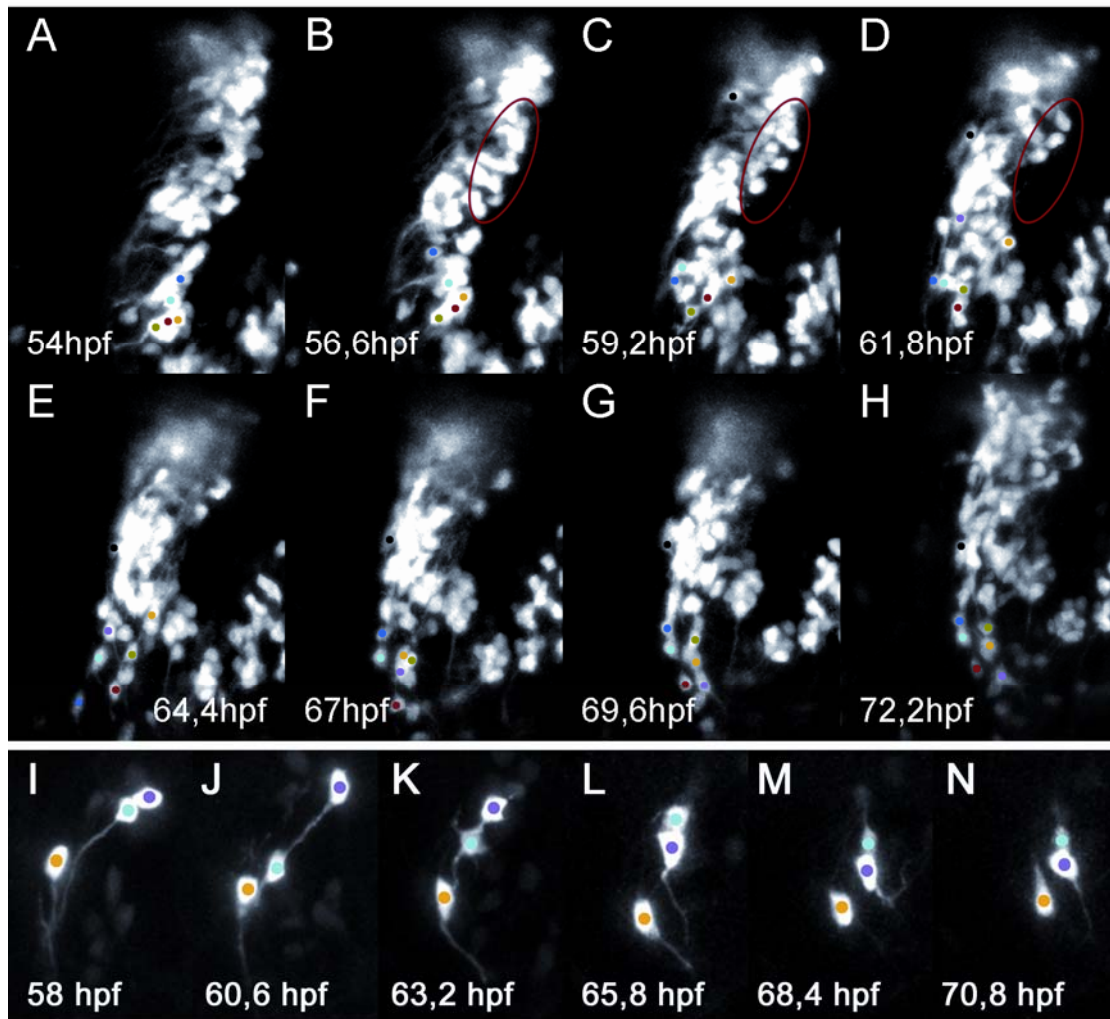


Fig. 13: Somal translocation of ECPs. Maximum brightness projections from individual time-points of time-lapse microscopy studies (compare supplementary movies 5 and 6). Anterior to the left, dorsal to the top. The coloured dots trace individual single cells. The zone encircled in red depicts clusters of cells that relocate by migration. **(A-H)**: Time lapse analysis of a Tg [*olig2*:GFP] embryo. **(I-N)**: Time lapse analysis of single ECPs that were transplanted from a transgenic *olig2*:GFP donor embryo onto a WT acceptor embryo. Note that axon formation occurs prior to somal translocation.

When using stable transgenic lines, in which expression of fluorescent proteins is driven by cis-regulatory elements, it is sometimes difficult to ascertain single cells and their dynamics. To overcome this problem, we performed time lapse analyses with chimeric embryos, which contain cells expressing fluorescent proteins in a mosaic manner. Such chimeras were generated by transplanting single cells from a Tg [*olig2*:GFP] donor into a WT host. Such homotopic-homochronic transplanted embryos were followed by laser scanning time-lapse microscopy. On the one hand these studies confirmed our observations from time lapse experiments with Tg [*olig2*:GFP]: the cell somata followed the developing axon towards the basal MHB and ventral positions. On the other hand, mosaic distribution of *olig2*:GFP fluorescent

ECs showed that, as cells relocated in the neuroepithelium, a high activity of filipodia-like processes occurred at the same time. Before ECPs progressed to develop their dendrites, filipodia projected towards several directions, finally giving rise to the dendrites. The formation of the dendrites was complete at around 80 hpf as judged by a cease of further denrite expansion. In terms of morphology, ECs had terminally differentiated at that stage. This observation indicates an intensive exploratory activity of ECPs prior to finally differentiating (supplementary movies 6 and 7, n=3).

From the time lapse analyses of the cellular behaviour, development of ECs can be divided into four phases: 1) onset of *olig2* expression and proliferation from 36 to 44hpf, 2) establishment of efferent connections between 45 and 50hpf, 3) migration and positioning in the medial cerebellum until 72hpf, 4) terminal differentiation- as indicated by cell morphology and acquisition of the ECs neurotransmitter phenotype- until 4dpf.

ECs are VZ-derived but glutamatergic (Fig. 4 and Fig. 8), a neurotransmitter phenotype that is usually confined to URL-derived neurons. In addition, no or only little overlap of *ptfla* and *olig2* expression was observed at 4 dpf (Fig. 7). In order to better explain this observation, double Tg [*olig2:dsRED*; *ptfla:GFP*] embryos were generated to follow the dynamics of both cell populations. 3D-reconstructions of stack recordings at 54 and 94 hpf revealed a progressive decline in the number of cells that were double positive for dsRED and GFP (Fig. 14 A-C). At 54 hpf, $81 \pm 5\%$ ($\cong 33,2 \pm 7,3 / 41,2 \pm 9,6$; numbers are evaluated cells per one cerebellar half \pm standard deviation, compare methods 2.2.4) of cerebellar *olig2*-expressing ECPs were positive for *ptfla* (Fig. 14 A, C). This degree of co-expression declined to $21 \pm 2\%$ ($13,4 \pm 4,6 / 64,2 \pm 18,5$) at 94 hpf (Fig. 14 B, C) (n=5 cerebellar halves, percentages have been evaluated in identical specimens at 54 and 94 hpf, respectively; numbers are average \pm standard deviation, p-value <0,005). One explanation for the relative decrease in the percentage of *olig2:dsRed*-positive ECs expressing *ptfla:GFP* could be an increase in the total number of cells after 54 hpf that exclusively express *olig2:dsRED*. To test this, the total number of cells expressing *olig2:dsRED* were evaluated. In fact the number of cells that expressed *olig2:dsRED* at 94 hpf increased by 156% compared to 54 hpf ($64,2 \pm 18,5 / 41,2 \pm 9,6$). If assuming that all cells that initiated expression of *olig2:dsRED* after 54 hpf were not concomitantly expressing *ptfla:GFP*, i.e. that the average of the number of double-positive cells per

one cerebellar half remained constant at $33,2 \pm 7,3$, the ratio of double-positive cells yet still would have been 52% at 94 hpf ($64,2 \pm 18,5 / 33,2 \pm 7,3$). However, as the number of *olig2*:dsRED-expressing cells increased, the number of cells that expressed both *olig2*:dsRED and *ptfla*:GFP decreased by 60% ($13,4 \pm 4,6 / 33,2 \pm 7,3$). Hence, both the net increase of ECPs expressing *olig2*:dsRED and the decline in the number of cells concomitantly expressing *olig2*:dsRED and *ptfla*:GFP caused the decline in ratio of ECPs expressing both *olig2*:dsRED and *ptfla*:GFP.

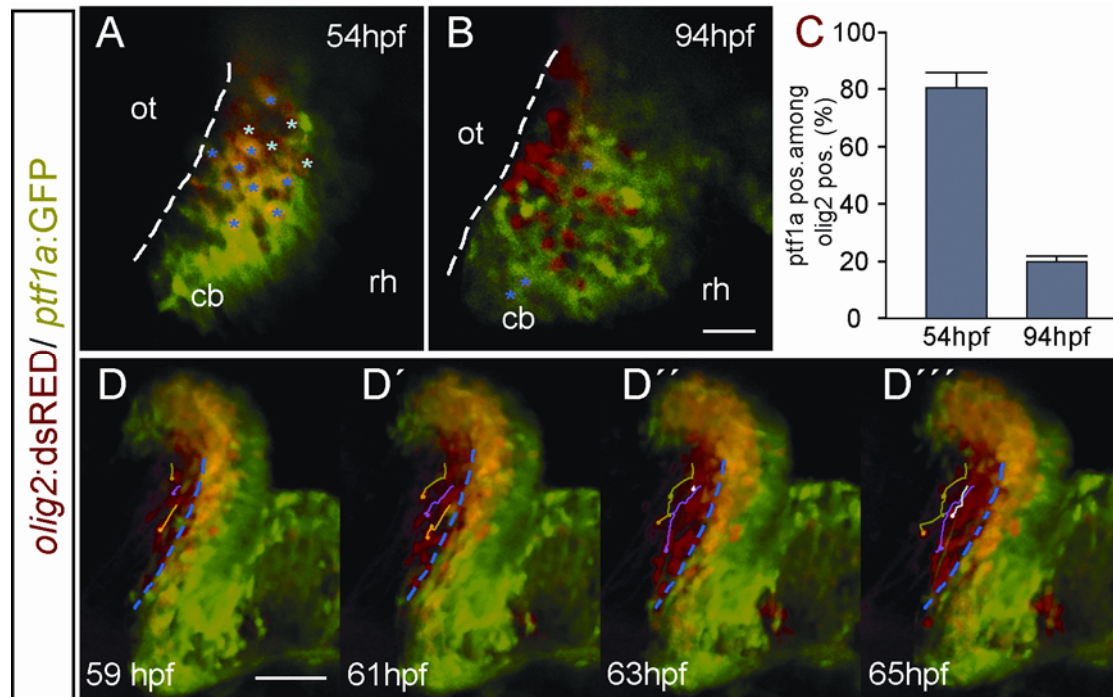


Fig. 14: Segregation of ECPs from the VZ. (A, B): Optical sections through double Tg [*olig2*:dsRED; *ptfla*:GFP] larvae at stages as indicated on the right top. Dorsal views of one cerebellar half, lateral to the top, anterior to the left. Cells expressing both dsRed and GFP are labelled with blue asterisks, while turquoise asterisks label cells that are positive only for *olig2*. (C): Quantification of the number of cells expressing both *ptfla*:GFP and *olig2*:dsRED, shown as a percentage of the dsRed-positive ECPs. Error bars are standard deviation (n=5 cerebellar halves, $p < 0,005$). (D-D''): Time lapse analysis of migrating ECPs in correlation to the remaining cells expressing GFP under the control of the *ptfla* enhancer. Brightest point projections of images of individual time-points are displayed. The blue dotted line demarks the border between segregated ECPs and the *ptfla* domain. Tracks delineate individual migrating ECPs. Stages are indicated in the bottom line. Magnification: 40x; scalebars: 20 μ m in (A), 50 μ m in (D). cb: cerebellum; ot: optic tectum; rh: rhombencephalon.

It is feasible though that ECs expressing *olig2*:dsRED accumulate after 54 hpf in the cerebellum, while cells co-expressing *olig2*:dsRED and *ptfla*:GFP migrate away from the relevant territory in which cells were quantified. Therefore, time lapse recordings of cerebellar neurons of double Tg [*olig2*:dsRED; *ptfla*:GFP] embryos were performed to trace the dynamics of ECPs in relation to residual VZ-derived

cells. Cellular movements typical for ECPs (i.e. axon protrusion towards the ventro-

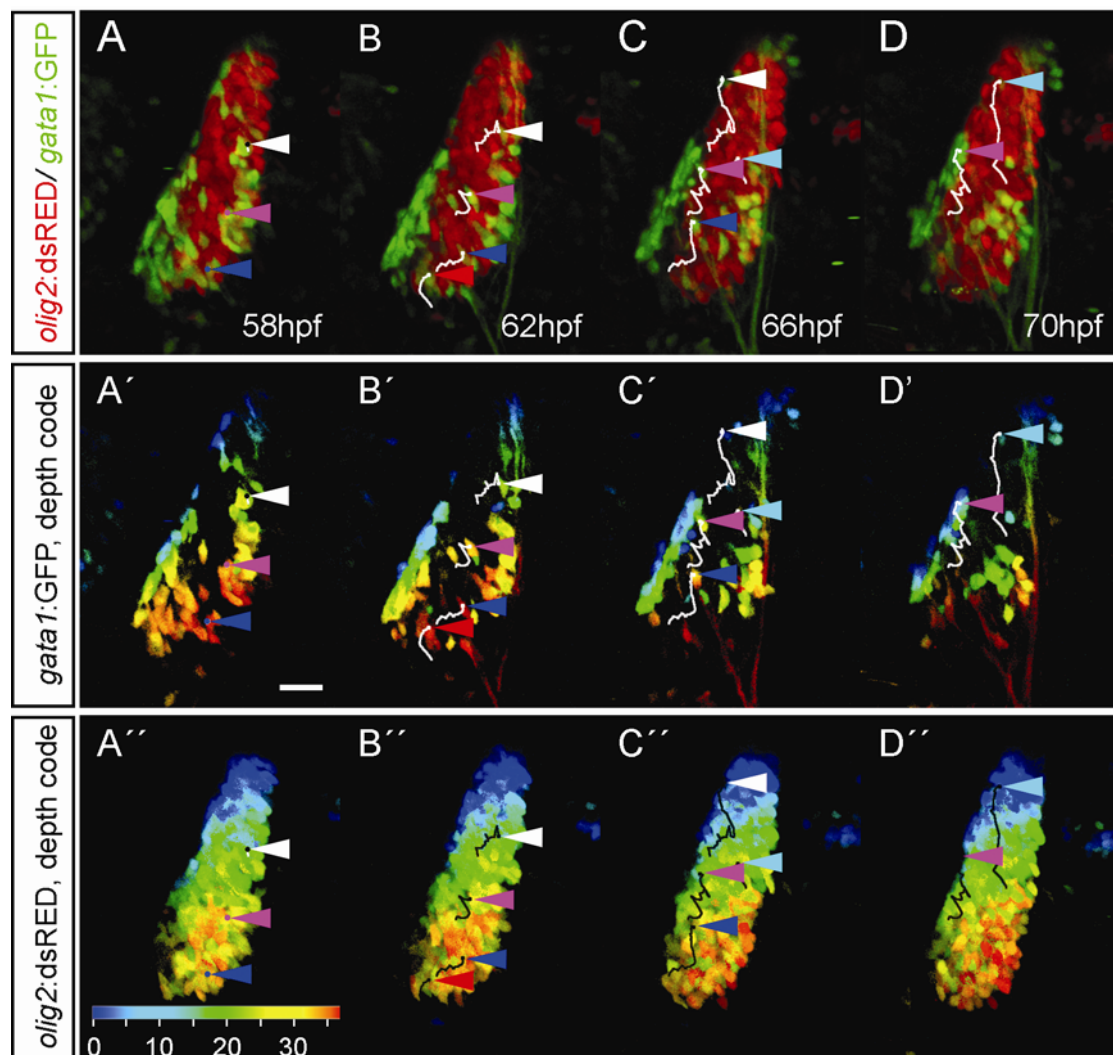


Fig. 15: Co-development of ECPs and GPCs. Anterior to the left, lateral to the top, stages of each column indicated bottom right of the top panel. Arrowheads trace individual migratory GCPs, solid lines trace their migratory paths. (A-D): Migration of GCP and the ECP, displayed by maximum brightness projections from individual time-points of a time-lapse microscopy study of a double tg [*olig2:dsRED*; *gata1:GFP*] embryo (compare supplementary movies 9 and 10). (A'-D', A''-D''): depth coding of stack recording displayed in (A-D). The color code indicates the depth of the cells within the tissue. Migrating GCPs migrate from the dorsally located URL towards ventral regions by passing EPCs above. Scalebar in A': 20 μ m. Coloured bar in A'' outlines the depth in μ m as indicated by the colour shades (blue: ventral, red: dorsal).

medial hindbrain bundle followed by translocation of the cell soma) in fact were restricted to the *olig2:dsRED*-expressing subpopulation of VZ-derived cells (Fig. 14 D-D'', supplementary movie 8, n=4). Cells expressing *ptf1a:GFP* also displayed motility, and the main direction of migration was also ventral, as far as single cells could be traced. Such cells however did not migrate anteriorly, as is typical for ECPs, and did not exhibit the characteristic axonal protrusions either. As a consequence, ECPs emigrate from the VZ in an antero-ventral direction (Fig. 14 D-E). These

cellular movements resulted in a segregation of the ECs from VZ-derived *ptfla*:GFP expressing cells (Fig. 14 D-D''', note the increase in cell number anterior to the blue dashed line separating the main expression domains of *olig2*:dsRED and *ptfla*:GFP). Both populations though do not completely separate to form distinct tissue layers, as seen in Fig. 14 B. Yet, no ECPs were observed to leave the area in which the cells were counted at 94 hpf, indicating that migration has no influence on the observed decline of *ptfla* expression by mature ECs.

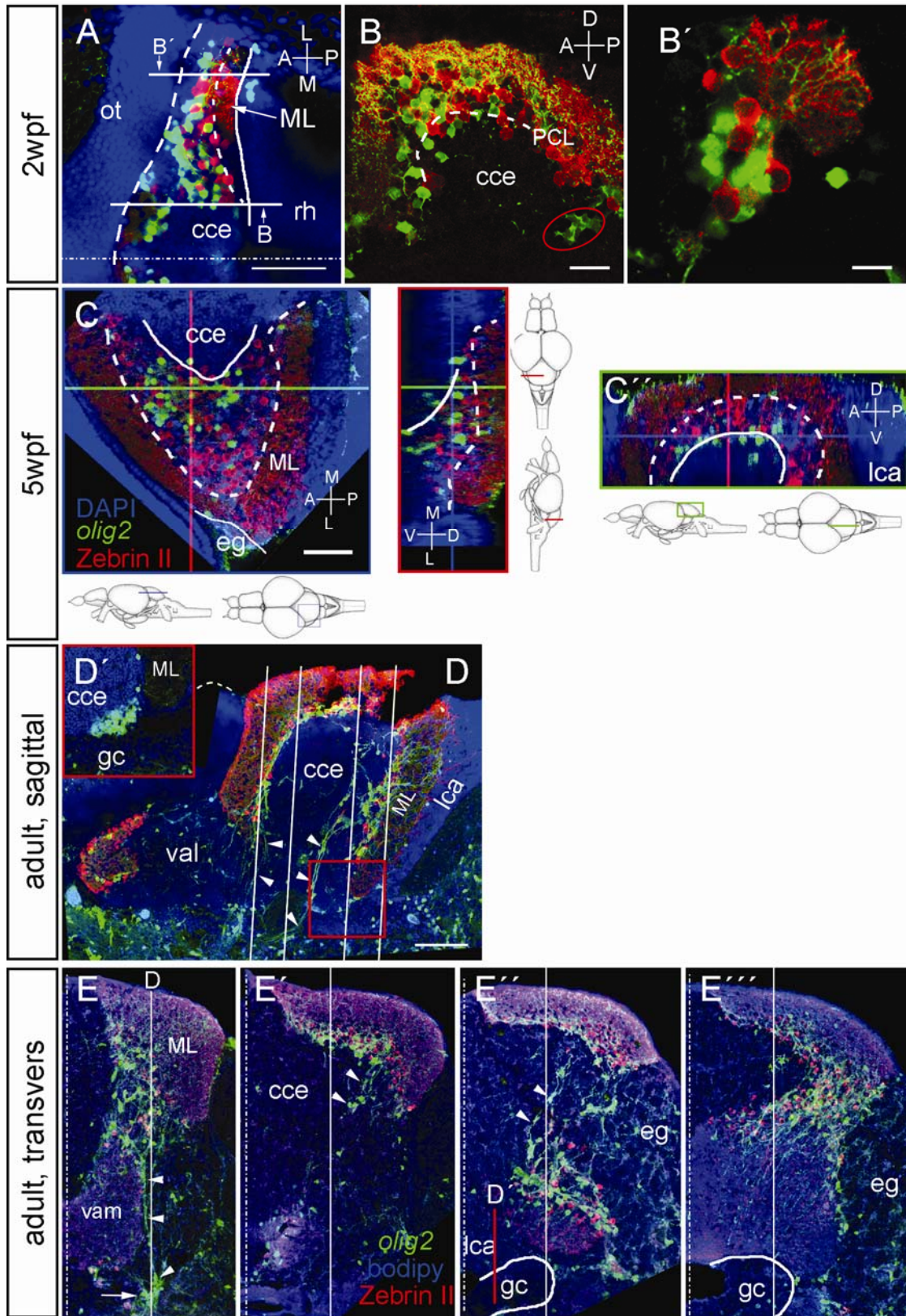
Since first glia appear only after 4 dpf, migrating zebrafish GCPs do not depend on glial interaction partners, namely Bergmann glia, but move by forming chain like structures extending from the apical towards the basal lamina, i.e. the MHB (Köster and Fraser, 2001; Rieger, 2008). GCPs initially arise dorsal to the ECPs in the URL. In the mature cerebellum however, granule neurons are found to be positioned ventrally to the ECs, which are distributed along the PCL (Fig. 16). In order to examine whether ECPs form a barrier for migrating GCPs or whether they cross the EC layer by intercalation, migration of GCPs and ECPs was assayed in Tg [*olig2*:dsRED; *gatal*:GFP] embryos (Fig. 15 and supplementary movies 9 and 10, n=5). Individual migrating cells were tracked via software-assisted visualization (ImageJ 1.34 S, Manual Tracking plug-in) to follow the migratory routes of GCPs respectively. Depiction of the confocal stack recordings using the depth code additionally enabled us to delineate the dorso-ventral positions of both ECPs and migrating GCPs. Starting at 50 hpf, GCPs rapidly moved towards the MHB in a chain-like manner. Comparison of the depths of the tracked GCPs with that of the ECPs revealed that the vast majority of GCPs passed the ECPs dorsally (note that coloured arrowheads in Fig. 15 point at the current position of migrating GCPs; ECPs at the respective position were located underneath migrating GCPs). Hence, it appears that GPC chain migration is accomplished without entering the ECP domain. However, sporadically migrating GCPs were observed that intercalated the cluster formed by the ECPs (arrowheads in supplementary movie 9), finally passing the ECPs ventrally. Thus, ECPs do not seem to form a rigid barrier for migrating GCPs *per se*. Remarkably, such GCPs originated in URL regions bearing GCPs that are considered to be predisposed to end up in the lca (Volkman et al., 2008). This predisposition might contain the ability to transverse the EC layer.

In the present study, it was shown that ECPs are born in the VZ and end up in the anterior cerebellum at 4 dpf (Fig. 4, Fig. 13, Fig. 14). The zebrafish cerebellum is

known to exhibit its layered organisation into ML, PCL and GCL by 8 dpf (Volkman et al., 2008). To further evaluate how ECs organise in the cerebellum after 4 dpf, the brains of Tg [*olig2*:GFP] and Tg [*olig2*:dsRED] fish were processed for IHC against GFP or DsRED and the PC marker Zebrin II at various stages until adulthood. Specimens were counterstained with DAPI, ToPro 3 or Bodipy 630/650-X to additionally outline the histological organisation of the cerebellum. Laser scanning confocal imaging of such preparations indicated that ECs remain located in rostral and lateral parts of the cerebellum at 2 wpf and 5 wpf (Fig. 16 A, B, C, C', C''). In the cerebellum of 3 month old fish, no imbalanced distribution of EC between anterior and posterior regions was observable (Fig. 16 D, E-E'''). At 2 wpf PCs tended to be present only in posterior regions of the cerebellum (Fig. 16 A, B), but were then distributed equally at developmental stages past 5 wpf (Fig. 16 C-E) with ECs being aligned along the PCL (Fig. 16 B, C', D, E-E'''). The layered organisation of the cerebellar tissue was found not as rigid as is known from the cerebella of higher vertebrates though: i.e. ECs as well as PCs were not strung in a single cell row. Instead, the PC layer consisted of a band of approximately 2 to 4 cells, in which ECs and PCs intermingled (Fig. 16 B, C'', E-E'''). Furthermore, ECs and to a lesser extent PCs were regularly found aside the PCL within the cce and the ML. Both ECs and PCs exhibited widespread dendritic arbours, which branched intensively in the ML and closely abutted to one another (Fig. 16 B, B', Fig. 10). The PCs occurred in two divergent types in terms of their connectivity: one subpopulation of the PCs exhibited only a short axon. A second group of PCs contained a long protruding axon projecting to the vestibular nucleus in the anterior hindbrain. These long distance PCs were found in lateral regions of the cerebellum. An additional cluster of cells expressing *olig2* was observed in 2 week old and adult fish (Fig. 16 B, D'). Such cells were located in a medial position at the posterior base of the cce, lining the rhombencephalic ventricle. The morphology of these *olig2*-expressing cells was apolar and of a small round shape bearing no detectable processes. Interestingly, different authors have identified this region as a niche for stem cells (Chapouton et al., 2006; Grandel et al., 2006; Zupanc et al., 2005). Such stem cells may provide a source of ongoing generation of cerebellar neurons such as ECs at larval and juvenile stages. To get to their destination, these cells might migrate dorsally towards the PCL, thereby passing the GCs of the cce (note ectopic *olig2*-expressing cells within the cce in Fig. 16 D, E' and E'').

In summary, the examination of the development of ECs revealed expression of *olig2* already when ECPs are in a proliferative state. ECPs initiate to extend axonal processes after becoming postmitotic and subsequently reposition their somata towards the efferent axon. About 80% of ECPs co-express the VZ marker *ptfla*:GFP at 54 hpf. This ratio declines to 20% at 4 dpf, probably due to active downregulation of *ptfla* in maturing ECs. GCPs, which develop simultaneously, appear to migrate independently of ECPs. At larval and juvenile stages, ECs are not equally distributed along the PCL but are instead positioned in cranial regions of the cerebellum. This imbalance is no longer apparent at adult stages. A potential source of ECs in the maturing cerebellum may be located at the ventral base of the posterior cerebellum.

Fig. 16 (following page): Development of the EC throughout juvenile and adult stages, and correlation of ECs and PCs. Immunological depiction of ECs and PCs in the cerebella of transgenic fish (tg [*olig2*:dsRED] in B, B'', C-C''; tg [*olig2*:GFP] in A, D, D', E-E'''). Colour code is as indicated in (C) except for E-E''', where blue colour indicates membranous and white matter staining using bodipy630/650-X. (A): optical section of a whole mount preparation using confocal laser microscopy. Bars indicate the approximate position of sagittal section depicted in B and B''. (B, B''): IHC on 18 µm cryosections. The caudo-ventral region highlighted by the red circle possibly bears *olig2*-expressing precursor- or stem cells. (C-C''): orthographic projection of a confocal stack recording of a whole mount brain from a 5 week old fish. The coloured frames are the respective cutting planes through the stack, indicated by the coloured lines in the schematic drawings. (C): dorsal view, anterior to the left, medial to the top. (C'): transversal view, medial to the top. (C''): lateral view, dorsal to the top. Note the absence of ECs in posterior regions bordering the lca (D, D'): IHC on sagittal cryosections (20 µm), anterior to the left, dorsal to the top. The solid lines indicate the position of E-E'''. The red boxed area in D indicates the ventro-caudal position of (D'). Arrowheads point towards efferents positive for *olig2*. Note the formation of the peduncle-like structure both cranially and caudally. (E-E'''): series of transverse cryosections (20 µm) processed by IHC and bodipy staining. Lateral to the right, dorsal to the top. Solid lines in E-E''' indicate the approximate sectioning plane shown in D, the red line in E'' indicates sectioning plane in D'. The dashed line indicates the midline. Arrowheads in (E) point to the anterior efferent bundle off of the corpus, the arrow points towards their destination, the medial longitudinal fascicle (MLF). (E', E''): arrowheads point to assumed migratory *olig2*-positive cells beyond the PCL. Magnification: 20x in D- E'', 40x in A-C''. Scale bars: (A): 50µm, (B): 20µm, (B'): 10µm, (C): 50µm, (D): 100µm. (D) and (E-E''') are of the same scale. cce: corpus cerebellaris; eg: eminentia granularis; gc: griseum centrale; lca: lobus caudalis; ot: optic tectum; rh: rhombencephalon; vam: medial division of the valvula; ML: molecular layer; PCL: Purkinje cell layer



3.2. Analysis of the protooncogene *nmyc* in the developing zebrafish cerebellum

3.2.1. Cloning of the zebrafish homologue of *nmyc* and functional variants of *zf nmyc*

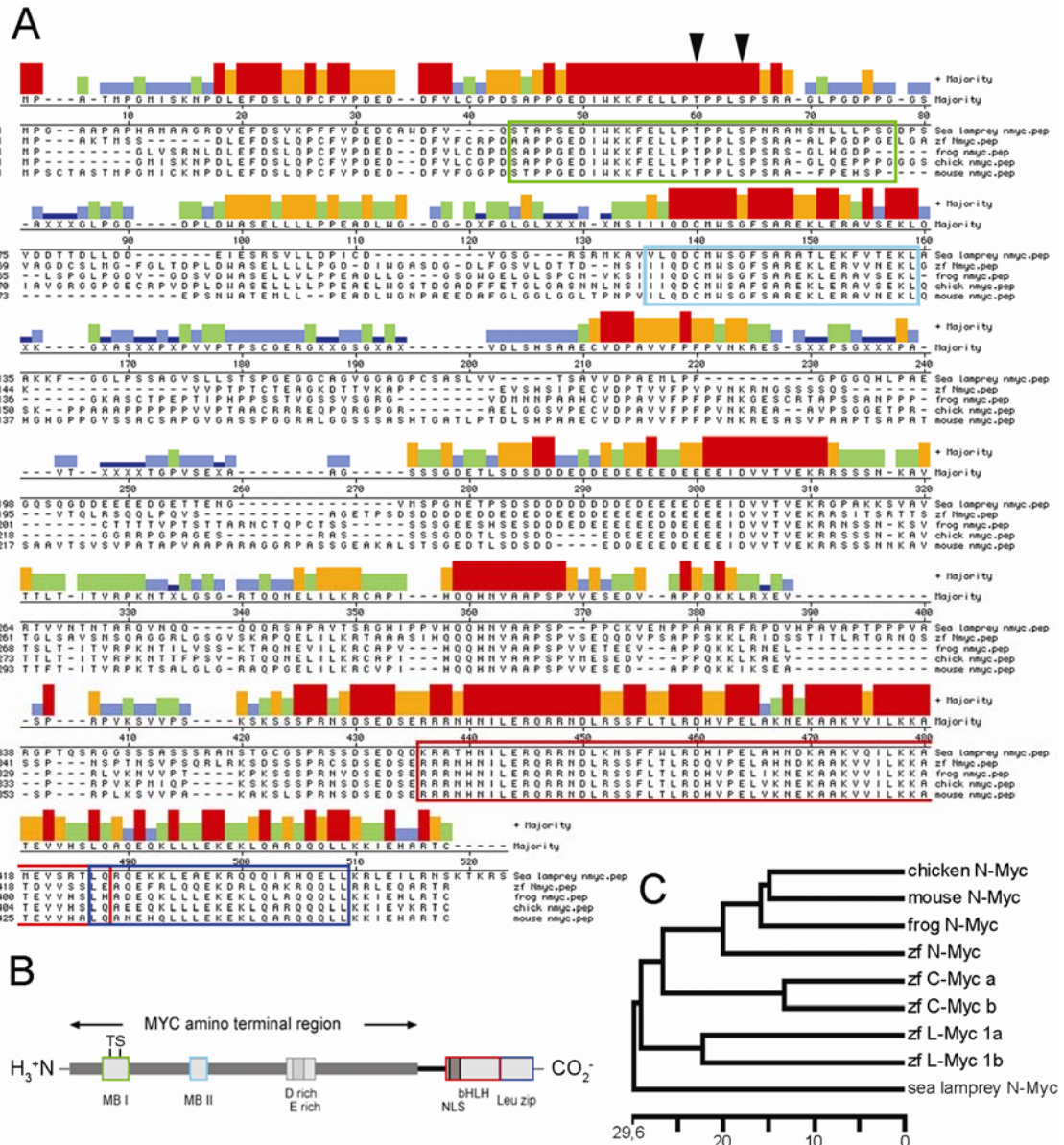


Fig. 17: Sequence analysis of *zf nmyc*. (A): Alignment of the putative zebrafish N-Myc homologue and N-Myc proteins from representatives of other vertebrate phyla (clustalW method). The degree of sequence identity is indicated by the coloured bars. Coloured boxes depict specific MYC domains, as shown also in (B). Arrowheads show highly conserved phosphorylation sites within the MB I domain. (B): A schematic drawing of the protein and its domains. The data set underlying the drawing was achieved using motifscan (http://myhits.isb-sib.ch/cgi-bin/motif_scan). Abbreviations: MB I, MB II: MYC box I and II; D, E, T, S: one letter AA code; NLS: nuclear localisation site; bHLH: basic helix-loop-helix; Leu zip: leucine zipper. (C): Phylogenetic tree of MYC proteins from zebrafish and N-Myc proteins from representatives of vertebrate phyla (clustalW method). Length of horizontal lines reflects the relative distance of the protein sequences. Note that similarity of the N-Myc proteins reflects the evolutionary relationship of the species.

nmyc has a major impact on brain development by preventing differentiation of neuronal precursors and promoting cell expansion (Knoepfler et al., 2002). In GCPs, *nmyc* transcription is activated by SHH secreted by PCs, whereas turnover of the protein is regulated by IGF and PI3K (Hatton et al., 2006; Kenney et al., 2003; Kenney et al., 2004; Oliver et al., 2003). MYC proteins are known oncogenes whose activity widely influences cells: MYC proteins modify the chromatin by directing acetylation of histones (Frank et al., 2003; McMahon et al., 1998; McMahon et al., 2000); they activate the transcription and translation machinery (Arabi et al., 2005; Cowling and Cole, 2007; Grandori et al., 2005) and also directly regulate transcription (Knoepfler et al., 2006).

Preliminary results demonstrated *nmyc* expression in the zebrafish cerebellum (R. Köster, personal communication). Interestingly, it was found that *nmyc* is expressed as early as 32 hpf, considerably before the time point at which GCPs are emigrating from the URL. Hence, the question arose which progenitors other than GCPs express *nmyc* at these early stages. In light of the proto-oncogenic properties of MYC proteins, such progenitor cells could provide an alternate source for malignancies such as medulloblastoma.

At the beginning of this study, only the 5' end of *zf nmyc* was available (Schreiber-Agus et al., 1993). In order to obtain the full length cDNA, the lacking 3' end was cloned by 3-prime RACE-PCR and TOPO-cloning. The full length cDNA was then constructed by cloning the 5' and 3' ends together, making use of an internal restriction site. *In-silico* analysis of the deduced amino acid sequence of the cloned cDNA using structural prediction databases displayed the presence of the conserved MYC domains (Fig. 17 B, A). Sequence comparison revealed a homology to other zebrafish *myc* genes of about 36% for the two *cmyc* homologues and 29% for the two *lmyc* homologues (Fig. 17 C). The sequence homology to *nmyc* genes of tetrapods was between 40 and 50% (*Xenopus laevis*: 49,2%, *Gallus gallus*: 49,4%, *Mus musculus*: 42,2%) while 33% to the *nmyc* homologue of the agnathan *Petromyzon marinus* (sea lamprey). The higher degree of homology to other *nmyc* genes of the osteichthyans phylum led to the conclusion that the cloned cDNA encodes for zebrafish *nmyc* rather than a member of the other *myc* subgroups. This finding was supported by a recent publication (Loeb-Hennard et al., 2005). The submitted sequence is identical on the AA level to that discovered in this study except for one additional AA within the E/ D-rich domain. While there are two homologues for each of *cmyc* and

lmyc in the zebrafish, up to now no second homologue of *nmyc* has been annotated in the zebrafish genome or could be found in the zebrafish genome by performing BLAST searches (status: ensemble release 48 of the zebrafish genome, 12/2007). In summary, comparison of the sequence of the obtained cDNA and analysis of the zebrafish genome revealed that the obtained cDNA encodes for the zebrafish homologue of N-Myc.

The isolated full-length cDNA of *nmyc* served as a template for PCR mutational approaches to establish variants of the *nmyc* gene for functional studies. MYC proteins contain highly conserved threonine and serine residues within the MB I domain (Fig. 17 A, B). Phosphorylation of these two residues has a major impact on the half-life of the protein, since this modification marks the protein for proteasomal degradation (Kenney et al., 2004; Niklinski et al., 2000; Sears et al., 2000). In order to study gain-of-function of N-MYC, a variant that is constitutively active due to its protection from degradation was constructed by targeted point mutagenesis. For this purpose, single bases of the cDNA were modified, which resulted in an exchange of the conserved threonine 49 (T49) and/or serine 53 (S53) to an alanine residue. Moreover, dominant negative variants of the cDNA were constructed to achieve an N-Myc loss-of-function approach. The MYC proteins contain two sites through which they bind their various interaction partners, the MB II domain and the leucine zipper domain. If one of these domains is removed, the truncated variant of the protein will still attach to a couple of interaction partners through the remaining binding site. Because these ligated proteins are no longer available to bind to the endogenous WT-form of the protein, expression of such dominant-negative variants leads to a functional loss of the MYC-protein. The leucine zipper was removed through PCR by introducing a stop codon 5 prime to this binding domain. In an alternative approach, the MB II domain was removed by targeted deletion of the entire region. These variants already were previously established with *myc*-homologues from other model organisms and have been demonstrated to mediate gain-of-function and loss-of-function (Brough et al., 1995; Kato et al., 1990; Kenney et al., 2003; Kenney et al., 2004; MacGregor et al., 1996; McMahon et al., 1998; Niklinski et al., 2000; Sears et al., 2000; Stone et al., 1987).

3.2.2. Expression of *nmyc* in the developing cerebellum

nmyc expression was previously detected in the retina, midbrain, posterior hindbrain, the spinal cord, in the endoderm and its derivatives as well as in branchial arches (Loeb-Hennard et al., 2005 138). To determine at which stages and in which cells *nmyc* is expressed in the developing zebrafish cerebellum, the expression pattern of *nmyc* was further investigated by ISH. At 24 hpf, *nmyc* expression in the cerebellum was confined to ventral areas of the cerebellum (Fig. 18 A). Expression in the embryonic cerebellum of *nmyc* was maximal at 32 hpf; at this stage, *nmyc* was expressed across the width of the cerebellum (Fig. 18 B). This was followed by the retraction of the *nmyc* expression domain to the posterior border of the cerebellum primordium at 48 hpf (Fig. 18 C). At 4 and 7 dpf, *nmyc* mRNA was detected along the lca of the cerebellum. *nmyc* mRNA was also present in a prominent proliferative zone of the cerebellum termed the rct (“rostral cerebellar thickening”, (Mueller and Wullimann, 2002; Wullimann and Knipp, 2000)), which gives rise to the vavula.

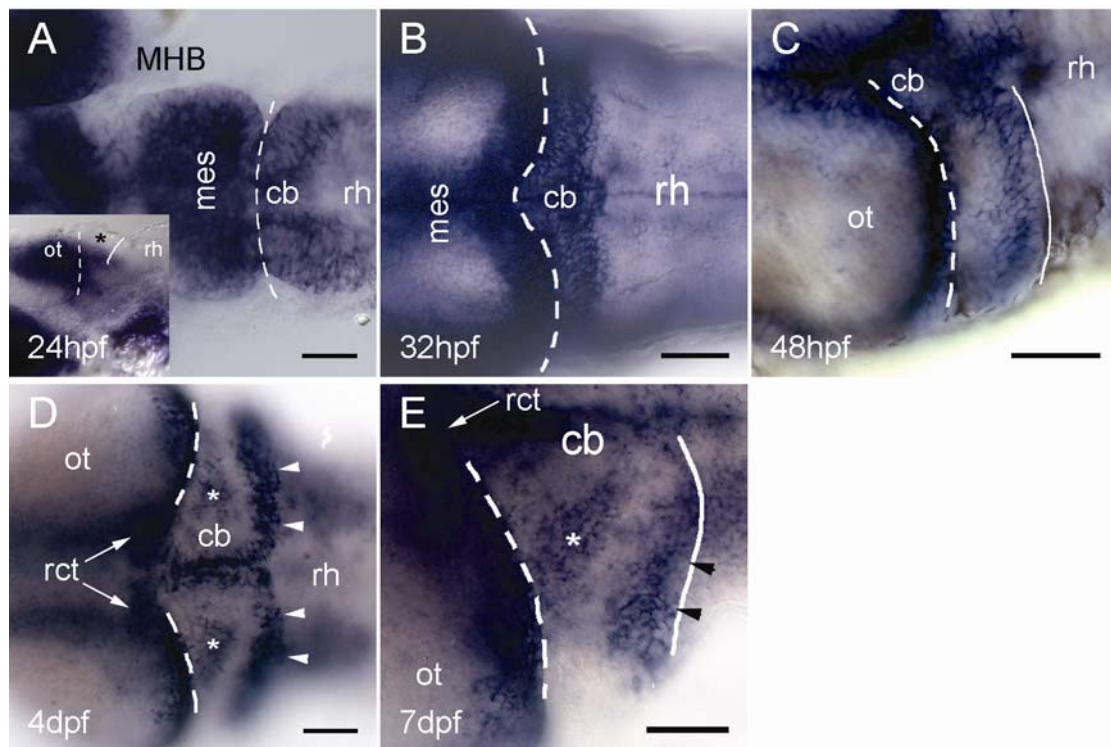


Fig. 18: Expression of *zf nmyc* in the developing cerebellum. Expression of *nmyc* revealed by in situ hybridization with a digoxigenin-labelled antisense riboprobe on whole mount embryos (A-C) and whole mount brains (D, E). Anterior left; dorsal views except inset in (A), lateral view; stages indicated bottom left of each panel. Scale bars: 50 μ m each. Asterisk in the inset in (A) indicates the absence of *nmyc* RNA in the dorsal cerebellum. Asterisks in (D) and (E) indicate *nmyc* expression in the cce. Arrowheads point to *nmyc* expression domain at the posterior border of the cerebellum, arrows highlight the rct (rostral cerebellar thickening). cb; cerebellum; mes: mesencephalon; ot: optic tectum; rh: rhombencephalon.

Furthermore, *N-myc* expression was detected in the centre of the forming cce (Fig. 18 D, E, white asterisk) and along the dorsal midline.

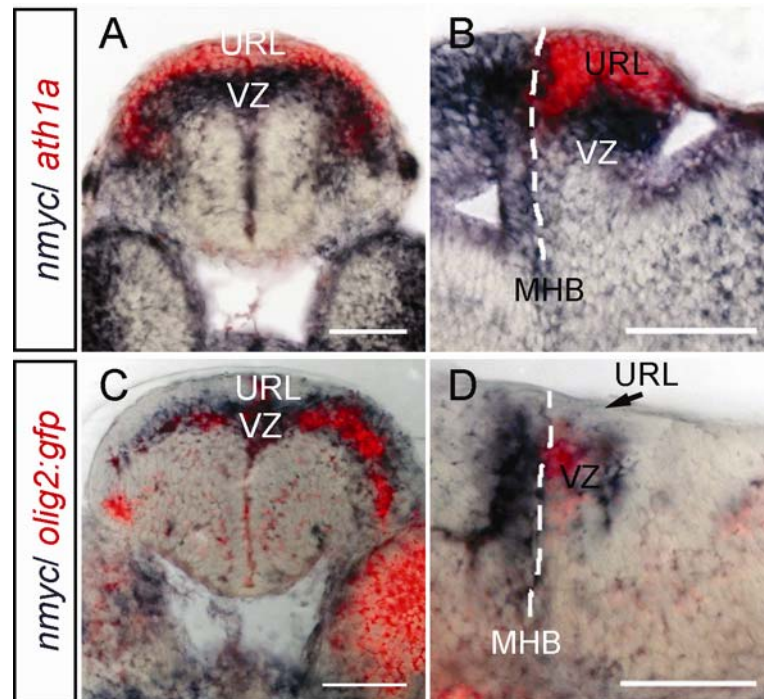


Fig. 19: Dorso-ventral localisation of the cerebellar *nmyc*-expression domain at 32 hpf. DISH was performed on whole Tg [*olig2*:GFP] embryos using antisense probes as indicated. Afterwards, specimens were sectioned on a vibratome transversally (A, C) and sagittally (B, D) (thickness: 25 μ m). The illustrations are a montage of the transmitted light picture and the corresponding fluorescent image, making use of the fluorescent properties of the fast red dye. (A, B): *ath1a* and *nmyc* form two distinct abutting expression domains in the cerebellum primordium. (C, D): *gfp* expression driven by the *olig2* enhancer widely overlaps with that of *N-myc* mRNA. Scalebars: 50 μ m; magnification: 40 fold. MHB: midbrain-hindbrain boundary; URL: upper rhombic lip; VZ: ventricular zone.

nmyc expression in the cerebellum at 32 hpf was detected in ventral regions. In other model organisms, *nmyc* has been demonstrated to stimulate proliferation in GCPs, which in contrast are derived from the dorsally located URL (Kenney et al., 2004; Oliver et al., 2003). To further clarify in which of the cerebellar precursor cells *N-myc* is expressed at the early cerebellar differentiation stages, double in situ hybridisation was performed using *ath1a* and *gfp* expression in Tg [*olig2*:GFP] embryos as markers for the URL and the ECP population, respectively, followed by vibratome sectioning. At 32 hpf, *nmyc* expression was absent in the URL, since co-expression with *ath1a* could not be detected (Fig. 19 A, B). Instead, the expression domains of *olig2*-enhancer driven *gfp* and *N-myc* showed overlap to a wide extent (Fig. 19 C, D). The expression domain of *N-myc* did not exceed the *olig2* domain further ventrally where the VZ marker *ptfla* continues to be expressed (see Fig. 4), thus showing that *N-myc* is not transcribed in the entire VZ but restricted to the

forming ECP population. Interestingly during this developmental stage ECPS have been found to go through their major phase of proliferation.

3.2.3. HH-signalling activates *nmyc* transcription at late cerebellum differentiation stages

HH signalling activates *nmyc* expression in GCPs of the mouse (Kenney et al., 2004; Oliver et al., 2003), and is thus a good candidate for activating *nmyc* expression in the cerebellum of zebrafish. First, we examined the expression of the various zebrafish homologues of *hh*. In gnathostomes, there are three orthologous groups of *hedgehog* genes: *desert*, *indian* and *sonic hedgehog* (*dhh*, *ihh*, *shh*) with partially overlapping and redundant functions (Ingham and McMahon, 2001). It has been postulated that there are additional *hedgehog* genes in teleosts due to the genome duplication event during teleost evolution (Amores et al., 1998; Zardoya et al., 1996a; Zardoya et al., 1996b). To date, five zebrafish *hh* genes have been identified: two members of the *sonic hedgehog* group (*shh* and *tiggy winkle hedgehog*, *twhh*) (Egger et al., 1995), two members of the *indian hedgehog* group (*ihha*, *ihhb*) (Avaron et al., 2006; Currie and Ingham, 1996) and *dhh* (Avaron et al., 2006), which is the vertebrate *hedgehog* closest related to *Drosophila hedgehog*. cDNAs of these five different zebrafish *hh* homologues were used to generate dig-labelled antisense probes for ISH. Also, the mRNA expression of the Hedgehog receptors *patched1* (*ptc1*) and *ptc2* and *smoothened* (*smo*) was analysed (Concordet et al., 1996; Varga et al., 2001). Two stages were investigated: 32 and 36 hpf (Fig. 20), which correspond to the first peak of *nmyc* expression, and 4 dpf, when *nmyc* expression is restricted to putative postembryonic proliferative cell pools (Fig. 21). Expression of *shh* and *twhh* (also referred to as *shh b*), which are known to have a major influence on the proliferation of EGL cells in the mouse cerebellum, was clearly absent from the cerebellum or neighbouring tissues (Fig. 20 A, B). *ihha* expression has only been reported for stages past 72 hpf (Avaron et al., 2006). While control experiments using a sense probe of the gene did not reveal any staining, the embryos labelled with antisense probe quickly developed a high degree of pale blue staining throughout the embryo, making it difficult to discriminate between background related to prolonged staining and low level transcription. To come to a conclusion though, subsets of embryos were exposed to variable staining intervals. At 32 hpf *ihha* mRNA was detected in the paraxial mesoderm, the eye and the fin buds. Additionally, *ihha* was asymmetrically present in

regions ventral to the somites, probably confined to the developing liver (Fig. 20 C, C'). In other model organisms, *ihh* was reported to act on the development of the vasculature and the blood cells (Dyer et al., 2001), the heart (Zhang et al., 2001), the endochondral skeleton (Vortkamp et al., 1996) and also to influence left/right asymmetry (Meyers and Martin, 1999). No specific expression in the CNS was observable though. *dhh* mRNA was detected in the fin buds, in the eye and in zones bordering the somites. Moreover, similar to *ihha*, *dhh* mRNA was detectable in a widespread manner that are difficult to specify (Fig. 20 D, D'). *dhh* as well has been described to be transcribed in many tissues throughout the entire organism (Parmantier et al., 1999). Finally *ihhb* (\equiv *ehh*) has been reported to be expressed exclusively in the notochord (Currie and Ingham, 1996).

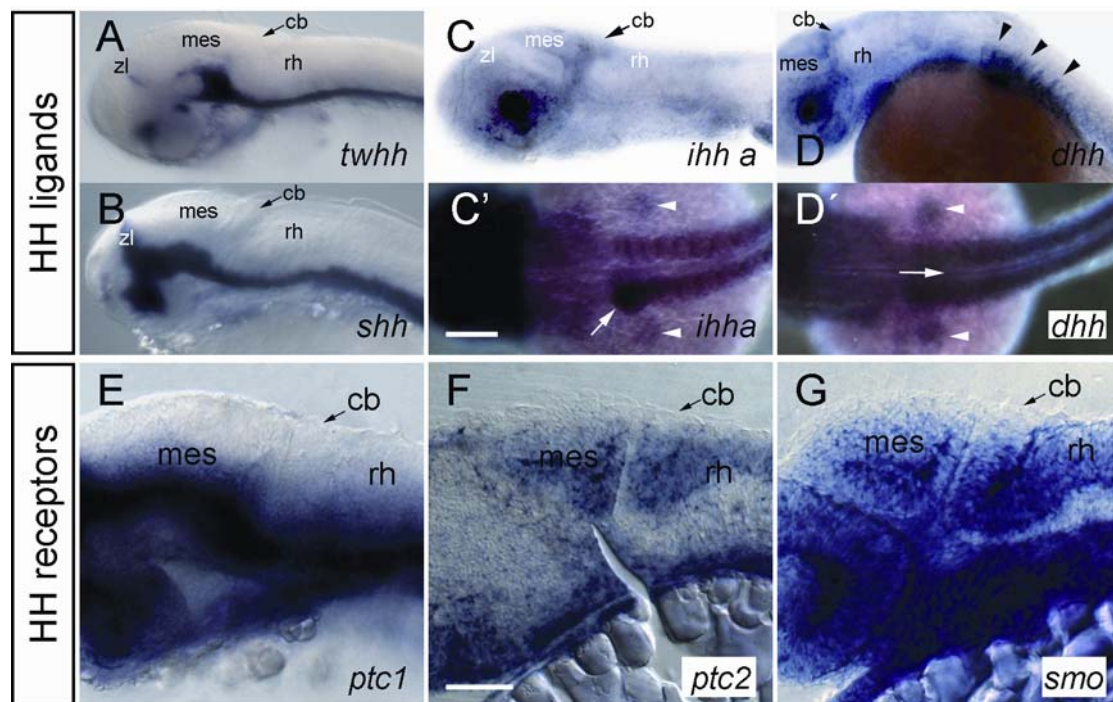


Fig. 20: Expression of components of the HH signalling cascade at the onset of neurogenesis in the cerebellum. In situ probes as indicated in the bottom right of each panel. Anterior to the left. (A, B): Both ligands of the *shh* subgroup were absent from the cerebellum at 36 hpf. Lateral view. (C, C'): Expression of *ihha* in the liver anlage (arrow), the paraxial mesoderm and the fin buds (arrowheads) at 32 hpf. Note the absence of NBT dye in the notochord and the yolk, arguing for the specificity of the ISH signal. (D, D'): *dhh* mRNA in the fin buds (arrowheads) and at the somite borders (arrowheads in D) 32 hpf. Again note absence of dye from the notochord (arrow) and yolk. (E-F): *ptc2* and *smo* are expressed in the ventral cerebellum at 32 hpf. In contrast, *ptc1* is absent at 36 hpf. (A-E): whole mount preparations; (F, G): sagittal vibratome sections (25 µm) after performing whole mount ISH. Magnification: 20x except in F, G: 5x binocular in C' and D'. Scalebars: 100 µm in C' for A to D, 50 µm in F for E to G. cb: cerebellum; mes: mesencephalon; ot: optic tectum; rh: rhombencephalon; zl: zona limitans.

To estimate the ability of cerebellar tissue to respond to HH signalling, expression of HH receptors was also examined. While *ptc1* expression was absent from the cerebellum (Fig. 20 E), mRNA coding for *ptc2* and the co-receptor *smo* was detectable in ventral parts of the cerebellum (Fig. 20 F, G). It is noteworthy though that *smo* mRNA was detected almost ubiquitously in the zebrafish embryo, possibly due to its role in transmitting the signal of all five HH ligands.

At 4 dpf, both *ptc1* and 2 and *smo* were found to be expressed in posterior regions of the lca of the cerebellum (Fig. 21 B-D), where also *nmyc* mRNA was localised (Fig. 18 D). Thus, cells of this caudal *nmyc* domain may be competent to respond to HH signalling. In addition, *shh* expression could be detected in two small domains in the dorsomedial parts of the cerebellum (Fig. 21 A). Their position in the cerebellum suggests that these *shh*-expressing cells are PCs.

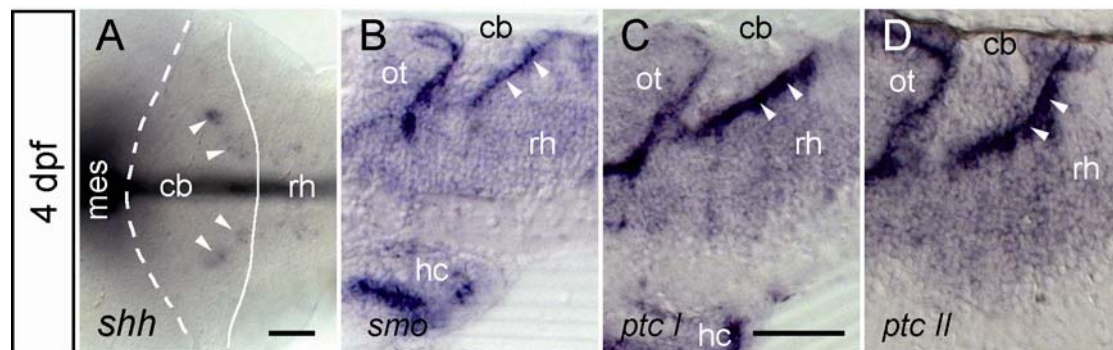


Fig. 21: Key components of the HH signalling pathway are present in the 4 dpf cerebellum. ISH for genes as indicated in the bottom left of each panel. Anterior to the left. (A): Whole mount preparation, dorsal view. (B-D): Sagittal vibratome sections (25 µm) after performing ISH. Magnification: 20x. Scalebars: 50 µm in A, 50 µm in C for B to C. cb; cerebellum; hc: caudal hypothalamus; mes: mesencephalon; ot: optic tectum; rh: rhombencephalon.

To determine whether *nmyc* expression is regulated by HH signalling, two independent approaches were performed. The *slow muscle omitted* mutant line (*smu*) carries a mutation in the *smoothened* gene that results in a loss-of-function variant of the receptor (Barresi et al., 2000; Varga et al., 2001). To obtain *smu*^{-/-} embryos, heterozygous carriers were mated in sibling crosses. Homozygous mutant embryos were sorted at 24 hpf based on the characteristic phenotype which becomes apparent by the bulky U-shaped somites, the ventral body curvature, the smaller-sized ventral forebrain and the reduced interocular distance (Varga et al., 2001). In agreement with the absence of transcripts for HH ligands in the cerebellum, an effect on the expression of *nmyc* was not observed when *smu*^{-/-} embryos were processed for ISH at 32 hpf (Fig. 22 A). Although up to now a second *smo* homologue has not been

identified in the zebrafish genome, a putative *smo2* may compensate the loss of *smo* in cerebellar HH-signalling. Therefore, a second approach was followed to block HH signalling by using the inhibitor cyclopamine, which is an alkaloid known to block signal transduction by the SMO protein (Frank-Kamenetsky et al., 2002; King, 2002). Cyclopamine was added to the embryo media at a final concentration of 100 nmol/ml in two parallel experiments at midblastula stage and at 20 hpf, thus controlling for secondary effects upon early loss of SMO activity. The effectiveness of cyclopamine was ascertained by phenocopy of the *smu* phenotype. As a control, the same volume of the solvent DMSO was added to two groups of embryos at midblastula stage and 20 hpf, respectively. Similar to the *smu* mutants, expression of *nmyc* in the cerebellum was unaffected at 32 hpf in embryos treated with cyclopamine (Fig. 22 B, C).

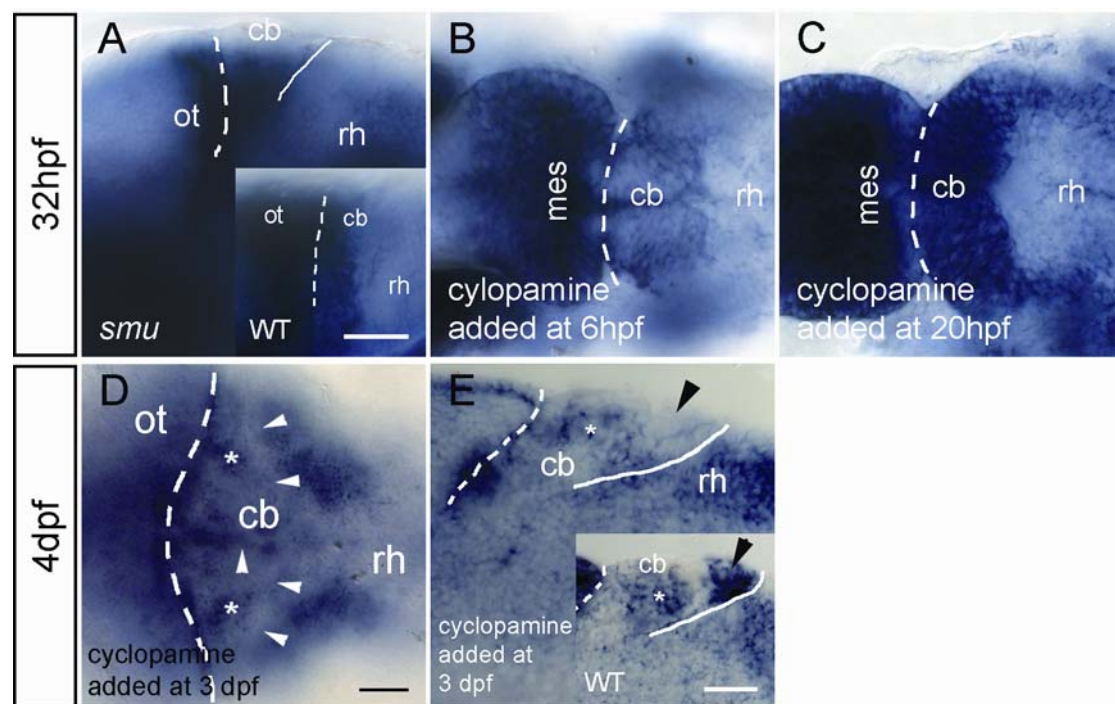


Fig. 22: Effect of loss of HH-signalling on *nmyc* expression. (A): ISH for *nmyc* on homozygous *smu*- mutant embryos. The inset shows a WT embryo for comparison. (B-E): ISH for *N-myc* was performed on embryos treated with cyclopamine at the indicated time points. (A-D): Whole mount preparations. (A): Lateral view; (B-D): Dorsal view. (E): Sagittal vibratome sections (25 μ m), inset: WT preparation for comparison. Arrowheads in D and E point towards domains in which *N-myc* expression is downregulated upon blocking HH signalling. Asterisks label areas in which cyclopamine treatment reveals no effect on *N-myc* expression. Compare (D) to Fig.18 D. Scale bars: 50 μ m in A for panels A to C, 50 μ m in D and, 20 μ m in E. cb; cerebellum; mes: mesencephalon; ot: optic tectum; rh: rhombencephalon.

In contrast, treatment of embryos with cyclopamine at 3 dpf led to a loss of *nmyc* expression in the posterior expression domain of the cerebellum at 4 dpf. *nmyc* expression was affected only in the regions where expression of HH receptors had

been detected (compare Fig. 21 B-D with Fig. 22 D, E), while still being present in cells of the cce and the rct despite cyclopamine treatment (Fig. 22 D, E). Similar results were achieved when 6 dpf larvae were treated with cyclopamine and processed for ISH the following day (not shown). Control embryos with solvent treatment only (1% DMSO) were indistinguishable from WT-embryos with respect to morphology and *nmyc* expression.

In summary, the cDNA encoding the zebrafish homologue of *nmyc* was isolated. This cDNA served as a template to create loss- and gain-of-function variants of *nmyc* for future studies regarding N-Myc function. The expression pattern of *nmyc* revealed its transcription to occur in a two phase mode. During a first phase between 24 hpf and 48 hpf, *nmyc* is expressed in a subset of the VZ of the cerebellar anlage, as indicated by the co-expression of *nmyc* and *olig2* at 32 hpf. At larval stages, *nmyc* expression appears again in distinct regions of the cerebellum, as *nmyc* mRNA was detected in the rct, the cce and the lca at 4 and at 7 dpf. Only at this time, HH regulates *nmyc* expression in the lca. These findings suggest additional roles of N-Myc during cerebellum development than solely regulating GCP proliferation.

4. Discussion

4.1. *olig2*: a potential regulator of neurogenesis in the zebrafish cerebellum

4.1.1. A comparative view on ECs and DCN neurons

Phylogeny of ECs and DCN neurons

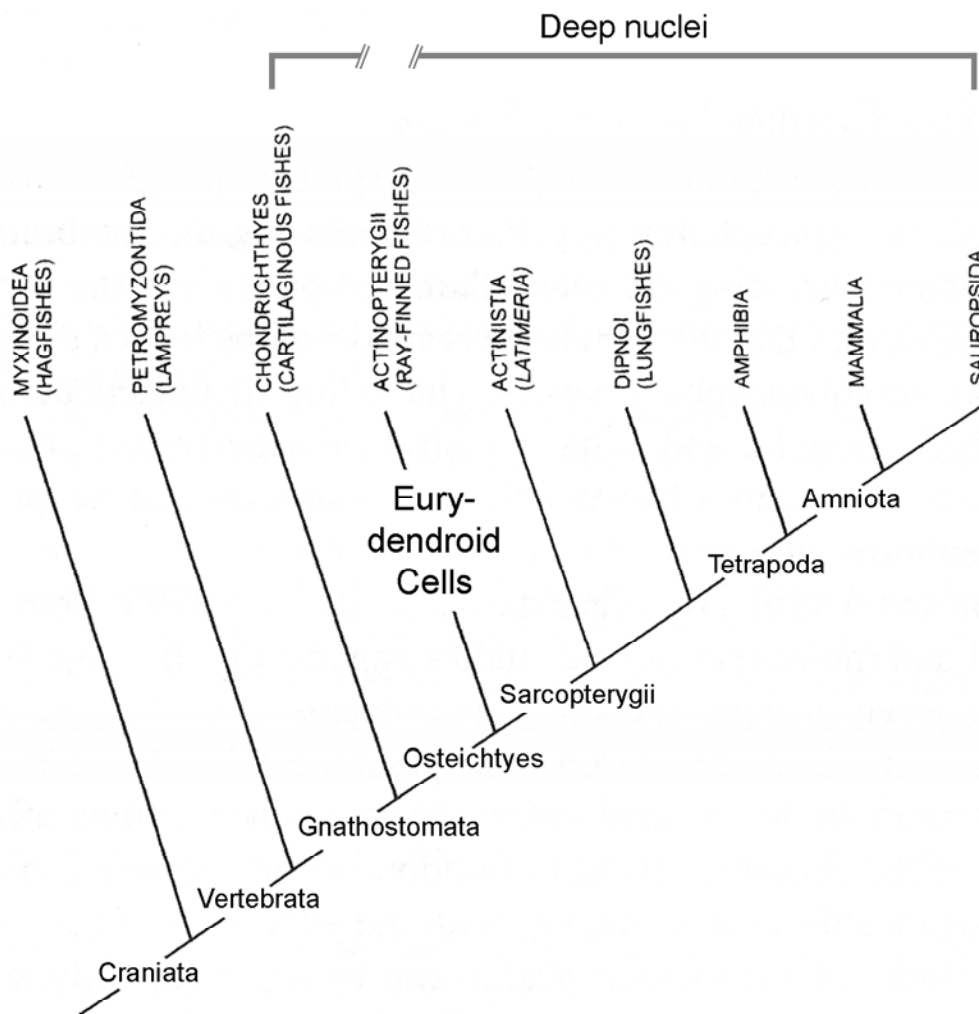


Fig. 24: Phylogeny of cerebellar efferents. Occurrence of a true cerebellum is restricted to jawed vertebrates (Murakami et al., 2005). Only the ray-finned fishes bear ECs, while the efferents of tetrapods and cartilaginous fishes are organised as nuclei. Modified from (Wullimann, 1998).

ECs are the teleosts' equivalent of the DCN of other gnathostomes (jawed vertebrates). Considering the neurophysiology of the EC network, they function equivalently to DCN efferents to the extent that both EC and DCN neurons project to

homologous territories within the CNS (Wulliman et al., 1996). T. Finger (Finger, 1978) considers the presence of efferent neurons innervated by PCs as the initial evolutionary situation rather than a convergent evolution, regardless whether efferents are organised in nuclear structures or as ECs. In fact, chondrichthyes (cartilaginous fish) as well as tetrapods harbour nuclear structures that provide the cerebellar output instead of ECs (Alvarez-Otero et al., 1996; Meek, 1992; Murakami et al., 2005; Nieuwenhuys, 1967). Noteworthy, the chondrichthyes clade separated from the osteichthyes (actinopterygii and sarcopterygii) before sarcopterygii (coelacanth, lungfish and tetrapods) evolved from the actinopterygii (ray-finned fishes). Hence organisation of cerebellar efferents in nuclear structures appears plesiomorphic, while allocation of the efferents, i.e. the EC, along the PCL seems apomorphic (Fig. 24).

Subsets of ECs express *olig2*

olig2 is a known key regulator of neuron specification and was shown in this thesis to be expressed in the cerebellum from embryonic stages onwards. The onset of expression coincides with the expression of the two prominent fate determinants in the cerebellum, *ath1a* and *ptfla*. To determine the cell type that arises from the *olig2* domain, co-expression of *olig2* with these known marker molecules was studied with the result that *olig2* and *ptfla* are co-expressed at 36 hpf. The neuronal identity of the precursors was revealed by the co-expression of HuC in *olig2*-expressing cells, co-expression of *vglut2.1* and the concomitant absence of glial marker expression. Furthermore, *olig2*-expressing precursors developed typical morphological features of neurons: widespread dendrites and long protruding axons. Despite the morphological similarities, it was ruled out that *olig2*-expressing precursors are designated to become PCs or a subset of PCs since co-expression of *olig2* and any of the PC markers tested could not be observed. Finally, the efferent character of these cells led us to define *olig2*-expressing neurons as ECs. Retrograde labelling in 7-day-old larvae revealed that at least subsets of *olig2*-expressing neurons project towards the contralateral half of the ventral mesencephalon (Fig. 10). The finding that not all ECs were retrogradely labelled may be a technical issue as not all EC axons may come into contact with the DiI crystal. It is also known that ECs innervate various brain regions. Hence application of DiI in one projection areal will miss projections in other brain regions. Noteworthy, not all of the cells labelled by the injected dye also contained *olig2*-promoter driven GFP. Absence of GFP fluorescence in DiI labelled cells may be due

to downregulation of *olig2*-promotor driven GFP expression after ECPs are finally established, as the transcription of proneural genes such as *ath1a* and *ptfla* terminates at around 2 dpf. Expression of *olig2* however persists up to adulthood, and it thus seems likely that ECs express *olig2* throughout their whole life span. This suggests that *olig2* expression is restricted to a subset of ECs.

DCN neurons, the equivalent of ECs in other species, similarly form a diverse group in terms of their morphology, their interconnections and their neurotransmitter phenotype. They have been classified into at least three subgroups: large glutamatergic neurons that innervate regions outside of the cerebellum, large GABAergic neurons that project to the ION and small GABAergic interneurons (Leto et al., 2006; Sultan et al., 2003). By definition, all efferents from the cerebellum are referred to as ECs, despite a wide variance in morphology and projection targets in the CNS. Indeed some recent publications use the more general term “efferent cells” instead of Eurydendroid Cells (Han et al., 2006; Shi et al., 2008). The heterogeneity of EC subtypes may be reflected by the divergence of expressed genes, such as *olig2*.

Properties of ECs in comparison to DCN neurons

Beyond their neurophysiological similarities, the morphology of DCN neurons and ECs bear substantial resemblances. ECs are multipolar projection neurons with tufted dendrites. DCN neurons have been classified into two major subgroups: “isodendritic” and “idiiodendritic”, with the first group consisting of neurons of a symmetric shape with dendrites that radiate in all directions and branch out to overlap with neighbouring nuclei; the second category is characterised by a polar shape with widely bifurcated dendrites and axons leaving their vicinity. The observed morphology of *olig2*-expressing cells displayed a striking similarity to that of the idiiodendritic DCN neurons described by Sultan and colleagues (Sultan et al., 2003).

Further studies addressing the molecular properties of ECs displayed homologies and differences between ECs and DCN neurons. ECs of the adult goldfish and subsets of the DCN neurons have been described to be immunoreactive for unbound L-Asp (Chen and Hillman, 1993; Ikenaga et al., 2005; Miranda-Contreras et al., 1999), which probably acts as a neurotransmitter (Bradford and Nadler, 2004; Gundersen and Storm-Mathisen, 2000; Kimura et al., 1985). However, cells immunoreactive for L-Asp could not be detected throughout the entire zebrafish CNS at 4 dpf in this study. Positive reactivity in chondrocytes of the notochord rules out a simple failure of the

IHC procedure. The role of unbound L-Asp as a neurotransmitter is under debate. L-Asp specifically activates post-synaptic NMDA receptors (Curras and Dingledine, 1992). Most of the postsynaptic current however is generated by non-NMDA receptors, which are insensitive for L-Asp; L-Asp thus might be involved in the NMDA receptor-dependent type of long-term potentiation or might trigger metabolic events in the brain (Gundersen and Storm-Mathisen, 2000). Perhaps not all of the properties of CNS neurons are yet fully developed at the larval stage in the zebrafish. Noteworthy, presence of unbound L-Asp does not exclude the presence of other neurotransmitters in an individual cell, regardless whether it is an excitatory or inhibitory neuron, i.e. presence of L-Asp does not exclude an excitatory glutamatergic phenotype (Chen and Hillman, 1993; Gundersen, 2008). Whether EC or other cells of the CNS are immunoreactive for L-Asp at alter stages should therefore be elucidated. Such studies should also investigate the expression of mRNA coding for NMDA receptor components in cells that are innervated by ECs.

Calretinin is an established marker of ECs (Castro et al., 2006; Diaz-Regueira and Anadon, 2000). In co-labelling experiments of this study, a wide overlap of α -Calret immunoreactivity and *olig2* expression was observed. DCN neurons of the mouse have been shown to express *calret* as well (Abbott and Jacobowitz, 1995; Rogers, 1989). In more detailed studies, the small GABAergic DCN interneurons were found to express Calretinin (Leto et al., 2006). By contrast, other laboratories regard Calretinin as a marker for glutamatergic DCN neurons, because Calretinin-immunoreactive DCN neurons were still detectable in *ptfla* knock-out mice. Because development of GABAergic neurons is *ptfla* dependent, the cerebellum of such mutants consequently should completely lack GABAergic neurons (Hoshino et al., 2005). Calcium binding proteins such as Calbindin, Calretinin and Calmodulin share a high degree of AA conservation. The cross-reactivity and lack of specificity of antibodies against Calcium binding proteins is a serious concern. For example, Schiffmann and colleagues detected Calret-immunoreactive cells even in *calretinin* knock-out mice (Schiffmann et al., 1999), and a study that addressed “Calretinin-like immunoreactivity in mormyrid and gymnarhid electrosensory and electromotor systems” reported pronounced cross-reactivity of Calbindin and Calretinin on the one hand and antisera against both proteins on the other hand (Friedman and Kawasaki, 1997). Various suppliers offer antibodies against Calretinin. In the present study, the antibody to detect Calretinin was provided by Chemicon (rabbit α Calretinin (guinea

pig), AB 149). Calb was detected using an antibody provided by Swant (rabbit α Calb (rat), Swant, CB 38). To examine the specificity of the antibodies used, cDNAs of both *calretinin* and *calbindin* were cloned by RT-PCR. Both cDNAs were subcloned into an expression vector and were transfected into HEK/T 293 cells. Western blot analyses of cell extracts using the various antibodies against Calretinin and Calbindin are being conducted and should identify more clearly the recognised epitope(s).

Because subsets of the DCN neurons are glutamatergic, it has been discussed that some ECs also use glutamate as a neurotransmitter (Ikenaga et al., 2005). *Olig2*-expressing ECs were found to express *vglut2.1*, which proves the glutamatergic phenotype of ECs (Fig. 8). The large projection neurons of the DCN express *vglut2* as well (Fink et al., 2006; Hisano et al., 2002). This finding shows that EC and DCN neurons share both neurophysiological properties and molecular features.

Is *olig2* a marker of DCN neurons?

The examination of molecular properties shared between EC and DCN neurons finally lead to the question of whether *olig2* is also labelling DCN neurons of other vertebrates. Up to now, a single publication addresses the effect of loss of *olig2* function on the development of the cerebellum, although without further commenting on the expression pattern of *olig2* in the cerebellum (Takebayashi et al., 2002). Intriguingly, *olig2* enhancer-mediated conditional expression of β -Galactoidase reveals *olig2* expression in the mouse cerebellum at E12,5 (Masahira et al., 2006). In addition, two gene expression databases report the expression of *olig2* in the cerebellum of developing mice embryos (Gong et al., 2003; Heintz, 2004; Magdaleno et al., 2006). In particular, *olig2* expression is found at E15.5 in regions resembling the NTZ, which is a transient differentiating zone that gives rise to the DCN. The time point as well as the localisation of *olig2* expression in the developing mouse cerebellum is in good agreement with expression of *olig2* in putative DCN neurons and their precursors.

DCN neurons were demonstrated to be URL-derived and dependent upon *math1* for proper development (Machold and Fishell, 2005; Wang et al., 2005). Fink *et al.* (2006) showed that these URL-derived DCN neurons are glutamatergic based on co-expression of *vglut2* and the DCN marker genes *tbr1* and *tbr2* (Fink et al., 2006). Previous works, in which clonal progeny of the URL was labelled in a mosaic manner, found occasional co-labelling of DCN and EGL or IGL neurons, suggesting

that the URL may not be the only source of DCN neurons (Lin et al., 2001; Mathis et al., 1997). Thus, Wang and colleagues conclude that “although some DN (=DCN neurons) share *math1* dependence with the granule neurons and migrate from the same region, they may still derive from different progenitors” (Wang et al., 2005). In another approach, the fate of VZ-derived cells was studied by making use of an inducible Cre-recombinase driven by regulatory elements of the proneuronal gene *ascl1/mash1* (*achaete-scute complex-like 1*, previously *mouse achaete scute homologue 1*) (Kim et al., 2008). Here, the authors found that DCN neurons that express *pax2*, which labels GABAergic neurons (Maricich and Herrup, 1999), are progeny of the VZ. In mice, V. Chizhikov and colleagues identified a population of cells that express *lmx1a* in a region they termed c3. The topology of the c3 domain resembles that of the NTZ. Neurons in the c3 domain contain a huge cell body, co-express Calret and do not express GABA, suggesting that at least some of the large glutamatergic DCN express *lmx1a*. However, *lmx1a*-expressing neurons do not originate from the rhombic lip migratory stream as they lack co-expression of lacZ and *lmx1a* in transgenic *math1*^{lacZ/+} embryos (Chizhikov et al., 2006). The authors hence suggested that progenitors located in the c3 domain could give rise to a previously unrecognized population of DCN neurons.

Future experiments studying co-expression of *olig2* and markers of the divergent DCN neurons should help to further assess homologies of ECs and DCN neurons. In addition, molecular homologies could reveal whether *olig2*-expressing ECs have a counterpart among DCN neurons in mammals and, if so, to which of the DCN neuron subclasses are ECs equivalent. For instance, the epitope of mAb Smi-32, *tbr1* and *tbr2* were described as molecular markers for the URL-derived large glutamatergic neurons (Fink et al., 2006; Hoshino et al., 2005). *ascl1/mash1* could be used as markers of VZ-derived DCN neurons (Kim et al., 2008), while *klc3* (*kinesin light chain 3*) was reported to label both glutamatergic and GABAergic DCN neurons (Chung et al., 2007) and thus could be used to depict *olig2*-expressing ECs and residual EC-populations. Finally, co-expression of *olig2* and *lmx1a* would strongly hint to a tight relationship of ECs and DCN neurons also on the molecular level.

4.1.2. *olig2*-expressing VZ-derived cells adopt the fate of glutamatergic projection neurons

Where it was shown that VZ-derived neurons differentiate into inhibitory GABAergic neurons in the mouse (Hoshino et al., 2005; Pascual et al., 2007), it was found in this study that *olig2*-expressing ECs are not immunoreactive for the key enzyme of GABA synthesis, GAD67, but instead express *vglut2.1*. This neurotransmitter phenotype is consistent with the loss of *ptfla* expression in EC precursors: cells that solely express *ptfla* were found to be GABAergic. While the entire *olig2* expression domain is a subdomain of the *ptfla* expression domain at 36 hpf (fig 5), the percentage of neurons co-expressing *ptfla*:GFP among neurons expressing *olig2*:dsRED decreased with ongoing brain differentiation from 81% at 54 hpf to 21% at 94 hpf. Three events could account for this observation: 1) after 54 hpf, there is an increase in the number of cells that express *olig2* and not *ptfla*. 2) The number of cells that solely express *olig2* after 54 hpf remains stable or decreases at a slower rate than does the number of cells expressing both genes, thus producing a relative decrease in the rate of co-expression. 3) Expression of both genes is terminated after 54 hpf, but GFP may have a longer half-life such that it is still detectable at 94 hpf, while dsRED protein is degraded more rapidly.

The evaluations of the net numbers of cells expressing *olig2* and both *olig2* and *ptfla* revealed that a net increase of *olig2*:dsRED expressing cells as well as a decline in the number of cells co-expressing *olig2*:dsRED and *ptfla*:GFP account for the overall decline of double positive ECPs at 94 hpf. It should be noted that maturation time of dsRED protein by far exceeds that of GFP (Verkhusha et al., 2001). Therefore, fluorescent mature dsRED protein occasionally reports transcription that has been activated already some time before. In this study, GFP fluorescence in Tg [*olig2*:GFP] embryos was detectable from 36 hpf on, while dsRED fluorescence could be observed only from 48 hpf onwards in Tg [*olig2*:dsRED] embryos. Red fluorescent cells that appear after 54 hpf thus might have initiated expression of *olig2* already about twelve hours before. Such cells probably do not co-express *ptfla* and thus could cause the accumulation of ECPs exclusively expressing *olig2*. Moreover it appears unlikely that the half-life of dsRED is shorter than that of GFP in zebrafish embryos and that a shortened half-life of dsRED caused the observed findings: In various cultured cells the half-life of GFP has been estimated to be around 24 h (Corish and Tyler-Smith, 1999; Verkhusha et al., 2003), while the half-life of dsRED has been

estimated to be 4,6 days (Verkhusha et al., 2003). Taken together it appears that expression of *ptfla* becomes actively downregulated in ECPs. In late born ECPs *ptfla* transcription seems not be initiated at all.

The *lmx1a*-expressing neurons of the c3 domain contribute to the DCN, but express neither *math1* nor *ptfla* (Chizhikov et al., 2006). In the URL, glutamatergic identity is induced by BMPs and GDF secreted from the roof plate (Alder et al., 1996; Chizhikov et al., 2006; Krizhanovsky and Ben-Arie, 2006), and *ptfla* is thought to prevent neuronal precursors from responding to such dorsalising signals, thereby abolishing expression of BMP-induced targets such as *math1*, *zic1/2* and *reelin* (Pascual et al., 2007). In the spinal cord, *olig2* specifies a subset of the p2-domain to form the pMN domain. Upon loss of *olig2*, V2 interneurons are found at the expense of pMN motoneurons. After neurogenesis is completed, loss of *olig2* causes the specification of astrocytes at the expense of oligodendrocytes (Lu et al., 2002; Park et al., 2002; Park et al., 2004; Takebayashi et al., 2002; Zhou and Anderson, 2002). Furthermore, it was demonstrated that OLIG2 acts as a transcriptional repressor (Lee et al., 2005b; Marshall et al., 2005; Novitch et al., 2001). The development of ECs in the zebrafish cerebellum might be accomplished by a mechanism analogous to motoneuron development. Comparable to the ventral spinal cord, *olig2* is expressed in a subset of the cerebellar VZ. Cerebellar *olig2*-expressing cells may adopt a fate distinct from residual VZ-derived cells (glutamatergic projection neurons vs. GABAergic interneurons). Expression of *ptfla* ceases in cells that express *olig2* or is even blocked completely. The following scenario may explain the molecular events of EC development: ECs are born in the VZ, begin at 36 hpf to express *olig2*, which then represses *ptfla* transcription, thus antagonising *ptfla*-mediated inhibition of the competence to respond to environmental cues, probably BMP or GDF released from the roof plate. In this context-dependent manner, external signals could specify ECPs to acquire their characteristic properties.

4.1.3. Dynamics of EC behaviour

As observed in studies using confocal laser scanning time lapse microscopy, proliferative EC precursors oscillate along the apical-basal axis periodically from 36 to 44 hpf. Characteristically, cells undergo mitosis when having reached the apical lamina of the neuroepithelium. The two daughter cells then move back towards the centre of the neuroepithelium, whereas URL-derived cells move towards the MHB.

Such movements of proliferative neuronal cells synchronous to the phases of the cell cycle are termed interkinetic nuclear migration (INM) {Murciano, 2002 #255; Götz, 2005 #109; Baye, 2008 #250;}. Although INM is not obligatory for promoting any phase of the cell cycle, its loss has an impact on neuronal development by causing premature cell cycle exit. INM is thought to allow for an increased density of proliferative cells of various fates in the neuroepithelium while remaining attached to the apical lamina (Frade, 2002). Maintenance of the apical-basal polarity and, as a consequence, tightly controlled responses to fate determining cues within the neuroepithelium appear to be crucial for cell commitment and concomitant control over the number of cells specified (Baye and Link, 2008). INM thus might be involved in controlling the number of ECPs by regulating cell cycle exit.

One prerequisite for correct development of the CNS is the ability of neural precursors to migrate away from germinal zones to their destined position within the CNS. In principal there are two modes of neuronal migration: tangential migration, i.e. movements of the cells parallel to the apical and basal lamina, and radial migration, during which cells move perpendicularly to the laminae. Radial migration in turn occurs in two distinguishable modes: Glia-independent neurophilic “somal translocation” and glia-guided “locomotion” (Baye and Link, 2008; Nadarajah, 2003). The present study demonstrated that, directly after exiting the cell cycle, EC precursors migrate radially to end up at the centre of the MHB and further migrate tangentially towards ventro-lateral positions over average distances of about 3-5 cell diameters. Notably, radial glia as well as oligodendroglia are absent at this developmental stage in zebrafish (Rieger, 2008). This suggests that the observed migratory mode parallels somal translocation: ECs initiate migration by first extending a leading process towards antero-ventrally directions and subsequent translocate the soma towards the leading process. The mode of formation of the leading processes of the ECs is remarkable in two aspects: first, considering the length and the target of these processes, they already bear the characteristics of the axons of the terminally differentiated ECs. In this regard, the time point at which these efferents are established seems early since formation of the axon is initiated at around 44 hpf immediately after EC precursors stop to further proliferate. In comparison, other cerebellar neuronal precursors such as GC precursors do not emigrate from the URL before 50 hpf (Volkman et al., 2008). The first neurons being immunoreactive for ZebrinII as a marker of terminally differentiating PCs appear from 60 hpf onwards

(R. W. Köster, personal communication). Second, EC precursors extend the leading process towards ventral areas of the cerebellum along the MHB. This mode of protrusion is atypical because the leading process is projected tangentially rather than radially. The data presented cannot answer whether this takes place in combination with the bifurcation of the original apical attaching process or whether it is detached and then guided ventrally. Ongoing studies in our laboratory using subcellular markers might provide deeper insights into the cell biology of migration of ECPs (Martin Distel, personal communication).

An issue of growing interest is to follow how adult structures form from their embryonic anlagen. To get insight into how the efferents of the mature cerebellum are organised, several larval and juvenile stages of Tg [*olig2*:GFP] fish were analysed. ECs first settle predominantly in the anterior part of the cerebellum, while PCs are found in posterior parts of the cce. Additional *olig2*-expressing cells were found to be located in a medial position, lining the rhombencephalic ventricle at the posterior base of the cce. The morphology and the position of these cells suggests that they may correspond to a population of neuronal stem cells (NSCs) described by others (Chapouton et al., 2006; Grandel et al., 2006; Zupanc et al., 2005). At 3 mpf, ECs are distributed along the entire PCL and intermingle with PCs. One possible mechanism may be that, *olig2*-expressing NSCs at the caudal base of the cerebellum account for the ongoing generation of ECs. To get to their destined position within the tissue, such NSCs would need to migrate radially away from their ventricular position through the tissue of the cce in a similar manner as has been described for PCs. As shown in Fig. 17 D, E' and E'', such putative migratory cells are encountered frequently. Co-labelling of putative *olig2*-expressing NSCs with known stem-cell markers (such as PDGFR α , SOX-2, Prominin and Nestin, (Colak et al., 2008; Lee et al., 2005a)) and birthdating-studies in which proliferating cells are labelled by injected BrdU could provide evidence to this assumption. This model hence provides a testable hypothesis for a mechanism of ongoing EC generation in juvenile and adult fish.

4.2. Analysis of *nmyc* expression and its regulation by HH signalling

4.2.1. The proto-oncogene *nmyc* is expressed in both VZ and URL-derived cells

Medulloblastoma (MB) are the most frequent brain tumours of childhood and are highly malignant. Despite multimodal therapy with surgery, radiation, and chemotherapy, still one third of the patients suffering of it die within 5 years (Packer et al., 1999). Although there are several variants of MB, the majority are described either as “desmoplastic” MB, which accounts for 15-20% of all cases, or “classic” MB (75-80%) (Read et al., 2006). One major effort to understand the aetiology and pathology of tumourigenesis is to determine the cell of origin of a tumour (Vescovi et al., 2006). Thus, recent approaches aimed to correlate different types of MB with their origin from the different cerebellar germinal zones. In a simplistic view, desmoplastic MB express markers associated with EGL derived cells (*ath1*, *zic1*), while classic MB express markers of VZ-derived cells such as *gfap* and *calbindin* (Buhren et al., 2000; Maria et al., 1990; Pelc et al., 2002; Salsano et al., 2004; Valtz et al., 1991; Yokota et al., 1996). The molecular mechanisms involved in the formation of desmoplastic MB have been studied in detail in mouse disease models and are often referred to as a consequence of poorly regulated mechanisms of foetal cerebellar development (e.g. (Marino, 2005; Rubin and Rowitch, 2002). The EGL in mice, which contains proliferating GCPs, persists until P15. Proliferation in this secondary germinal tissue relies on secretion of SHH by PCs ventral to the EGL. GCPs receive the SHH signal and in turn respond to it with a significant induction of critical regulators of cell cycle progression, especially *nmyc* (Kenney et al., 2003; Oliver et al., 2003). Overexpression of components of this cascade was demonstrated to be sufficient to cause desmoplastic MB in adult mice (Browd et al., 2006; Hatton et al., 2006). In addition, expression studies of human MB tissue detected an upregulation of *nmyc* merely in desmoplastic, i.e. GCP derived MB (Pomeroy et al., 2002).

At embryonic stages, *nmyc* expression was found in the ventral cerebellum of the zebrafish. As revealed by DISH, *nmyc* and *olig2* are co-expressed in the VZ at 32 hpf. At 4 dpf and at 7 dpf, *nmyc* expression is detectable in three distinct regions of the cerebellum: the rostral cerebellar thickening (rct), the cce and the lca. The results of the present study showed that expression of *nmyc* is more widespread in the

cerebellum than solely in the EGL; consequently it ought to function both in URL and VZ-derived cells in a temporally shifted manner.

4.2.2. HH signalling regulates *nmyc* expression at larval stages

Besides *nmyc*, cells within the lca express *ptc2* and *smo* at 4 dpf. At that stage, also expression of *shh* was found in small lateral clusters located in the posterior cerebellum. Consistent with the absence of mRNA encoding HH receptors, *nmyc* expression in the cce and the rct was not affected upon the inhibition of HH signalling by cyclopamine treatment. By contrast, *nmyc* expression in the lca was abolished when HH signalling was impaired by cyclopamine treatment. The lca is a known proliferative zone in the zebrafish cerebellum during juvenile and adult stages (Chapouton et al., 2007; Grandel et al., 2006; Volkmann et al., 2008). These findings suggest that the signalling cascade regulating ongoing growth and proliferation in the lca of the cerebellum in postnatal and larval stages is conserved between mammals and teleosts. Due to its proliferative properties and the molecular mechanism regulating proliferation, the lca appears to be the equivalent of the EGL of mammals and birds. Since *nmyc* expression in the cce and the rct is not HH dependent, additional cues ought to be responsible to control *nmyc* expression in these regions. Likewise, *nmyc* expression is not exclusively regulated by SHH in the foetal mouse cerebellum (Corrales et al., 2006).

nmyc expression could be observed already at embryonic stages. At 32 hpf, expression of *nmyc* overlaps to a significant extent with that of *olig2* and is absent in URL-located, *zath1a*-expressing cells. *Olig2* in turn was shown to be expressed by ECPs, which are the VZ-derived equivalent of DCN neurons. Expression studies of human MB tissue associated upregulated expression of *nmyc* merely with desmoplastic, i.e. GCP derived MB (Pomeroy et al., 2002). Other studies however point to a more significant role for N-MYC in tumourigenesis of MB (Lee et al., 2003; Tomlinson et al., 1994). Assuming that *nmyc* is one of the key factors in neuroblastoma formation in general (Lutz et al., 2002), the findings of this study raise the possibility that the precursors of cerebellar efferent neurons as well could account for the formation of MB.

It was demonstrated in this study that early expression of *nmyc* is not affected by the loss of HH signalling. This was expected given that none of the five *hh* genes are expressed in the cerebellum or in adjacent regions at embryonic stages such that the

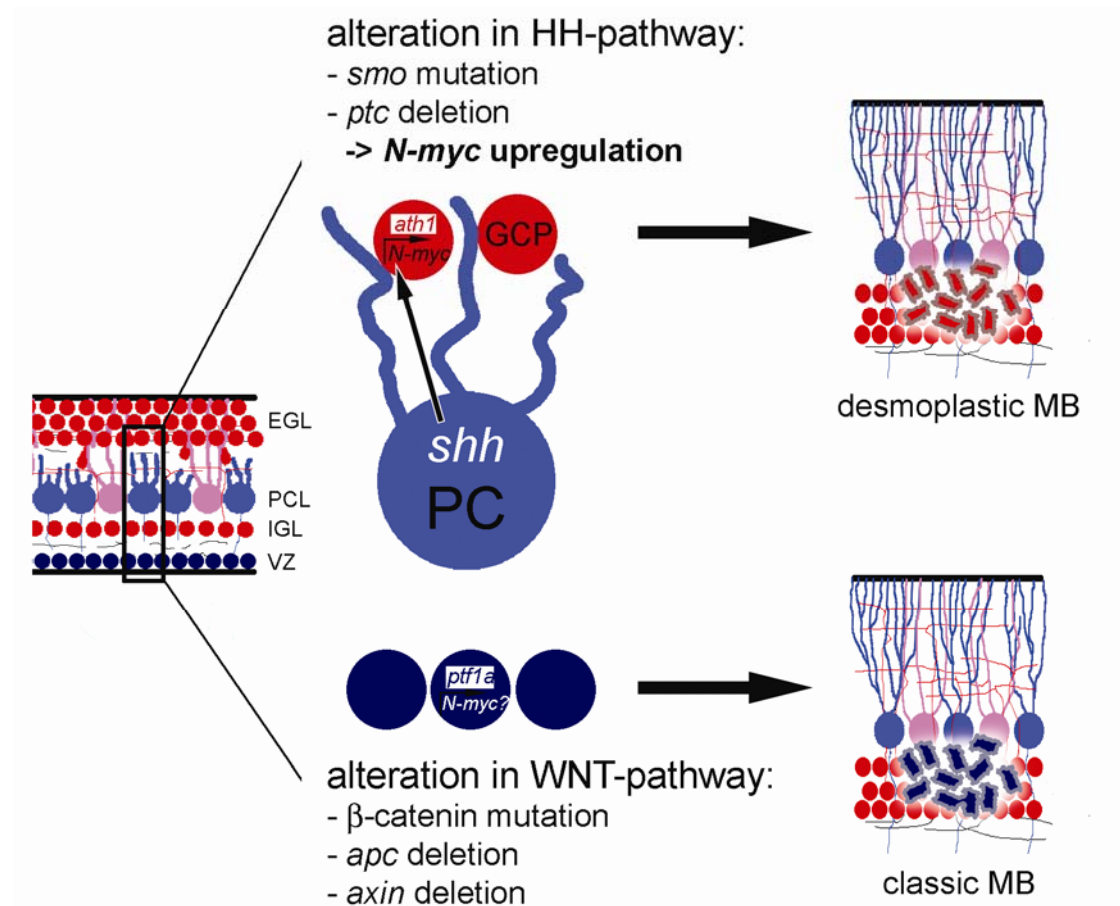


Fig. 24: Potential origin of medulloblastoma subtypes. Aberrations in undifferentiated precursors of the two germinal zones are thought to constitute the main cause of the formation of MB. Classic MB is thought to develop from VZ-derived progenitors and has been linked with alterations in the WNT signalling pathway. The desmoplastic variant of MB is supposed to derive from GPCs from the EGL. The results of the present work suggest that *nmyc* might play a role in both HH- and WNT-related MB.

secreted ligand could directly signal to cells in the cerebellum. As in the rct and the cce at larval stages, morphogenetic cascades other than HH signalling regulate *nmyc* expression in the VZ. Similarly, early expression of *nmyc* in the developing mouse cerebellum precedes the expression of *shh* and is hence not regulated by SHH (Corrales et al., 2004; Knoepfler et al., 2002). Interestingly, *olig2* expression was demonstrated to be downstream of WNT signalling (McFarland et al., 2008). Moreover, WNT signalling is implicated in many malignancies through its regulation of the expression of MYC family members (Grigoryan et al., 2008; Karim et al., 2004). Thus, it seems possible that WNT regulates *nmyc* as well. Genomic studies found a correlation between alterations in components of the WNT cascade and the classic type of MB (Clifford et al., 2006; Ellison et al., 2005; Thompson et al., 2006). Classic MB in turn exhibits marker molecules of VZ-derived cells (Maria et al., 1990;

Pelc et al., 2002; Valtz et al., 1991). Up to now, an animal model to study WNT-dependent MB tumorigenesis is not available (Gilbertson and Ellison, 2008).

4.3. Future perspective

This report is one of the first to address the development of ECs. Besides a detailed description of their origin and the cellular dynamics throughout development, ECs were also characterised at the molecular level. The transcription factor *olig2* may play a pivotal role for development of ECs. To test this hypothesis, approaches manipulating *olig2* function are currently underway. Since morpholino-mediated knockdown of *olig2* function caused severe defects already during neurulation, while EC specification in the cerebellum takes place after 36 hpf, heat-shock inducible functional variants of *olig2* were constructed. WT-*olig2* and dominant-interfering forms of *olig2* (Marshall et al., 2005; Novitsch et al., 2001) were subcloned into vectors carrying 8xHSE sites, which allow for temporal control over expression of *olig2* and *olig2* variants, and a fluorescent reporter protein for monitoring cell behaviour. These constructs provide the experimental setup for investigating gain- and loss-of-function of *olig2*. In the case that OLIG2 directly represses *ptfla*, ectopic expression of an OLIG2 variant in which the DNA binding bHLH domain has been fused to the VP16 domain (“dominant interfering”, (Marshall et al., 2005)), ought to yield ectopic expression of *ptfla* outside the VZ. If *olig2* is necessary to induce EC fate, expression of a dominant interfering OLIG2 should cause ECPs to mimic the development of common VZ-derived cells such as PCs. Accordingly, if *olig2* also is sufficient to initiate EC development, ectopic expression of WT-*olig2* should result in the generation of ectopic ECs or EC-like cells. Such experiments are expected to establish *olig2* as a new proneural factor in the developing cerebellum.

The examination of *nmyc* expression and HH regulation provides necessary information towards establishing a novel *in vivo* model of MB tumorigenesis. Using zebrafish as a model organism offers various opportunities to complement the insights into MB formation gained from the classical *ptc* mutant mouse model. Zebrafish embryos are optically transparent; they develop extracorporally and rapidly. Making use of the Gal4 system will allow the cell type specific expression of functional variants of *nmyc*. One crucial step will be to study the role of *nmyc* at embryonic stages. As mentioned, it might be possible that *nmyc* might not only control proliferation. MYC proteins have been implicated in a wide range of cellular

processes such as cell growth, proliferation, apoptosis and differentiation (Grandori et al., 2000). In the developing mouse CNS, *nmyc* was shown to play a role in expansion and differentiation of neuronal precursors; in the frog, *c-myc* was demonstrated to initially induce neural crest precursors downstream of WNT signalling (Bellmeyer et al., 2003; Light et al., 2005). With the knowledge of the precise function of *nmyc*, subsequent experiments in which constitutively active variants of *nmyc* are expressed in a cell type specific manner could be used to induce malignant growth of neuronal precursors. Genesis of such medulloblastoma-like tumours ought to be monitored by using *in vivo* time-lapse imaging, offering the possibility to observe MB formation from its origin onwards.

5. References

- Abbott, L. C. and Jacobowitz, D. M.** (1995). Development of calretinin-immunoreactive unipolar brush-like cells and an afferent pathway to the embryonic and early postnatal mouse cerebellum. *Anat Embryol (Berl)* **191**, 541-59.
- Acampora, D., Avantaggiato, V., Tuorto, F. and Simeone, A.** (1997). Genetic control of brain morphogenesis through Otx gene dosage requirement. *Development* **124**, 3639-50.
- Adolf, B., Bellipanni, G., Huber, V. and Bally-Cuif, L.** (2004). atoh1.2 and beta3.1 are two new bHLH-encoding genes expressed in selective precursor cells of the zebrafish anterior hindbrain. *Gene Expr Patterns* **5**, 35-41.
- Ahn, A. H., Dziennis, S., Hawkes, R. and Herrup, K.** (1994). The cloning of zebrin II reveals its identity with aldolase C. *Development* **120**, 2081-90.
- Alder, J., Cho, N. K. and Hatten, M. E.** (1996). Embryonic precursor cells from the rhombic lip are specified to a cerebellar granule neuron identity. *Neuron* **17**, 389-99.
- Alder, J., Lee, K. J., Jessell, T. M. and Hatten, M. E.** (1999). Generation of cerebellar granule neurons in vivo by transplantation of BMP-treated neural progenitor cells. *Nat Neurosci* **2**, 535-40.
- Altman, J. and Bayer, S. A.** (1978). Prenatal development of the cerebellar system in the rat. I. Cytogenesis and histogenesis of the deep nuclei and the cortex of the cerebellum. *J Comp Neurol* **179**, 23-48.
- Altman, J. and Bayer, S. A.** (1985a). Embryonic development of the rat cerebellum. II. Translocation and regional distribution of the deep neurons. *J Comp Neurol* **231**, 27-41.
- Altman, J. and Bayer, S. A.** (1985b). Embryonic development of the rat cerebellum. III. Regional differences in the time of origin, migration, and settling of Purkinje cells. *J Comp Neurol* **231**, 42-65.
- Altman, J. and Bayer, S. A.** (1997). Development of the Cerebellar System. In Relation to Its Evolution, Structure, and Functions. Boca Raton, FL: CRC Press, Inc.
- Alvarez-Otero, R., Perez, S. E., Rodriguez, M. A. and Anadon, R.** (1996). Organisation of the cerebellar nucleus of the dogfish, *Scyliorhinus canicula* L.: a light microscopic, immunocytochemical, and ultrastructural study. *J Comp Neurol* **368**, 487-502.
- Amores, A., Force, A., Yan, Y. L., Joly, L., Amemiya, C., Fritz, A., Ho, R. K., Langeland, J., Prince, V., Wang, Y. L. et al.** (1998). Zebrafish hox clusters and vertebrate genome evolution. *Science* **282**, 1711-4.
- Apps, R. and Garwicz, M.** (2005). Anatomical and physiological foundations of cerebellar information processing. *Nat Rev Neurosci* **6**, 297-311.
- Arabi, A., Wu, S., Ridderstrale, K., Bierhoff, H., Shiue, C., Fatyol, K., Fahlen, S., Hydbring, P., Soderberg, O., Grummt, I. et al.** (2005). c-Myc associates with ribosomal DNA and activates RNA polymerase I transcription. *Nat Cell Biol* **7**, 303-10.
- Avaron, F., Hoffman, L., Guay, D. and Akimenko, M. A.** (2006). Characterization of two new zebrafish members of the hedgehog family: atypical expression of a zebrafish indian hedgehog gene in skeletal elements of both endochondral and dermal origins. *Dev Dyn* **235**, 478-89.
- Ayer, D. E., Kretzner, L. and Eisenman, R. N.** (1993). Mad: a heterodimeric partner for Max that antagonizes Myc transcriptional activity. *Cell* **72**, 211-22.
- Ayer, D. E., Lawrence, Q. A. and Eisenman, R. N.** (1995). Mad-Max transcriptional repression is mediated by ternary complex formation with mammalian homologs of yeast repressor Sin3. *Cell* **80**, 767-76.
- Barresi, M. J., Stickney, H. L. and Devoto, S. H.** (2000). The zebrafish slow-muscle-omitted gene product is required for Hedgehog signal transduction and the development of slow muscle identity. *Development* **127**, 2189-99.
- Basson, M. A., Echevarria, D., Ahn, C. P., Sudarov, A., Joyner, A. L., Mason, I. J., Martinez, S. and Martin, G. R.** (2008). Specific regions within the embryonic midbrain and cerebellum require different levels of FGF signaling during development. *Development* **135**, 889-98.
- Baye, L. M. and Link, B. A.** (2008). Nuclear migration during retinal development. *Brain Res* **1192**, 29-36.
- Bellmeyer, A., Krase, J., Lindgren, J. and LaBonne, C.** (2003). The protooncogene c-myc is an essential regulator of neural crest formation in xenopus. *Dev Cell* **4**, 827-39.
- Belting, H. G., Hauptmann, G., Meyer, D., Abdelilah-Seyfried, S., Chitnis, A., Eschbach, C., Soll, I., Thisse, C., Thisse, B., Artinger, K. B. et al.** (2001). spiel ohne grenzen/pou2 is required during establishment of the zebrafish midbrain-hindbrain boundary organizer. *Development* **128**, 4165-76.

- Ben-Arie, N., Bellen, H. J., Armstrong, D. L., McCall, A. E., Gordadze, P. R., Guo, Q., Matzuk, M. M. and Zoghbi, H. Y.** (1997). Math1 is essential for genesis of cerebellar granule neurons. *Nature* **390**, 169-72.
- Ben-Arie, N., McCall, A. E., Berkman, S., Eichele, G., Bellen, H. J. and Zoghbi, H. Y.** (1996). Evolutionary conservation of sequence and expression of the bHLH protein Atonal suggests a conserved role in neurogenesis. *Hum Mol Genet* **5**, 1207-16.
- Bertrand, N., Castro, D. S. and Guillemot, F.** (2002). Proneural genes and the specification of neural cell types. *Nat Rev Neurosci* **3**, 517-30.
- Blackwood, E. M. and Eisenman, R. N.** (1991). Max: a helix-loop-helix zipper protein that forms a sequence-specific DNA-binding complex with Myc. *Science* **251**, 1211-7.
- Bolivar, F. and Backman, K.** (1979). Plasmids of Escherichia coli as cloning vectors. *Methods Enzymol* **68**, 245-67.
- Bourrat, F. and Sotelo, C.** (1986). Neuronal migration and dendritic maturation of the medial cerebellar nucleus in rat embryos: an HRP in vitro study using cerebellar slabs. *Brain Res* **378**, 69-85.
- Bradford, S. E. and Nadler, J. V.** (2004). Aspartate release from rat hippocampal synaptosomes. *Neuroscience* **128**, 751-65.
- Braunstein, M., Sobel, R. E., Allis, C. D., Turner, B. M. and Broach, J. R.** (1996). Efficient transcriptional silencing in Saccharomyces cerevisiae requires a heterochromatin histone acetylation pattern. *Mol Cell Biol* **16**, 4349-56.
- Broccoli, V., Boncinelli, E. and Wurst, W.** (1999). The caudal limit of Otx2 expression positions the isthmic organizer. *Nature* **401**, 164-8.
- Brochu, G., Maler, L. and Hawkes, R.** (1990). Zebrin II: a polypeptide antigen expressed selectively by Purkinje cells reveals compartments in rat and fish cerebellum. *J Comp Neurol* **291**, 538-52.
- Brösamle, C. and Halpern, M. E.** (2002). Characterization of myelination in the developing zebrafish. *Glia* **39**, 47-57.
- Brough, D. E., Hofmann, T. J., Ellwood, K. B., Townley, R. A. and Cole, M. D.** (1995). An essential domain of the c-myc protein interacts with a nuclear factor that is also required for E1A-mediated transformation. *Mol Cell Biol* **15**, 1536-44.
- Browd, S. R., Kenney, A. M., Gottfried, O. N., Yoon, J. W., Walterhouse, D., Pedone, C. A. and Fuhs, D. W.** (2006). N-myc can substitute for insulin-like growth factor signaling in a mouse model of sonic hedgehog-induced medulloblastoma. *Cancer Res* **66**, 2666-72.
- Buhren, J., Christoph, A. H., Buslei, R., Albrecht, S., Wiestler, O. D. and Pietsch, T.** (2000). Expression of the neurotrophin receptor p75NTR in medulloblastomas is correlated with distinct histological and clinical features: evidence for a medulloblastoma subtype derived from the external granule cell layer. *J Neuropathol Exp Neurol* **59**, 229-40.
- Bullock, W. O., Fernandez, J.M., Short, J.M.** (1987). X11-Blue: A High Efficiency Plasmid Transforming recA Escherichia coli Strain With Beta-Galactosidase Selection. *BioTechniques* **5**, 376-379.
- Carnegie, P. R.** (1971). Amino acid sequence of the encephalitogenic basic protein from human myelin. *Biochem J* **123**, 57-67.
- Castro, A., Becerra, M., Manso, M. J. and Anadon, R.** (2006). Calretinin immunoreactivity in the brain of the zebrafish, Danio rerio: distribution and comparison with some neuropeptides and neurotransmitter-synthesizing enzymes. II. Midbrain, hindbrain, and rostral spinal cord. *J Comp Neurol* **494**, 792-814.
- Celio, M. R., Baier, W., Scharer, L., Gregersen, H. J., de Viragh, P. A. and Norman, A. W.** (1990). Monoclonal antibodies directed against the calcium binding protein Calbindin D-28k. *Cell Calcium* **11**, 599-602.
- Cerda, J., Conrad, M., Markl, J., Brand, M. and Herrmann, H.** (1998). Zebrafish vimentin: molecular characterization, assembly properties and developmental expression. *Eur J Cell Biol* **77**, 175-87.
- Chapouton, P., Adolf, B., Leucht, C., Tannhauser, B., Ryu, S., Driever, W. and Bally-Cuif, L.** (2006). her5 expression reveals a pool of neural stem cells in the adult zebrafish midbrain. *Development* **133**, 4293-303.
- Chapouton, P., Jagasia, R. and Bally-Cuif, L.** (2007). Adult neurogenesis in non-mammalian vertebrates. *Bioessays* **29**, 745-57.
- Chen, S. and Hillman, D. E.** (1993). Colocalization of neurotransmitters in the deep cerebellar nuclei. *J Neurocytol* **22**, 81-91.
- Cheng, S. W., Davies, K. P., Yung, E., Beltran, R. J., Yu, J. and Kalpana, G. V.** (1999). c-MYC interacts with INI1/hSNF5 and requires the SWI/SNF complex for transactivation function. *Nat Genet* **22**, 102-5.

- Chizhikov, V. V., Lindgren, A. G., Curre, D. S., Rose, M. F., Monuki, E. S. and Millen, K. J.** (2006). The roof plate regulates cerebellar cell-type specification and proliferation. *Development* **133**, 2793-804.
- Chung, S., Zhang, Y., Van Der Hoorn, F. and Hawkes, R.** (2007). The anatomy of the cerebellar nuclei in the normal and scrambler mouse as revealed by the expression of the microtubule-associated protein kinesin light chain 3. *Brain Res* **1140**, 120-31.
- Clifford, S. C., Lusher, M. E., Lindsey, J. C., Langdon, J. A., Gilbertson, R. J., Straughton, D. and Ellison, D. W.** (2006). Wnt/Wingless pathway activation and chromosome 6 loss characterize a distinct molecular sub-group of medulloblastomas associated with a favorable prognosis. *Cell Cycle* **5**, 2666-70.
- Cohen, S. N., Chang, A. C. and Hsu, L.** (1972). Nonchromosomal antibiotic resistance in bacteria: genetic transformation of *Escherichia coli* by R-factor DNA. *Proc Natl Acad Sci U S A* **69**, 2110-4.
- Colak, D., Mori, T., Brill, M. S., Pfeifer, A., Falk, S., Deng, C., Monteiro, R., Mummery, C., Sommer, L. and Gotz, M.** (2008). Adult neurogenesis requires Smad4-mediated bone morphogenic protein signaling in stem cells. *J Neurosci* **28**, 434-46.
- Concordet, J. P., Lewis, K. E., Moore, J. W., Goodrich, L. V., Johnson, R. L., Scott, M. P. and Ingham, P. W.** (1996). Spatial regulation of a zebrafish patched homologue reflects the roles of sonic hedgehog and protein kinase A in neural tube and somite patterning. *Development* **122**, 2835-46.
- Corcoran, R. B. and Scott, M. P.** (2001). A mouse model for medulloblastoma and basal cell nevus syndrome. *J Neurooncol* **53**, 307-18.
- Corish, P. and Tyler-Smith, C.** (1999). Attenuation of green fluorescent protein half-life in mammalian cells. *Protein Eng* **12**, 1035-40.
- Corrales, J. D., Blaess, S., Mahoney, E. M. and Joyner, A. L.** (2006). The level of sonic hedgehog signaling regulates the complexity of cerebellar foliation. *Development* **133**, 1811-21.
- Corrales, J. D., Rocco, G. L., Blaess, S., Guo, Q. and Joyner, A. L.** (2004). Spatial pattern of sonic hedgehog signaling through Gli genes during cerebellum development. *Development* **131**, 5581-90.
- Cowling, V. H. and Cole, M. D.** (2007). The Myc transactivation domain promotes global phosphorylation of the RNA polymerase II carboxy-terminal domain independently of direct DNA binding. *Mol Cell Biol* **27**, 2059-73.
- Curras, M. C. and Dingledine, R.** (1992). Selectivity of amino acid transmitters acting at N-methyl-D-aspartate and amino-3-hydroxy-5-methyl-4-isoxazolepropionate receptors. *Mol Pharmacol* **41**, 520-6.
- Currie, P. D. and Ingham, P. W.** (1996). Induction of a specific muscle cell type by a hedgehog-like protein in zebrafish. *Nature* **382**, 452-5.
- Dahmane, N. and Ruiz i Altaba, A.** (1999). Sonic hedgehog regulates the growth and patterning of the cerebellum. *Development* **126**, 3089-100.
- De Zeeuw, C. I. and Berrebi, A. S.** (1995). Postsynaptic targets of Purkinje cell terminals in the cerebellar and vestibular nuclei of the rat. *Eur J Neurosci* **7**, 2322-33.
- Delaney, C. L., Brenner, M. and Messing, A.** (1996). Conditional ablation of cerebellar astrocytes in postnatal transgenic mice. *J Neurosci* **16**, 6908-18.
- Diaz-Regueira, S. and Anadon, R.** (2000). Calretinin expression in specific neuronal systems in the brain of an advanced teleost, the grey mullet (*Chelon labrosus*). *J Comp Neurol* **426**, 81-105.
- Distel, M., Babaryka, A. and Köster, R. W.** (2006). Multicolor in vivo time-lapse imaging at cellular resolution by stereomicroscopy. *Dev Dyn* **235**, 1100-06.
- Distel, M. and Köster, R. W.** (2007). In Vivo Time-Lapse Imaging of Zebrafish Embryonic Development. *Cold Spring Harbor Protocols* **2007**, pdb.prot4816-.
- Dudek, H., Datta, S. R., Franke, T. F., Birnbaum, M. J., Yao, R., Cooper, G. M., Segal, R. A., Kaplan, D. R. and Greenberg, M. E.** (1997). Regulation of neuronal survival by the serine-threonine protein kinase Akt. *Science* **275**, 661-5.
- Dullin, J. P., Locker, M., Robach, M., Henningfeld, K. A., Parain, K., Afelik, S., Pieler, T. and Perron, M.** (2007). Ptf1a triggers GABAergic neuronal cell fates in the retina. *BMC Dev Biol* **7**, 110.
- Dyer, M. A., Farrington, S. M., Mohn, D., Munday, J. R. and Baron, M. H.** (2001). Indian hedgehog activates hematopoiesis and vasculogenesis and can respecify prospective neurectodermal cell fate in the mouse embryo. *Development* **128**, 1717-30.
- Edmondson, J. C. and Hatten, M. E.** (1987). Glial-guided granule neuron migration in vitro: a high-resolution time-lapse video microscopic study. *J Neurosci* **7**, 1928-34.
- Ekker, S. C., Ungar, A. R., Greenstein, P., von Kessler, D. P., Porter, J. A., Moon, R. T. and Beachy, P. A.** (1995). Patterning activities of vertebrate hedgehog proteins in the developing eye and brain. *Curr Biol* **5**, 944-55.

- Ellison, D. W., Onilude, O. E., Lindsey, J. C., Lusher, M. E., Weston, C. L., Taylor, R. E., Pearson, A. D. and Clifford, S. C.** (2005). beta-Catenin status predicts a favorable outcome in childhood medulloblastoma: the United Kingdom Children's Cancer Study Group Brain Tumour Committee. *J Clin Oncol* **23**, 7951-7.
- Finger, T. E.** (1978). Efferent neurons of the teleost cerebellum. *Brain Res* **153**, 608-14.
- Fink, A. J., Englund, C., Daza, R. A., Pham, D., Lau, C., Nivison, M., Kowalczyk, T. and Hevner, R. F.** (2006). Development of the deep cerebellar nuclei: transcription factors and cell migration from the rhombic lip. *J Neurosci* **26**, 3066-76.
- Folgueira, M., Anadon, R. and Yanez, J.** (2006). Afferent and efferent connections of the cerebellum of a salmonid, the rainbow trout (*Oncorhynchus mykiss*): a tract-tracing study. *J Comp Neurol* **497**, 542-65.
- Frade, J. M.** (2002). Interkinetic nuclear movement in the vertebrate neuroepithelium: encounters with an old acquaintance. *Prog Brain Res* **136**, 67-71.
- Frank-Kamenetsky, M., Zhang, X. M., Bottega, S., Guicherit, O., Wichterle, H., Dudek, H., Bumcrot, D., Wang, F. Y., Jones, S., Shulok, J. et al.** (2002). Small-molecule modulators of Hedgehog signaling: identification and characterization of Smoothed agonists and antagonists. *J Biol* **1**, 10.
- Frank, S. R., Parisi, T., Taubert, S., Fernandez, P., Fuchs, M., Chan, H. M., Livingston, D. M. and Amati, B.** (2003). MYC recruits the TIP60 histone acetyltransferase complex to chromatin. *EMBO Rep* **4**, 575-80.
- Friedman, M. A. and Kawasaki, M.** (1997). Calretinin-like immunoreactivity in mormyrid and gymnoarchid electrosensory and electromotor systems. *J Comp Neurol* **387**, 341-57.
- Gazit, R., Krizhanovsky, V. and Ben-Arie, N.** (2004). Math1 controls cerebellar granule cell differentiation by regulating multiple components of the Notch signaling pathway. *Development* **131**, 903-13.
- Gilbertson, R. J. and Ellison, D. W.** (2008). The origins of medulloblastoma subtypes. *Annu Rev Pathol* **3**, 341-65.
- Gilthorpe, J. D., Papantoniou, E. K., Chedotal, A., Lumsden, A. and Wingate, R. J.** (2002). The migration of cerebellar rhombic lip derivatives. *Development* **129**, 4719-28.
- Glasgow, S. M., Henke, R. M., Macdonald, R. J., Wright, C. V. and Johnson, J. E.** (2005). Ptf1a determines GABAergic over glutamatergic neuronal cell fate in the spinal cord dorsal horn. *Development* **132**, 5461-9.
- Glickstein, M.** (1997). Mossy-fibre sensory input to the cerebellum. *Prog Brain Res* **114**, 251-9.
- Godinho, L., Mumm, J. S., Williams, P. R., Schroeter, E. H., Koerber, A., Park, S. W., Leach, S. D. and Wong, R. O.** (2005). Targeting of amacrine cell neurites to appropriate synaptic laminae in the developing zebrafish retina. *Development* **132**, 5069-79.
- Goldowitz, D. and Hamre, K.** (1998). The cells and molecules that make a cerebellum. *Trends Neurosci* **21**, 375-82.
- Gona, A. G.** (1976). Autoradiographic studies of cerebellar histogenesis in the bullfrog tadpole during metamorphosis: the external granular layer. *J Comp Neurol* **165**, 77-87.
- Gong, S., Zheng, C., Doughty, M. L., Losos, K., Didkovsky, N., Schambra, U. B., Nowak, N. J., Joyner, A., Leblanc, G., Hatten, M. E. et al.** (2003). A gene expression atlas of the central nervous system based on bacterial artificial chromosomes. *Nature* **425**, 917-25.
- Goodrich, L. V., Milenkovic, L., Higgins, K. M. and Scott, M. P.** (1997). Altered neural cell fates and medulloblastoma in mouse patched mutants. *Science* **277**, 1109-13.
- Götz, M. and Huttner, W. B.** (2005). The cell biology of neurogenesis. *Nat Rev Mol Cell Biol* **6**, 777-88.
- Grandel, H., Kaslin, J., Ganz, J., Wenzel, I. and Brand, M.** (2006). Neural stem cells and neurogenesis in the adult zebrafish brain: origin, proliferation dynamics, migration and cell fate. *Dev Biol* **295**, 263-77.
- Grandori, C., Cowley, S. M., James, L. P. and Eisenman, R. N.** (2000). The Myc/Max/Mad network and the transcriptional control of cell behavior. *Annu Rev Cell Dev Biol* **16**, 653-99.
- Grandori, C., Gomez-Roman, N., Felton-Edkins, Z. A., Ngouenet, C., Galloway, D. A., Eisenman, R. N. and White, R. J.** (2005). c-Myc binds to human ribosomal DNA and stimulates transcription of rRNA genes by RNA polymerase I. *Nat Cell Biol* **7**, 311-8.
- Grigoryan, T., Wend, P., Klaus, A. and Birchmeier, W.** (2008). Deciphering the function of canonical Wnt signals in development and disease: conditional loss- and gain-of-function mutations of beta-catenin in mice. *Genes Dev* **22**, 2308-41.
- Gundersen, V.** (2008). Co-localization of excitatory and inhibitory transmitters in the brain *Acta Neurologica Scandinavica* **117**, 29-33.

- Gundersen, V. and Storm-Mathisen, J.** (2000). Aspartate-neurochemical evidence for a transmitter role. München: Elsevier.
- Hallonet, M. E., Teillet, M. A. and Le Douarin, N. M.** (1990). A new approach to the development of the cerebellum provided by the quail-chick marker system. *Development* **108**, 19-31.
- Han, V. Z., Meek, J., Campbell, H. R. and Bell, C. C.** (2006). Cell morphology and circuitry in the central lobes of the mormyrid cerebellum. *J Comp Neurol* **497**, 309-25.
- Hassig, C. A., Fleischer, T. C., Billin, A. N., Schreiber, S. L. and Ayer, D. E.** (1997). Histone deacetylase activity is required for full transcriptional repression by mSin3A. *Cell* **89**, 341-7.
- Hatten, M. E.** (1990). Riding the glial monorail: a common mechanism for glial-guided neuronal migration in different regions of the developing mammalian brain. *Trends Neurosci* **13**, 179-84.
- Hatten, M. E.** (1999). Central nervous system neuronal migration. *Annu Rev Neurosci* **22**, 511-39.
- Hatten, M. E., Alder, J., Zimmerman, K. and Heintz, N.** (1997). Genes involved in cerebellar cell specification and differentiation. *Curr Opin Neurobiol* **7**, 40-7.
- Hatton, B. A., Knoepfler, P. S., Kenney, A. M., Rowitch, D. H., de Alboran, I. M., Olson, J. M. and Eisenman, R. N.** (2006). N-myc is an essential downstream effector of Shh signaling during both normal and neoplastic cerebellar growth. *Cancer Res* **66**, 8655-61.
- Hauptmann, G. and Gerster, T.** (1996). Complex expression of the zp-50 pou gene in the embryonic zebrafish brain is altered by overexpression of sonic hedgehog. *Development* **122**, 1769-80.
- Heintz, N.** (2004). Gene expression nervous system atlas (GENSAT). *Nat Neurosci* **7**, 483.
- Higashijima, S., Mandel, G. and Fetcho, J. R.** (2004). Distribution of prospective glutamatergic, glycinergic, and GABAergic neurons in embryonic and larval zebrafish. *J Comp Neurol* **480**, 1-18.
- Hisano, S., Sawada, K., Kawano, M., Kanemoto, M., Xiong, G., Mogi, K., Sakata-Haga, H., Takeda, J., Fukui, Y. and Nogami, H.** (2002). Expression of inorganic phosphate/vesicular glutamate transporters (BNPI/VGLUT1 and DNPI/VGLUT2) in the cerebellum and precerebellar nuclei of the rat. *Brain Res Mol Brain Res* **107**, 23-31.
- Hoshino, M., Nakamura, S., Mori, K., Kawachi, T., Terao, M., Nishimura, Y. V., Fukuda, A., Fuse, T., Matsuo, N., Sone, M. et al.** (2005). Ptf1a, a bHLH transcriptional gene, defines GABAergic neuronal fates in cerebellum. *Neuron* **47**, 201-13.
- Hurlin, P. J., Queva, C. and Eisenman, R. N.** (1997). Mnt, a novel Max-interacting protein is coexpressed with Myc in proliferating cells and mediates repression at Myc binding sites. *Genes Dev* **11**, 44-58.
- Ikenaga, T., Yoshida, M. and Uematsu, K.** (2005). Morphology and immunohistochemistry of efferent neurons of the goldfish corpus cerebelli. *J Comp Neurol* **487**, 300-11.
- Ikenaga, T., Yoshida, M. and Uematsu, K.** (2006). Cerebellar efferent neurons in teleost fish. *Cerebellum* **5**, 268-74.
- Ingham, P. W. and McMahon, A. P.** (2001). Hedgehog signaling in animal development: paradigms and principles. *Genes Dev* **15**, 3059-87.
- Irving, C. and Mason, I.** (2000). Signalling by FGF8 from the isthmus patterns anterior hindbrain and establishes the anterior limit of Hox gene expression. *Development* **127**, 177-86.
- Jakab, R. L. and Hamori, J.** (1988). Quantitative morphology and synaptology of cerebellar glomeruli in the rat. *Anat Embryol (Berl)* **179**, 81-8.
- Jansen, J. and Brodal, A.** (1958). Das Kleinhirn: Ergänzung zu Band IV/1. Handbuch der mikroskopischen Anatomie des Menschen Berlin: Springer.
- Jansen, J. and Brodal, A. e.** (1954). Aspects of Cerebellar Anatomy. Oslo: Johan Grunft Tanum.
- Kaneko, T. and Fujiyama, F.** (2002). Complementary distribution of vesicular glutamate transporters in the central nervous system. *Neurosci Res* **42**, 243-50.
- Karim, R., Tse, G., Putti, T., Scolyer, R. and Lee, S.** (2004). The significance of the Wnt pathway in the pathology of human cancers. *Pathology* **36**, 120-8.
- Kato, G. J., Barrett, J., Villa-Garcia, M. and Dang, C. V.** (1990). An amino-terminal c-myc domain required for neoplastic transformation activates transcription. *Mol Cell Biol* **10**, 5914-20.
- Kato, K.** (1990). Sequence of a novel carbonic anhydrase-related polypeptide and its exclusive presence in Purkinje cells. *FEBS Lett* **271**, 137-40.
- Kenney, A. M., Cole, M. D. and Rowitch, D. H.** (2003). Nmyc upregulation by sonic hedgehog signaling promotes proliferation in developing cerebellar granule neuron precursors. *Development* **130**, 15-28.
- Kenney, A. M. and Rowitch, D. H.** (2000). Sonic hedgehog promotes G(1) cyclin expression and sustained cell cycle progression in mammalian neuronal precursors. *Mol Cell Biol* **20**, 9055-67.
- Kenney, A. M., Widlund, H. R. and Rowitch, D. H.** (2004). Hedgehog and PI-3 kinase signaling converge on Nmyc1 to promote cell cycle progression in cerebellar neuronal precursors. *Development* **131**, 217-28.

- Kim, C. H., Bae, Y. K., Yamanaka, Y., Yamashita, S., Shimizu, T., Fujii, R., Park, H. C., Yeo, S. Y., Huh, T. L., Hibi, M. et al.** (1997). Overexpression of neurogenin induces ectopic expression of HuC in zebrafish. *Neurosci Lett* **239**, 113-6.
- Kim, E. J., Battiste, J., Nakagawa, Y. and Johnson, J. E.** (2008). Ascl1 (Mash1) lineage cells contribute to discrete cell populations in CNS architecture. *Mol Cell Neurosci* **38**, 595-606.
- Kimmel, C. B., Ballard, W. W., Kimmel, S. R., Ullmann, B. and Schilling, T. F.** (1995). Stages of embryonic development of the zebrafish. *Dev Dyn* **203**, 253-310.
- Kimura, H., Okamoto, K. and Sakai, Y.** (1985). Pharmacological evidence for L-aspartate as the neurotransmitter of cerebellar climbing fibres in the guinea-pig. *J Physiol* **365**, 103-19.
- King, R. W.** (2002). Roughing up Smoothed: chemical modulators of hedgehog signaling. *J Biol* **1**, 8.
- Knoepfler, P. S., Cheng, P. F. and Eisenman, R. N.** (2002). N-myc is essential during neurogenesis for the rapid expansion of progenitor cell populations and the inhibition of neuronal differentiation. *Genes Dev* **16**, 2699-712.
- Knoepfler, P. S., Zhang, X. Y., Cheng, P. F., Gafken, P. R., McMahon, S. B. and Eisenman, R. N.** (2006). Myc influences global chromatin structure. *EMBO J* **25**, 2723-34.
- Kobayashi, Y., Kaufman, D. L. and Tobin, A. J.** (1987). Glutamic acid decarboxylase cDNA: nucleotide sequence encoding an enzymatically active fusion protein. *J Neurosci* **7**, 2768-72.
- Komuro, H. and Rakic, P.** (1995). Dynamics of granule cell migration: a confocal microscopic study in acute cerebellar slice preparations. *J Neurosci* **15**, 1110-20.
- Komuro, H. and Yacubova, E.** (2003). Recent advances in cerebellar granule cell migration. *Cell Mol Life Sci* **60**, 1084-98.
- Komuro, H., Yacubova, E., Yacubova, E. and Rakic, P.** (2001). Mode and tempo of tangential cell migration in the cerebellar external granular layer. *J Neurosci* **21**, 527-40.
- Koppel, H. and Lewis, P. D.** (1983). Cell proliferation and DNA-synthesis in the external granular layer of the postnatal rat cerebellum: a quantitative study. *Neuropathol Appl Neurobiol* **9**, 207-14.
- Köster, R. W. and Fraser, S. E.** (2001). Direct imaging of in vivo neuronal migration in the developing cerebellum. *Curr Biol* **11**, 1858-63.
- Köster, R. W. and Fraser, S. E.** (2004). Time-lapse microscopy of brain development. *Methods Cell Biol* **76**, 207-35.
- Köster, R. W. and Fraser, S. E.** (2006). FGF signaling mediates regeneration of the differentiating cerebellum through repatterning of the anterior hindbrain and reinitiation of neuronal migration. *J Neurosci* **26**, 7293-304.
- Krizhanovskiy, V. and Ben-Arie, N.** (2006). A novel role for the choroid plexus in BMP-mediated inhibition of differentiation of cerebellar neural progenitors. *Mech Dev* **123**, 67-75.
- Lakkis, M. M., O'Shea, K. S. and Tashian, R. E.** (1997). Differential expression of the carbonic anhydrase genes for CA VII (Car7) and CA-RP VIII (Car8) in mouse brain. *J Histochem Cytochem* **45**, 657-62.
- Landsberg, R. L., Awatramani, R. B., Hunter, N. L., Farago, A. F., DiPietrantonio, H. J., Rodriguez, C. I. and Dymecki, S. M.** (2005). Hindbrain rhombic lip is comprised of discrete progenitor cell populations allocated by Pax6. *Neuron* **48**, 933-47.
- Lannoo, M. J., Ross, L., Maler, L. and Hawkes, R.** (1991). Development of the cerebellum and its extracerebellar Purkinje cell projection in teleost fishes as determined by zebrin II immunocytochemistry. *Prog Neurobiol* **37**, 329-63.
- Larouche, M., Che, P. M. and Hawkes, R.** (2006). Neurogranin expression identifies a novel array of Purkinje cell parasagittal stripes during mouse cerebellar development. *J Comp Neurol* **494**, 215-27.
- Lee, A., Kessler, J. D., Read, T. A., Kaiser, C., Corbeil, D., Huttner, W. B., Johnson, J. E. and Wechsler-Reya, R. J.** (2005a). Isolation of neural stem cells from the postnatal cerebellum. *Nat Neurosci* **8**, 723-9.
- Lee, S. K., Lee, B., Ruiz, E. C. and Pfaff, S. L.** (2005b). Olig2 and Ngn2 function in opposition to modulate gene expression in motor neuron progenitor cells. *Genes Dev* **19**, 282-94.
- Lee, Y., Miller, H. L., Jensen, P., Hernan, R., Connelly, M., Wetmore, C., Zindy, F., Roussel, M. F., Curran, T., Gilbertson, R. J. et al.** (2003). A molecular fingerprint for medulloblastoma. *Cancer Res* **63**, 5428-37.
- Leto, K., Carletti, B., Williams, I. M., Magrassi, L. and Rossi, F.** (2006). Different types of cerebellar GABAergic interneurons originate from a common pool of multipotent progenitor cells. *J Neurosci* **26**, 11682-94.
- Lichtman, J. W. and Fraser, S. E.** (2001). The neuronal naturalist: watching neurons in their native habitat. *Nat Neurosci* **4 Suppl**, 1215-20.

- Light, W., Vernon, A. E., Lasorella, A., Iavarone, A. and LaBonne, C.** (2005). Xenopus Id3 is required downstream of Myc for the formation of multipotent neural crest progenitor cells. *Development* **132**, 1831-41.
- Lin, J. C., Cai, L. and Cepko, C. L.** (2001). The external granule layer of the developing chick cerebellum generates granule cells and cells of the isthmus and rostral hindbrain. *J Neurosci* **21**, 159-68.
- Lin, J. W., Biankin, A. V., Horb, M. E., Ghosh, B., Prasad, N. B., Yee, N. S., Pack, M. A. and Leach, S. D.** (2004). Differential requirement for ptf1a in endocrine and exocrine lineages of developing zebrafish pancreas. *Dev Biol* **270**, 474-86.
- Livet, J., Weissman, T. A., Kang, H., Draft, R. W., Lu, J., Bennis, R. A., Sanes, J. R. and Lichtman, J. W.** (2007). Transgenic strategies for combinatorial expression of fluorescent proteins in the nervous system. *Nature* **450**, 56-62.
- Loeb-Hennard, C., Kremmer, E. and Bally-Cuif, L.** (2005). Prominent transcription of zebrafish N-myc (nmyc1) in tectal and retinal growth zones during embryonic and early larval development. *Gene Expr Patterns* **5**, 341-7.
- Long, Q., Meng, A., Wang, H., Jessen, J. R., Farrell, M. J. and Lin, S.** (1997). GATA-1 expression pattern can be recapitulated in living transgenic zebrafish using GFP reporter gene. *Development* **124**, 4105-11.
- Lordkipanidze, T. and Dunaevsky, A.** (2005). Purkinje cell dendrites grow in alignment with Bergmann glia. *Glia* **51**, 229-34.
- Lowery, L. A. and Sive, H.** (2005). Initial formation of zebrafish brain ventricles occurs independently of circulation and requires the nagie oko and snakehead/atp1a1a.1 gene products. *Development* **132**, 2057-67.
- Lu, Q. R., Sun, T., Zhu, Z., Ma, N., Garcia, M., Stiles, C. D. and Rowitch, D. H.** (2002). Common developmental requirement for Olig function indicates a motor neuron/oligodendrocyte connection. *Cell* **109**, 75-86.
- Lu, Q. R., Yuk, D., Alberta, J. A., Zhu, Z., Pawlitzky, I., Chan, J., McMahon, A. P., Stiles, C. D. and Rowitch, D. H.** (2000). Sonic hedgehog--regulated oligodendrocyte lineage genes encoding bHLH proteins in the mammalian central nervous system. *Neuron* **25**, 317-29.
- Lutz, W., Leon, J. and Eilers, M.** (2002). Contributions of Myc to tumorigenesis. *Biochim Biophys Acta* **1602**, 61-71.
- MacGregor, D., Li, L. H. and Ziff, E. B.** (1996). Dominant negative mutants of Myc inhibit cooperation of both Myc and adenovirus serotype-5 E1a with Ras. *J Cell Physiol* **167**, 95-105.
- Machold, R. and Fishell, G.** (2005). Math1 is expressed in temporally discrete pools of cerebellar rhombic-lip neural progenitors. *Neuron* **48**, 17-24.
- Machold, R. P., Kittell, D. J. and Fishell, G. J.** (2007). Antagonism between Notch and bone morphogenetic protein receptor signaling regulates neurogenesis in the cerebellar rhombic lip. *Neural Develop* **2**, 5.
- Magdaleno, S., Jensen, P., Brumwell, C. L., Seal, A., Lehman, K., Asbury, A., Cheung, T., Cornelius, T., Batten, D. M., Eden, C. et al.** (2006). BGEM: an in situ hybridization database of gene expression in the embryonic and adult mouse nervous system. *PLoS Biol* **4**, e86.
- Maria, B. L., Wong, D. and Kalnins, V. I.** (1990). Dibutyl cyclic AMP induces vimentin and GFAP expression in cultured medulloblastoma cells. *Can J Neurol Sci* **17**, 15-20.
- Maricich, S. M. and Herrup, K.** (1999). Pax-2 expression defines a subset of GABAergic interneurons and their precursors in the developing murine cerebellum. *J Neurobiol* **41**, 281-94.
- Marino, S.** (2005). Medulloblastoma: developmental mechanisms out of control. *Trends Mol Med* **11**, 17-22.
- Marshall, C. A., Novitsch, B. G. and Goldman, J. E.** (2005). Olig2 directs astrocyte and oligodendrocyte formation in postnatal subventricular zone cells. *J Neurosci* **25**, 7289-98.
- Masahira, N., Takebayashi, H., Ono, K., Watanabe, K., Ding, L., Furusho, M., Ogawa, Y., Nabeshima, Y., Alvarez-Buylla, A., Shimizu, K. et al.** (2006). Olig2-positive progenitors in the embryonic spinal cord give rise not only to motoneurons and oligodendrocytes, but also to a subset of astrocytes and ependymal cells. *Dev Biol* **293**, 358-69.
- Mathis, L., Bonnerot, C., Puelles, L. and Nicolas, J. F.** (1997). Retrospective clonal analysis of the cerebellum using genetic lacZ/lacZ mouse mosaics. *Development* **124**, 4089-104.
- McFarland, K. A., Topczewska, J. M., Weidinger, G., Dorsky, R. I. and Appel, B.** (2008). Hh and Wnt signaling regulate formation of olig2(+) neurons in the zebrafish cerebellum. *Dev Biol*.
- McMahon, S. B., Van Buskirk, H. A., Dugan, K. A., Copeland, T. D. and Cole, M. D.** (1998). The novel ATM-related protein TRRAP is an essential cofactor for the c-Myc and E2F oncoproteins. *Cell* **94**, 363-74.

- McMahon, S. B., Wood, M. A. and Cole, M. D.** (2000). The essential cofactor TRRAP recruits the histone acetyltransferase hGCN5 to c-Myc. *Mol Cell Biol* **20**, 556-62.
- Meek, J.** (1992). Comparative aspects of cerebellar organization. From mormyrids to mammals. *Eur J Morphol* **30**, 37-51.
- Meek, J., Hafmans, T. G., Maler, L. and Hawkes, R.** (1992). Distribution of zebrin II in the gigantocerebellum of the mormyrid fish *Gnathonemus petersii* compared with other teleosts. *J Comp Neurol* **316**, 17-31.
- Meyers, E. N. and Martin, G. R.** (1999). Differences in left-right axis pathways in mouse and chick: functions of FGF8 and SHH. *Science* **285**, 403-6.
- Miale, I. L. and Sidman, R. L.** (1961). An autoradiographic analysis of histogenesis in the mouse cerebellum. *Exp Neurol* **4**, 277-96.
- Mikami, Y., Yoshida, T., Matsuda, N. and Mishina, M.** (2004). Expression of zebrafish glutamate receptor delta2 in neurons with cerebellum-like wiring. *Biochem Biophys Res Commun* **322**, 168-76.
- Millet, S., Bloch-Gallego, E., Simeone, A. and Alvarado-Mallart, R. M.** (1996). The caudal limit of Otx2 gene expression as a marker of the midbrain/hindbrain boundary: a study using in situ hybridisation and chick/quail homotopic grafts. *Development* **122**, 3785-97.
- Millet, S., Campbell, K., Epstein, D. J., Losos, K., Harris, E. and Joyner, A. L.** (1999). A role for Gbx2 in repression of Otx2 and positioning the mid/hindbrain organizer. *Nature* **401**, 161-4.
- Miranda-Contreras, L., Benitez-Diaz, P. R., Mendoza-Briceno, R. V., Delgado-Saez, M. C. and Palacios-Pru, E. L.** (1999). Levels of amino acid neurotransmitters during mouse cerebellar neurogenesis and in histotypic cerebellar cultures. *Dev Neurosci* **21**, 147-58.
- Mueller, T. and Wullimann, M. F.** (2002). BrdU-, neuroD (nrd)- and Hu-studies reveal unusual non-ventricular neurogenesis in the postembryonic zebrafish forebrain. *Mech Dev* **117**, 123-35.
- Mugnaini, E. and Floris, A.** (1994). The unipolar brush cell: a neglected neuron of the mammalian cerebellar cortex. *J Comp Neurol* **339**, 174-80.
- Murakami, T. and Morita, Y.** (1987). Morphology and distribution of the projection neurons in the cerebellum in a teleost, *Sebastiscus marmoratus*. *J Comp Neurol* **256**, 607-23.
- Murakami, Y., Uchida, K., Rijli, F. M. and Kuratani, S.** (2005). Evolution of the brain developmental plan: Insights from agnathans. *Dev Biol* **280**, 249-59.
- Murciano, A., Zamora, J., Lopez-Sanchez, J. and Frade, J. M.** (2002). Interkinetic nuclear movement may provide spatial clues to the regulation of neurogenesis. *Mol Cell Neurosci* **21**, 285-300.
- Nadarajah, B.** (2003). Radial glia and somal translocation of radial neurons in the developing cerebral cortex. *Glia* **43**, 33-6.
- Nadarajah, B. and Parnavelas, J. G.** (2002). Modes of neuronal migration in the developing cerebral cortex. *Nat Rev Neurosci* **3**, 423-32.
- Nakhai, H., Sel, S., Favor, J., Mendoza-Torres, L., Paulsen, F., Duncker, G. I. and Schmid, R. M.** (2007). Ptf1a is essential for the differentiation of GABAergic and glycinergic amacrine cells and horizontal cells in the mouse retina. *Development* **134**, 1151-60.
- Nieuwenhuys, R.** (1967). Comparative anatomy of the cerebellum. *Prog Brain Res* **25**, 1-93.
- Nieuwenhuys, R., Pouwels, E. and Smulders-Kersten, E.** (1974). The neuronal organization of cerebellar lobe C1 in the mormyrid fish *Gnathonemus Petersii* (teleostei). *Z Anat Entwicklungsgesch* **144**, 315-36.
- Niklinski, J., Claassen, G., Meyers, C., Gregory, M. A., Allegra, C. J., Kaye, F. J., Hann, S. R. and Zajac-Kaye, M.** (2000). Disruption of Myc-tubulin interaction by hyperphosphorylation of c-Myc during mitosis or by constitutive hyperphosphorylation of mutant c-Myc in Burkitt's lymphoma. *Mol Cell Biol* **20**, 5276-84.
- Novitsch, B. G., Chen, A. I. and Jessell, T. M.** (2001). Coordinate regulation of motor neuron subtype identity and pan-neuronal properties by the bHLH repressor Olig2. *Neuron* **31**, 773-89.
- Obata, J., Yano, M., Mimura, H., Goto, T., Nakayama, R., Mibu, Y., Oka, C. and Kawaichi, M.** (2001). p48 subunit of mouse PTF1 binds to RBP-Jkappa/CBF-1, the intracellular mediator of Notch signalling, and is expressed in the neural tube of early stage embryos. *Genes Cells* **6**, 345-60.
- Oliver, T. G., Grasfeder, L. L., Carroll, A. L., Kaiser, C., Gillingham, C. L., Lin, S. M., Wickramasinghe, R., Scott, M. P. and Wechsler-Reya, R. J.** (2003). Transcriptional profiling of the Sonic hedgehog response: a critical role for N-myc in proliferation of neuronal precursors. *Proc Natl Acad Sci U S A* **100**, 7331-6.
- Packer, R. J., Goldwein, J., Nicholson, H. S., Vezina, L. G., Allen, J. C., Ris, M. D., Muraszko, K., Rorke, L. B., Wara, W. M., Cohen, B. H. et al.** (1999). Treatment of children with medulloblastomas with reduced-dose craniospinal radiation therapy and adjuvant chemotherapy: A Children's Cancer Group Study. *J Clin Oncol* **17**, 2127-36.

- Park, H. C., Mehta, A., Richardson, J. S. and Appel, B.** (2002). *olig2* is required for zebrafish primary motor neuron and oligodendrocyte development. *Dev Biol* **248**, 356-68.
- Park, H. C., Shin, J. and Appel, B.** (2004). Spatial and temporal regulation of ventral spinal cord precursor specification by Hedgehog signaling. *Development* **131**, 5959-69.
- Parmantier, E., Lynn, B., Lawson, D., Turmaine, M., Namini, S. S., Chakrabarti, L., McMahon, A. P., Jessen, K. R. and Mirsky, R.** (1999). Schwann cell-derived Desert hedgehog controls the development of peripheral nerve sheaths. *Neuron* **23**, 713-24.
- Pascual, M., Abasolo, I., Mingorance-Le Meur, A., Martinez, A., Del Rio, J. A., Wright, C. V., Real, F. X. and Soriano, E.** (2007). Cerebellar GABAergic progenitors adopt an external granule cell-like phenotype in the absence of *Ptf1a* transcription factor expression. *Proc Natl Acad Sci U S A* **104**, 5193-8.
- Pelc, K., Vincent, S., Ruchoux, M. M., Kiss, R., Pochet, R., Sariban, E., Decaestecker, C. and Heizmann, C. W.** (2002). Calbindin-d(28k): a marker of recurrence for medulloblastomas. *Cancer* **95**, 410-9.
- Pomeroy, S. L., Tamayo, P., Gaasenbeek, M., Sturla, L. M., Angelo, M., McLaughlin, M. E., Kim, J. Y., Goumnerova, L. C., Black, P. M., Lau, C. et al.** (2002). Prediction of central nervous system embryonal tumour outcome based on gene expression. *Nature* **415**, 436-42.
- Pouwels, E.** (1978). On the development of the cerebellum of the trout, *Salmo gairdneri*. IV. Development of the pattern of connectivity. *Anat Embryol (Berl)* **153**, 55-65.
- Prendergast, G. C., Lawe, D. and Ziff, E. B.** (1991). Association of *Myn*, the murine homolog of *max*, with *c-Myc* stimulates methylation-sensitive DNA binding and *ras* cotransformation. *Cell* **65**, 395-407.
- Qin, L., Wine-Lee, L., Ahn, K. J. and Crenshaw, E. B., 3rd.** (2006). Genetic analyses demonstrate that bone morphogenetic protein signaling is required for embryonic cerebellar development. *J Neurosci* **26**, 1896-905.
- Rakic, P.** (1971). Neuron-glia relationship during granule cell migration in developing cerebellar cortex. A Golgi and electronmicroscopic study in *Macacus Rhesus*. *J Comp Neurol* **141**, 283-312.
- Rakic, P.** (1990). Principles of neural cell migration. *Experientia* **46**, 882-91.
- Rakic, P., Cameron, R. S. and Komuro, H.** (1994). Recognition, adhesion, transmembrane signaling and cell motility in guided neuronal migration. *Curr Opin Neurobiol* **4**, 63-9.
- Rakic, P. and Sidman, R. L.** (1970). Histogenesis of cortical layers in human cerebellum, particularly the lamina dissecans. *J Comp Neurol* **139**, 473-500.
- Rakic, P. and Sidman, R. L.** (1973). Weaver mutant mouse cerebellum: defective neuronal migration secondary to abnormality of Bergmann glia. *Proc Natl Acad Sci U S A* **70**, 240-4.
- Read, T. A., Hegedus, B., Wechsler-Reya, R. and Gutmann, D. H.** (2006). The neurobiology of neurooncology. *Ann Neurol* **60**, 3-11.
- Rice, D. S. and Curran, T.** (2001). Role of the reelin signaling pathway in central nervous system development. *Annu Rev Neurosci* **24**, 1005-39.
- Rieger, S.** (2008). The regulation of neuronal progenitor cell migration by cell-cell adhesion factors during zebrafish cerebellar development In *Fakultät Wissenschaftszentrum Weihenstephan für Ernährung, Landnutzung und Umwelt der Technischen Universität München*, (ed., pp. 154. Munich: technical university munich.
- Rieger, S., Volkman, K. and Köster, R. W.** (2008). Polysialyltransferase expression is linked to neuronal migration in the developing and adult zebrafish. *Dev Dyn* **237**, 276-85.
- Rogers, J. H.** (1989). Immunoreactivity for calretinin and other calcium-binding proteins in cerebellum. *Neuroscience* **31**, 711-21.
- Rollenhagen, A. and Lubke, J. H.** (2006). The morphology of excitatory central synapses: from structure to function. *Cell Tissue Res* **326**, 221-37.
- Rubin, J. B. and Rowitch, D. H.** (2002). Medulloblastoma: a problem of developmental biology. *Cancer Cell* **2**, 7-8.
- Rupp, R. A., Snider, L. and Weintraub, H.** (1994). *Xenopus* embryos regulate the nuclear localization of XMyoD. *Genes Dev* **8**, 1311-23.
- Salsano, E., Pollo, B., Eoli, M., Giordana, M. T. and Finocchiaro, G.** (2004). Expression of MATH1, a marker of cerebellar granule cell progenitors, identifies different medulloblastoma subtypes. *Neurosci Lett* **370**, 180-5.
- Sambrook, a. F., .** (2001). Molecular Cloning. Cold Spring Harbor.
- Sato, T., Araki, I. and Nakamura, H.** (2001). Inductive signal and tissue responsiveness defining the tectum and the cerebellum. *Development* **128**, 2461-9.

- Sato, T. and Nakamura, H.** (2004). The Fgf8 signal causes cerebellar differentiation by activating the Ras-ERK signaling pathway. *Development* **131**, 4275-85.
- Schiffmann, S. N., Cheron, G., Lohof, A., d'Alcantara, P., Meyer, M., Parmentier, M. and Schurmans, S.** (1999). Impaired motor coordination and Purkinje cell excitability in mice lacking calretinin. *Proc Natl Acad Sci U S A* **96**, 5257-62.
- Schnitzer, J., Franke, W. W. and Schachner, M.** (1981). Immunocytochemical demonstration of vimentin in astrocytes and ependymal cells of developing and adult mouse nervous system. *J Cell Biol* **90**, 435-47.
- Schreiber-Agus, N., Horner, J., Torres, R., Chiu, F. C. and DePinho, R. A.** (1993). Zebra fish myc family and max genes: differential expression and oncogenic activity throughout vertebrate evolution. *Mol Cell Biol* **13**, 2765-75.
- Sears, R., Nuckolls, F., Haura, E., Taya, Y., Tamai, K. and Nevins, J. R.** (2000). Multiple Ras-dependent phosphorylation pathways regulate Myc protein stability. *Genes Dev* **14**, 2501-14.
- Sgaier, S. K., Millet, S., Villanueva, M. P., Berenshteyn, F., Song, C. and Joyner, A. L.** (2005). Morphogenetic and cellular movements that shape the mouse cerebellum; insights from genetic fate mapping. *Neuron* **45**, 27-40.
- Shi, Z., Zhang, Y., Meek, J., Qiao, J. and Han, V. Z.** (2008). The neuronal organization of a unique cerebellar specialization: The valvula cerebelli of a mormyrid fish. *J Comp Neurol* **509**, spc1.
- Shin, J., Park, H. C., Topczewska, J. M., Mawdsley, D. J. and Appel, B.** (2003). Neural cell fate analysis in zebrafish using olig2 BAC transgenics. *Methods Cell Sci* **25**, 7-14.
- Sjostrom, S. K., Finn, G., Hahn, W. C., Rowitch, D. H. and Kenney, A. M.** (2005). The Cdk1 complex plays a prime role in regulating N-myc phosphorylation and turnover in neural precursors. *Dev Cell* **9**, 327-38.
- Smeyne, R. J., Chu, T., Lewin, A., Bian, F., Sanlioglu, S., Kunsch, C., Lira, S. A. and Oberdick, J.** (1995). Local control of granule cell generation by cerebellar Purkinje cells. *Mol Cell Neurosci* **6**, 230-51.
- Sotelo, C.** (2004). Cellular and genetic regulation of the development of the cerebellar system. *Prog Neurobiol* **72**, 295-339.
- Sotelo, C., Alvarado-Mallart, R. M., Frain, M. and Vernet, M.** (1994). Molecular plasticity of adult Bergmann fibers is associated with radial migration of grafted Purkinje cells. *J Neurosci* **14**, 124-33.
- Stone, J., de Lange, T., Ramsay, G., Jakobovits, E., Bishop, J. M., Varmus, H. and Lee, W.** (1987). Definition of regions in human c-myc that are involved in transformation and nuclear localization. *Mol Cell Biol* **7**, 1697-709.
- Suda, Y., Matsuo, I. and Aizawa, S.** (1997). Cooperation between Otx1 and Otx2 genes in developmental patterning of rostral brain. *Mech Dev* **69**, 125-41.
- Sultan, F., Czubayko, U. and Thier, P.** (2003). Morphological classification of the rat lateral cerebellar nuclear neurons by principal component analysis. *J Comp Neurol* **455**, 139-55.
- Takamori, S., Rhee, J. S., Rosenmund, C. and Jahn, R.** (2000). Identification of a vesicular glutamate transporter that defines a glutamatergic phenotype in neurons. *Nature* **407**, 189-94.
- Takamori, S., Rhee, J. S., Rosenmund, C. and Jahn, R.** (2001). Identification of differentiation-associated brain-specific phosphate transporter as a second vesicular glutamate transporter (VGLUT2). *J Neurosci* **21**, RC182.
- Takebayashi, H., Nabeshima, Y., Yoshida, S., Chisaka, O., Ikenaka, K. and Nabeshima, Y.** (2002). The basic helix-loop-helix factor olig2 is essential for the development of motoneuron and oligodendrocyte lineages. *Curr Biol* **12**, 1157-63.
- Thompson, M. C., Fuller, C., Hogg, T. L., Dalton, J., Finkelstein, D., Lau, C. C., Chintagumpala, M., Adesina, A., Ashley, D. M., Kellie, S. J. et al.** (2006). Genomics identifies medulloblastoma subgroups that are enriched for specific genetic alterations. *J Clin Oncol* **24**, 1924-31.
- Tomlinson, F. H., Jenkins, R. B., Scheithauer, B. W., Keelan, P. A., Ritland, S., Parisi, J. E., Cunningham, J. and Olsen, K. D.** (1994). Aggressive medulloblastoma with high-level N-myc amplification. *Mayo Clin Proc* **69**, 359-65.
- Tsurushima, H., Yuasa, S., Kawamura, K. and Nose, T.** (1993). Expression of tenascin and BDNF during the migration and differentiation of grafted Purkinje and granule cells in the adult rat cerebellum. *Neurosci Res* **18**, 109-20.
- Valtz, N. L., Hayes, T. E., Norregaard, T., Liu, S. M. and McKay, R. D.** (1991). An embryonic origin for medulloblastoma. *New Biol* **3**, 364-71.
- Varga, Z. M., Amores, A., Lewis, K. E., Yan, Y. L., Postlethwait, J. H., Eisen, J. S. and Westerfield, M.** (2001). Zebrafish smoothed functions in ventral neural tube specification and axon tract formation. *Development* **128**, 3497-509.

- Verkhusha, V. V., Akovbian, N. A., Efremenko, E. N., Varfolomeyev, S. D. and Vrzheshch, P. V.** (2001). Kinetic analysis of maturation and denaturation of DsRed, a coral-derived red fluorescent protein. *Biochemistry (Mosc)* **66**, 1342-51.
- Verkhusha, V. V., Kuznetsova, I. M., Stepanenko, O. V., Zaisky, A. G., Shavlovsky, M. M., Turoverov, K. K. and Uversky, V. N.** (2003). High stability of Discosoma DsRed as compared to Aequorea EGFP. *Biochemistry* **42**, 7879-84.
- Vescovi, A. L., Galli, R. and Reynolds, B. A.** (2006). Brain tumour stem cells. *Nat Rev Cancer* **6**, 425-36.
- Vogel, M. W., Caston, J., Yuzaki, M. and Mariani, J.** (2007). The Lurcher mouse: fresh insights from an old mutant. *Brain Res* **1140**, 4-18.
- Volkman, K. and Köster, R. W.** (2007). In Vivo Retrograde Labeling of Neurons in the Zebrafish Embryo or Larva with Rhodamine Dextran. *Cold Spring Harbor Protocols* **2007**, pdb.prot4832-.
- Volkman, K., Rieger, S., Babaryka, A. and Köster, R. W.** (2008). The zebrafish cerebellar rhombic lip is spatially patterned in producing granule cell populations of different functional compartments. *Dev Biol* **313**, 167-80.
- von der Lehr, N., Johansson, S. and Larsson, L. G.** (2003). Implication of the ubiquitin/proteasome system in Myc-regulated transcription. *Cell Cycle* **2**, 403-7.
- Voogd, J. and Glickstein, M.** (1998). The anatomy of the cerebellum. *Trends Neurosci* **21**, 370-5.
- Vortkamp, A., Lee, K., Lanske, B., Segre, G. V., Kronenberg, H. M. and Tabin, C. J.** (1996). Regulation of rate of cartilage differentiation by Indian hedgehog and PTH-related protein. *Science* **273**, 613-22.
- Wakamatsu, Y. and Weston, J. A.** (1997). Sequential expression and role of Hu RNA-binding proteins during neurogenesis. *Development* **124**, 3449-60.
- Wallace, V. A.** (1999). Purkinje-cell-derived Sonic hedgehog regulates granule neuron precursor cell proliferation in the developing mouse cerebellum. *Curr Biol* **9**, 445-8.
- Wang, V. Y., Rose, M. F. and Zoghbi, H. Y.** (2005). Math1 expression redefines the rhombic lip derivatives and reveals novel lineages within the brainstem and cerebellum. *Neuron* **48**, 31-43.
- Wang, V. Y. and Zoghbi, H. Y.** (2001). Genetic regulation of cerebellar development. *Nat Rev Neurosci* **2**, 484-91.
- Warming, S., Costantino, N., Court, D. L., Jenkins, N. A. and Copeland, N. G.** (2005). Simple and highly efficient BAC recombineering using galK selection. *Nucleic Acids Res* **33**, e36.
- Wechsler-Reya, R. J. and Scott, M. P.** (1999). Control of neuronal precursor proliferation in the cerebellum by Sonic Hedgehog. *Neuron* **22**, 103-14.
- Westerfield, M.** (2000). The zebrafish book. A guide for the laboratory use of zebrafish (*Danio rerio*). Eugene, OR: Univ. of Oregon Press.
- Wilson, L. J. and Wingate, R. J.** (2006). Temporal identity transition in the avian cerebellar rhombic lip. *Dev Biol* **297**, 508-21.
- Wingate, R.** (2005). Math-Map(ic)s. *Neuron* **48**, 1-4.
- Wingate, R. J. and Hatten, M. E.** (1999). The role of the rhombic lip in avian cerebellum development. *Development* **126**, 4395-404.
- Wulliman, M., Rupp, B. and Reichert, H.** (1996). Neuroanatomy of the Zebrafish Brain: A Topological Atlas. Basel: Birkhäuser Verlag.
- Wullimann, M. F.** (1998). The central nervous system. In *Physiology of fishes*, (ed. D. H. Evans).
- Wullimann, M. F., Hofmann, M. H. and Meyer, D. L.** (1991). Histochemical, connectional and cytoarchitectonic evidence for a secondary reduction of the pretectum in the European eel, *Anguilla anguilla*: a case of parallel evolution. *Brain Behav Evol* **38**, 290-301.
- Wullimann, M. F. and Knipp, S.** (2000). Proliferation pattern changes in the zebrafish brain from embryonic through early postembryonic stages. *Anat Embryol (Berl)* **202**, 385-400.
- Wullimann, M. F. and Northcutt, R. G.** (1989). Afferent connections of the valvula cerebelli in two teleosts, the common goldfish and the green sunfish. *J Comp Neurol* **289**, 554-67.
- Wurst, W. and Bally-Cuif, L.** (2001). Neural plate patterning: upstream and downstream of the isthmic organizer. *Nat Rev Neurosci* **2**, 99-108.
- Yamada, K., Fukaya, M., Shibata, T., Kurihara, H., Tanaka, K., Inoue, Y. and Watanabe, M.** (2000). Dynamic transformation of Bergmann glial fibers proceeds in correlation with dendritic outgrowth and synapse formation of cerebellar Purkinje cells. *J Comp Neurol* **418**, 106-20.
- Yamada, K. and Watanabe, M.** (2002). Cytodifferentiation of Bergmann glia and its relationship with Purkinje cells. *Anat Sci Int* **77**, 94-108.
- Yamada, M., Terao, M., Terashima, T., Fujiyama, T., Kawaguchi, Y., Nabeshima, Y. and Hoshino, M.** (2007). Origin of climbing fiber neurons and their developmental dependence on Ptf1a. *J Neurosci* **27**, 10924-34.

- Yokota, N., Aruga, J., Takai, S., Yamada, K., Hamazaki, M., Iwase, T., Sugimura, H. and Mikoshiba, K.** (1996). Predominant expression of human *zic* in cerebellar granule cell lineage and medulloblastoma. *Cancer Res* **56**, 377-83.
- Zardoya, R., Abouheif, E. and Meyer, A.** (1996a). Evolution and orthology of hedgehog genes. *Trends Genet* **12**, 496-7.
- Zardoya, R., Abouheif, E. and Meyer, A.** (1996b). Evolutionary analyses of hedgehog and Hoxd-10 genes in fish species closely related to the zebrafish. *Proc Natl Acad Sci U S A* **93**, 13036-41.
- Zervas, M., Millet, S., Ahn, S. and Joyner, A. L.** (2004). Cell behaviors and genetic lineages of the mesencephalon and rhombomere 1. *Neuron* **43**, 345-57.
- Zhang, L. and Goldman, J. E.** (1996). Developmental fates and migratory pathways of dividing progenitors in the postnatal rat cerebellum. *J Comp Neurol* **370**, 536-50.
- Zhang, X. M., Ramalho-Santos, M. and McMahon, A. P.** (2001). Smoothed mutants reveal redundant roles for Shh and Ihh signaling including regulation of L/R symmetry by the mouse node. *Cell* **106**, 781-92.
- Zhou, Q. and Anderson, D. J.** (2002). The bHLH transcription factors OLIG2 and OLIG1 couple neuronal and glial subtype specification. *Cell* **109**, 61-73.
- Zhou, Q., Wang, S. and Anderson, D. J.** (2000). Identification of a novel family of oligodendrocyte lineage-specific basic helix-loop-helix transcription factors. *Neuron* **25**, 331-43.
- Zupanc, G. K., Hirsch, K. and Gage, F. H.** (2005). Proliferation, migration, neuronal differentiation, and long-term survival of new cells in the adult zebrafish brain. *J Comp Neurol* **488**, 290-319.

6. Appendix

6.1. Movie legends

Supplementary movie 1

Supplementary movie 1 shows the rotation of the cerebellar anlage from a dorsal view. The movie starts at 18 hpf and ends at 32 hpf. During that period, the fourth ventricle continues to widen. Concomitantly the hindbrain anlage condenses; the neuroepithelium remains bound at the position of the MHB, and the cerebellar lobes reposition from an initial anterior-posterior into a medial-lateral orientation.

Individual stacks of the embryo were recorded in intervals of 12 min using a motorized fluorescence stereomicroscope (MZ16FA, Leica, Planapo 5.0 objective) equipped with a digital camera (DFC350FX, Leica). Capturing data from three-dimensions rather than from a single plane allowed out-of-focus signal to be efficiently eliminated by deconvolution. Taken from (Distel, Babaryka and Köster, 2006). Abbreviations: cb: cerebellum; Mes: mesencephalon; MHB: midbrain-hindbrain boundary; IV: fourth ventricle, rh: rhombencephalon.

Supplementary movie 2

This movie shows a series of a confocal stack recording of a Tg [*olig2*:GFP] larva at 7 dpf from a dorsal view, starting at the dorsal side of the cerebellum and ending at its ventral base. At 6 dpf, DiI was injected into the ventral mesencephalon (asterisk). The dye retrogradly diffused along the axonal processes of the ECs, eventually ending up in the somata of ECs in cerebellum (encircled area). EC somata and axons labelled by DiI frequently co-expressed GFP (arrowheads).

The stack was recorded using a 20x objective. The thickness of the optical slices was 5 μm , the distance between each slice was 2,5 μm . The recorded pictures were rendered using Adobe Photoshop 7.0 and displayed as a movie sequence using QuickTime Pro 7.2.

Abbreviations: cb: cerebellum; mes: mesencephalon; rh: rhombencephalon.

Supplementary movie 3

The movie is a subset of a time lapse recording of a Tg [*olig2*:GFP] embryo demonstrating interkinetic nuclear movements of proliferating ECPs. During this period, ECPs continuously oscillated back and forth within the neuroepithelium. When having reached the apical lamina, ECPs underwent cytokinesis (arrows).

Stacks were recorded every 12 minutes in optical sections of 5,7 μm thickness using a 40x objective; the distance between the sections was 3 μm . Each stack was projected into a single image for each time point, rendered using Adobe Photoshop 7.0 and displayed as a movie sequence using QuickTime Pro 7.2. Abbreviations: cb: cerebellum; mes: mesencephalon; MHB: midbrain-hindbrain boundary; IV: fourth ventricle.

Supplementary movie 4

This movie shows the formation of the efferent protrusions of ECPs between 44 and 50 hpf in a Tg [*olig2*:GFP] embryo from a lateral view. ECPs initiated to extend processes anteriorly towards the MHB. The growing axons further extended ventrally along the MHB, ending up in the ventromedial hindbrain bundle. The cell somas of the ECs remained static in the central area of the dorsal cerebellum. Coloured arrowheads indicate individual growing processes, associated cell clusters are indicated by coloured circles.

Stacks were recorded every 12 minutes in optical sections of 3,5 μm thickness using a 40x objective; the distance between the sections was 1,75 μm . Maximum brightness projections from individual time-points of these stacks were rendered using Adobe Photoshop 7.0 and displayed as a movie sequence using QuickTime Pro 7.2.

Supplementary movie 5

The movie is a subset of the same time lapse recording shown in supplementary movie 4, but depicts cellular migration of ECPs between 54 and 72 hpf. ECPs migrate away from the VZ in an anterior direction over distances of around 3 to 5 cell diameters. Coloured dots trace individual migratory cells; the VZ is demarcated by the red circle. Stack recording and image rendering were as described for supplementary movie 4.

Supplementary movie 6

To get a closer view on the cellular events during migration, single cells of a Tg [*olig2*:GFP] embryo at the 1000-cell stage were transplanted into a WT host embryo of the same age, resulting in mosaic expression of GFP driven by the *olig2* enhancer. Each of the three migratory ECPs already contained a fully extended axon.

Stacks were recorded every 12 minutes in optical sections of 2,3 μm thickness using a 40x objective; the distance between the sections was 1,2 μm . Maximum brightness projections from individual time-points of these stacks were rendered using

Adobe Photoshop 7.0 and displayed as a movie sequence using QuickTime Pro 7.2. Abbreviations: cb: cerebellum; mes: mesencephalon; MHB: midbrain-hindbrain boundary.

Supplementary movie 7

The specimen was generated as described for supplementary movie 6. The movie shows the formation of the dendrites of ECPs between 48 and 92 hpf. Barely detectable in this view, the traced cell already have developed an efferent axon. As the cell extended and retracted fillipodia like structures repeatedly, the cell seemingly explored the surrounding environment prior to extending its dendrites.

Stacks were recorded every 12 minutes in optical sections of 3 μm thickness using a 40x objective; the distance between the sections was 2 μm . Maximum brightness projections from individual time-points of these stacks were rendered using Adobe Photoshop 7.0 and displayed as a movie sequence using QuickTime Pro 7.2. Abbreviations: cb: cerebellum; mes: mesencephalon; rh: rhombencephalon; rhod: rhodamine dextrane; MHB: midbrain-hindbrain boundary; IV: fourth ventricle.

Supplementary movie 8

This movie shows how ECPs separate from residual VZ- derived cells. Lateral view of a Tg [*olig2:dsRED*; *ptfla:GFP*] embryo. Individual cells and their migratory paths are delineated by the coloured dots and lines, respectively. ECPs, but not residual VZ derived cells moved towards anterior. This migratory behaviour appears to be a characteristic of ECPs.

Stacks were recorded every 12 minutes in optical sections of 4 μm thickness using a 40x objective; the distance between the sections was 3 μm . Maximum brightness projections from individual time-points of these stacks were rendered using Adobe Photoshop 7.0 and displayed as a movie sequence using QuickTime Pro 7.2. Abbreviations: cb: cerebellum; mes: mesencephalon; rh: rhombencephalon; MHB: midbrain-hindbrain boundary.

Supplementary movie 9

Time lapse recording of a Tg [*olig2:dsRED*; *gatal:GFP*] embryo, dorsal view on one cerebellar hemisphere. GCPs migrated towards the MHB in a chain-like manner and pass ECPs dorsally. GPC chain migration apparently is accomplished without intercalating with ECPs. Individual migrating GCPs and their migratory routes are

labelled by the coloured dots and lines, respectively. Sporadically migrating GCPs entered the cluster formed by the ECPs (arrowheads).

Stacks were recorded every 12 minutes in optical sections of 3 µm thickness using a 40x objective; the distance between the sections was 2 µm. Maximum brightness projections from individual time-points of these stacks were rendered using Adobe Photoshop 7.0 and displayed as a movie sequence using QuickTime Pro 7.2.

Supplementary movie 10

Time lapse recording of a Tg [*olig2:dsRED*; *gata1:GFP*] embryo, lateral view. GCPs rapidly moved towards their in a chain-like manner.

Stacks were recorded every 12 minutes in optical sections of 3 µm thickness using a 40x objective; the distance between the sections was 2,5 µm. Maximum brightness projections from individual time-points of these stacks were rendered using Adobe Photoshop 7.0 and displayed as a movie sequence using QuickTime Pro 7.2. Abbreviations: cb: cerebellum; mes: mesencephalon; rh: rhombencephalon; MHB: midbrain-hindbrain boundary.

6.2. Nucleotide sequences

pCS Kozac *N-myc* WT GI

```
TGGGAGGTCTATATAAGCAATGCTCGTTTAGGGAACCGCCATTCTGCCTGGGGACGTCGGAGCAAGCTTGATT
TAGGTGACTATAGAATACAAGCTACTTGTCTTTTTGCAGGATCCCATCGATTCCAATTCGCCGCCACCATGCC
AGCTAAAACCATGAGCTCAGATCTGGAGTTTGACTCCTTGCAGCCGTGTTTCTACCCGGACGAGGATGACTTCTAC
TTCTGCAGACCAGACGCCGACCCGCTGGTGAGGACATCTGGAAGAAAATTCGAGCTGCTGCCACTCCTCTGT
CCATCACCAGCAGCAGCGCTTCCAGGGGACCCGGGGGAGCTGGGCGCGGTGGCTGGGGATTGCTCGTGGGCT
TTGGATTAACCGACCCGTTGGACTGGGCTTCCGAGCTTCTGCTTTTACCGGGAGACGACATTTGGGGGGCGTCGGA
CGGGGACCTTTGGCTCCGTTTTGGATACTACGGACAATCCATCATCATTAGGACTGCATGTGGAGCGGCTTC
TCGGCGGAGAGAAAAGTGGAGCGGGTTGTGAATGAGAAAAGTGGCAAAGTCTTCTACTCCAACCTGTACTGAA
GCCGGTAAAGACACGACAGTCAAAGCGCCCGAAGTGAGCCACTCTATACCGGAGTGTGTGGACCCTACCGTGGTT
TTCCCTTATCCAGTCAACAAAAGAAACGGGAGCAGCAGCAGCCAAAGTGTGACACAAGTGGAGCCAAACAATTG
CCTCAAGTCAAGTGCAGGCGAGACTCCGAGCGACTCTGATGATGATGATGAGGATGATGAAGATGAGGATGATGAG
GAAGATGATGAAGAAGAGGAAGAAGATGAAGAAGAGGAAGAGATTGATGTCGTCACGGTGGAGAAGAGGCGTTC
CCATCACCAGCAGCAACCAGCACTGGACTGTCTGCTTCCAACCTCTCAGGAGGAGGGGAGGAGGAGGAGGAGG
GGGTGAGCAAAGCTCCGCAGGAAGTCAATTTAAAGAGGACAGCAGCAGCCTCCATCACCAGCAGCAACATAACT
ACGCAGCCCATCCCTTACTCCGAACAGCAAGACGTTCCAGCGCTCCTCCAAGCAAAGAACTCAGGATCGACA
GCAGCACTATAACTTACGCACTGGCAGGAACAGAGCTCTTCTCCAACCTCCCTACCAACAGCGTACCAAGTCA
GCGCTTGAGGAAGAGCGACTCCAGCAGCCCCAGATGTCCGACTCGGAGGACAGCGAACGACAGCAACCACA
ACATCTGGAGCGTCAGCGGCCAATGACCTGCGGTCTAGCTTCTCACTCTGCGGGATCAGGTGCTGAGCTCGC
ACACAACGACAAGGAGCAAAAGGTGGTATCCTAAAGAAGGCCACTGATTACGTCAGCTCCCTGGAGGCTCAGGA
GTTCCGACTCCAGCAGGAGAAAGACAGATTGCAAGCAAACGACAACAGCTCCTCCGAGACTTGAGCAGGCCAG
GACTCGTAATACAGAAGTATAGTGAGTCGTATTACTCGACCGATCCTGAGAaCTTCAC
```

pCS Kozac *N-myc* ΔMBII GI

```
CAAGTACATCCCCATTGACGTCATGGGAGGGGCAATGACGCAAATGGGGCTTCCATTGACGTAATGGGGC
GTAGGCGTGCTAATGGGAGGTCTATATAAGCAATGCTCGTTTAGGGAACCGCCATTCTGCCTGGGGACGTCGGA
GCAAGCTTGATTTAGGTGACACTATAGAATACAAGCTACTTGTCTTTTTGCAGGATCCCATCGATTCCAATTCGCC
GCCACCATGCCAGCTAAAACCATGAGCTCAGATCTGGAGTTTGACTCCTTGCAGCCGTGTTTCTACCCGGACGAGG
ATGACTTCTACTTCTGCAGACCAGACGCCGACCCGCTGGTGAGGACATCTGGAAGAAAATTCGAGCTGTGCCAC
TCCTCTCTGTCCCGAGCCGGCAGCGCTTCCAGGGGACCCGGGGGAGCTGGGCGCGGTGGCTGGGGATTGCTC
GCTGATGGGCTTTGGATTAACCGACCCGTTGGACTGGGCTTCCGAGCTTCTGCTTTTACCGGGAGACGACATTTGG
GGGGCGTCGGACGGGACCTTTTGGCTCCGTTTTGGATACTACGGACAATCCATCATCATTACGCGAGAGAAAAC
TGGAGCGGGTTGTGAATGAGAAAAGTGGCAAAGTCTTCTACTCCAACCTGTACTGAAGCCGGTAAAGACACGA
CAGTCAAAGCGCCGAAGTGAGCCACTCTATACCGGAGTGTGTGGACCCTACCGTGGTTTTCCCTTATCCAGTCAA
```

CAAAAGAAACGGGAGCAGCAGCAGCCAAAGTGTGACACAACCTGAGGAGCCAACAATTGCCTCAAGTCAGTGCAG
GCGAGACTCCGAGCGACTCTGATGATGATGATGAGGATGATGAAGATGAGGATGATGAGGAAGATGATGAAGAA
GAGGAAGAAGATGAAGAAGAGGAAGAGATTGATGTCGTCACGGTGGAGAAGAGGGCTTCCATCACCAGCAGGAC
AACCAGCACTGGACTGTCTGCTGTCTCCAACTCTCAGGCAGGAGGGCGACTGGGCTCAGGGGTGAGCAAAGCTCC
GCAGGAACCTATTTAAAGAGGACAGCAGCAGCCTCCATCCACCAGCAGCAACATAACTACGCAGCCCCATCCCC
TTACTCCGAACAGCAAGACGTTCCAGCGCTCCTCCAAGCAAGAACTCAGGATCGACAGCAGCACTATAACTCT
ACGCACTGGCAGGAACAGAGCTCTTCTCCAACTCCCCTACCAACAGCGTACCAAGTCAGCGCTTGAGGAAGAG
CGACTCCAGCAGCCCCAGATGCTCCGACTCGGAGGACAGCAACAGCAGCAGCAACCAACATCTTGGAGCGTCA
GCGGCGCAATGACCTGCGGTCTAGCTTCTCCTACTCTGCGGGATCAGGTGCCTGAGCTCGCACACAACGACAAGGC
AGCAAAGGTGGTCATCCTAAAGAAGGCCACTGATTACGTCAGCTCCTGGAGGCTCAGGAGTTCGACTCCAGCA
GGAGAAAGACAGATTGCAAGCCAAACGACAACAGCTCCTCCGAGACTTGAGCAGGCCAGGACTCGCTAATACA
GAACTATAGTGAGTCGATTACTCGACCGATCCTgAGaACTTCAGG

pCS *N-myc* Koz Δzip-GI

GCGGTAGGCGTGCCTAATGGGAGGTCTATATAAGCAATGCTCGTTTAGGGAACCGCCATTCTGCCTGGGGACG
TCGGAGCAAGCTTGATTTAGGTGACACTATAGAATACAAGCTACTTGTCTTTTTGCAGGATCCCATCGATTGAA
TTCCGCCACCACATGCCAGCTAAAACCATGAGCTCAGATCTGGAGTTGACTCCTTGCAGCCGTGTTTCTACCCGG
ACGAGGATGACTTCTACTTCTGCAGACCAGACGCCGACCCGCTGGTGAGGACATCTGGAAGAAATTCGAGCTGC
TGCCCACTCCTCTGTCTCCCGAGCCGGGACCGCTTCCAGGGGACCCGGGGAGCTGGGCGCGGTGGCTGGGG
ATTGCTCGTGTAGTGGCTTTGGATTAACCGACCCGTTGGACTGGGCTTCCGAGCTTCTGCTTTTACCGGGAGACAA
CATTGGGGGGCGTCCGACGGGGACCTCTTTGGCTCCGTTTGGATACTACGGACAATTCCATCATCATTACAGGAC
TGCATGTGGAGCGGCTTCTCGGCGCAGAGAACTGGAGCGGGTTGTGAATGAGAACTCGGCAAGTCTGTTCTCT
ACTCCAACCTGTACTGAAGCCGTAAGACACGACAGTCAAAGCGCCCGAAGTGAGCCACTCTATACCCGGAGTGT
GTGGACCTACCGTGGTTTTCCCTTATCCAGTCAACAAAAGAAACGGGAGCAGCAGCAAAAGTGTGACACAA
CTGAGGAGCCAACAATTGCCTCAAGTCAGTGCAGGCGAGACTCCGAGCGACTCTGATGATGATGATGAGGATGAT
GAAGATGAGGATGATGAGGAAGATGATGAAGAAGAGGAAGAAGATGAAGAAGAGGAAGAGATTGATGTCGTC
CGGTGGAGAAGAGCGTTCATCACCAGCAGGACAACCAGCACTGGACTGTCTGCTGTCTCCAACTCTCAGGAC
GAGGGCGACTGGGCTCAGGGGTGAGCAAAGCTCCGAGGAACTCATTTTAAAGAGGACAGCAGCAGCTCCATCC
ACCAGCAGCAACATAACTACGCAGCCCCATCCCCTTACTCCGAACAGCAAGACGTTCCAGCGCTCCTCCAAGCA
AGAACTCAGGATCGACAGCAGCACTATAACTCTACGACTGGCAGGAACCAGAGCTCTTCTCCAACTCCCCTA
CCAACAGCGTACCAAGTCAGCGCTTGAGGAAGAGCGACTCCAGCAGCCCCAGATGCTCCGACTCGGAGGACAGGC
AACGCAGACGCAACCACAACATCTTGAGCGTACGCGCGCAATGACCTGCGGTCTAGCTTCTCCTACTCTGCGGG
ATCAGGTGCCTGAGCTCGCACACAACGACAAGGCAGCAAAAGGTGGTCATCCTAAAGAAGGCCACTGATTACGTCA
GCTCCCTGGAGGCTCAGGAGTTCGATAATACTAGAACTATAGTGAGTCGATTACTCGACCGATCTGAGAACTT
CAGGGTGAGTTGGGGACCCCTGATTGTTCTTTCTTTTCGCTATTGTAATAATTCATGTTATATGGAGGGGGCAAGG
TTTTCAGGTG

pCS Koz *N-myc* T49AS53A GI

GTGCCTAATGGGAGGTCTATATAAGCAATGCTCGTTTAGGGAACCGCCATTCTGCCTGGGGACGTCGGAGCAA
GCTTGATTTAGGTGACACTATAGAATACAAGCTACTTGTCTTTTTGCAGGATCCCATCGATTGAAATTCGCCGCCA
CCATGCCAGTAAAACCATGAGCTCAGATCTGGAGTTGACTCCTTGCAGCCGTGTTTCTACCCGGACGAGGATGA
CTTCTACTTCTGCAGACCAGACGCCGACCCGCTGGTGAGGACATCTGGAAGAAATTCGAGCTGCTGCCGCTCCT
CCTTGGCCCCGAGCCGGGACGCGCTTCCAGGGGACCCGGGGAGCTGGGCGCGGTGGCTGGGGATTGCTCGCTG
ATGGGCTTTGGATTAACCGACCCGTTGGACTGGGCTTCCGAGCTTCTGCTTTTACCGGGAGACGACATTTGGGGGG
CTGGACCGGGACCTCTTTGGCTCCGTTTGGATACTACGGACAATTCCATCATCATTACGGACTGCATGTGGAG
CGGCTTCTCGGCGCAGAGAACTGGAGCGGGTTGTGAATGAGAACTCGGCAAAAGTCTTCTACTCCAACCTG
TACTGAAGCCGGTAAAGACACGACAGTCAAAGCGCCCGAAGTGAGCCACTCTATACCCGGAGTGTGTGGACCCTAC
CGTGGTTTTCCCTTATCCAGTCAACAAAAGAAACGGGAGCAGCAGCAAAAGTGTGACACAACCTGAGGAGCCA
ACAATTGCCTCAAGTGCAGGCGAGACTCCGAGCGACTCTGATGATGATGATGATGATGATGATGATGATGATGATG
TGATGAGGAAGATGATGAAGAAGAGGAAGAAGATGAAGAAGAGGAAGAGATTGATGTCGTCACGGTGGAGAAG
AGGCGTTCATCACCAGCAGGACAACCAGCACTGGACTGTCTGCTGTCTCCAACTCTCAGGCAGGAGGGCGACTG
GGCTCAGGGGTGAGCAAAGCTCCGAGGAACTCATTTTAAAGAGGACAGCAGCAGCCTCCATCCACCAGCAGCAA
CATAACTACGCAGCCCCATCCCCTTACTCCGAACAGCAAGACGTTCCAGCGCTCCTCAAGCAAGAACTCAGG
ATCGACAGCAGCACTATAACTCTACGCACTGGCAGGAACCAGAGCTTCTTCCAACTCCCCTACCAACAGCGTAC
CAAGTCAGCGCTTGAGGAAGAGCGACTCCAGCAGCCCCAGATGCTCCGACTCGGAGGACAGCGAACGCAGACGC
AACCACAACATCTTGAGCGYACGCGCGCAATGACCTGCGGTCTAGCTTCTCCTACTCTGCGGGATCAGGTGCCTG
AGCTCGCACACAACGACAAGGCAGCAAAGGTGGTCATCCTAAAGAAGGCCACTGATTACGTCAGCTCCTGGAGG
CTCAGGAGTTCGACTCCAGCAGGAGAAAGACAGATTGCAAGCCAAACGACAACAGCTCCTCCGAGACTTGAGC
AGGCCAGGACTCGCTAATACAGAACTATAGTGAGTCGATTACTCGACCGATCCTAGA

pCS Koz *N-myc* T49A GI

TGGGAGTCTATATAAGCAATGCTCGTTTAGGGAACCGCCATTCTGCCTGGGGACGTCGGAGCAAGCTTGATT
TAGGTGACACTATAGAATACAAGCTACTTGTCTTTTTGCAGGATCCCATCGATTGAAATTCGCCGCCACCATGCC
AGCTAAAACCATGAGCTCAGATCTGGAGTTGACTCCTTGCAGCCGTGTTTCTACCCGGACGAGGATGACTTCTAC
TTCTGCAGACCAGACGCCGACCCGCTGGTGAGGACATCTGGAAGAAATTCGAGCTGCTGCCCTCCTCCTCTGT
CCCCGAGCCGGGACGCTTCCAGGGGACCCGGGGAGCTGGGCGCGGTGGCTGGGGATTGCTCGCTGATGGGCT
TTGGATTAACCGACCCGTTGGACTGGGCTTCCGAGCTTCTGCTTTTACCGGGAGACGACATTTGGGGGGCGTCGGA
CGGGGACCTTTGGCTCCGTTTTGGATACTACGGACAATTCCATCATCATTACGGACTGCATGTGGAGCGGCTC

TCGGCGGAGAGAACTGGAGCGGGTTGTGAATGAGAACTCGGC AAAAGTCGTTCTACTCCAACCTGTACTGAA
GCCGGTAAAGCACACGACAGTCAAAGCGCCCGAAGTGAGCCACTCTATAACCGGAGTGTGTGGACCCTACCGTGGTT
TTCCCTTATCCAGTCAACAAAAGAAACGGGAGCAGCAGCAGCAGCAAAGTGTGACACAACCTGAGGAGCCAACAATTG
CCTCAAGTCAGTGCAGGCGAGACTCCGAGCGACTCTGATGATGATGATGAGGATGATGAAGATGAGGATGATGAG
GAAGATGATGAAGAAGAGGAAGAAGATGAAGAAGAGGAAGAGATTGATGTCGTCACGGTGGAGAAGAGCGCTT
CCATCACCAGCAGGACAACCAGCACTGGACTGTCTGCTGTCTCCAACCTCTCAGGCAGGAGGGCGACTGGGCTCAG
GGGTGAGCAAAGCTCCGCAGGAACTCATTTTAAAGAGGACAGCAGCAGCCTCCATC_cACCAGCAGCAACATAACT
ACGCAGCCCCATCCCCTTACTCCGAACAGCAAGACGTTCCAGCGCTCCTCCAAGCAAGAAACTCAGGATCGACA
GCAGCACTATAACTCTACGCACTGGCAGGAACCAGAGCTCTTCTCCAACCTCCCCTACCAACAGCGTACCAAGTCA
GCGCTTGAGGAAGAGCGACTCCAGCAGCCCCAGATGCTCCGACTCGGAGGACAGCGAACGCAGACGCAACCACA
ACATCTTGAGCGCTCAGCGGCGCAATGACCTGCGGTCTAGCTTCTCACTCTGCGGGATCAGGTGCCTGAGCTCGC
ACACAACGACAAGGCAGCAAAGGTGGTATCCTAAAGAAGGCCACTGATTACGTCAGCTCCCTGGAGGCTCAGGA
GTTCCGACTCCAGCAGGAGAAAGACAGATTGCAAGCCAAACGACAACAGCTCCTCCGAGACTTGAGCAGGCCAG
GACTCGTAATACAGAACTATAGTGAGTCGTATTACTCGACCGATCCTGAGAACTTAC

pCS Koz *N-myc* S53A GI

TGGGAGGTCTATATAAGCAATGCTCGTTT_{AGGGA}ACCGCCATTCTGCCTGGGGACGTCGGAGCAAGCTTGATT
TAGGTGACACTATAGAATACAAGCTACTTGTCTTTTTGCAGGATCCCATCGATTCCAATTTCGCCGCCACCATGCC
AGCTAAAACCATGAGCTCAGATCTGGAGTTTACTCCTTGCAGCCGTGTTTCTACCCGGACGAGGATGACTTCTAC
TTCTGCAGACAGCAGCCCGCACCCTGGTGAGACATCTGGAAGAAATTCGAGCTGCTGCCACTCCTCCTCTGG
CCCCGAGCCGGGACGCTTCCAGGGGACCCGGGGAGCTGGGCGCGGTGGCTGGGGATTGCTCGTGATGGGCT
TTGGATTAACCGACCCGTTGGACTGGGCTTCCGAGCTTCTGCTTTTACCGGGAGACGACATTTGGGGGGCGTCGGA
CCGGGACCTCTTTGGCTCCGTTTTGGATACTACGGACAATTCCATCATCATTGAGGACTGCATGTGGAGCGGCTTC
TCGGCGCAGAGAAAACCTGGAGCGGGTTGTGAATGAGAAAACCTCGGCAAAGTCGTTCTACTCCAACCTGACTGAA
GCCGGTAAAGACACGACAGTCAAAGCGCCCGAAGTGAGCCACTCTATAACCGGAGTGTGTGGACCCTACCGTGGTT
TTCCCTTATCCAGTCAACAAAAGAAACGGGAGCAGCAGCAGCAAAGTGTGACACAACCTGAGGAGCCAACAATTG
CCTCAAGTCAGTGCAGGCGAGACTCCGAGCGACTCTGATGATGATGATGAGGATGATGAAGATGAGGATGATGAG
GAAGATGATGAAGAAGAGGAAGAAGATGAAGAAGAGGAAGATTGATGTCGTCACGGTGGAGAAGAGCGCTT
CCATCACCAGCAGGACAACCAGCACTGGACTGTCTGCTGTCTCCAACCTCTCAGGCAGGAGGGCGACTGGGCTCAG
GGGTGAGCAAAGCTCCGCAGGAACTCATTTTAAAGAGGACAGCAGCAGCCTCCATC_cACCAGCAGCAACATAACT
ACGCAGCCCCATCCCCTTACTCCGAACAGCAAGACGTTCCAGCGCTCCTCCAAGCAAGAAAACCTCAGGATCGACA
GCAGCACTATAACTCTACGCACTGGCAGGAACCAGAGCTCTTCTCCAACCTCCCCTACCAACAGCGTACCAAGTCA
GCGCTTGAGGAAGAGCGACTCCAGCAGCCCCAGATGCTCCGACTCGGAGGACAGCGAACGCAGACGCAACCACA
ACATCTTGAGCGCTCAGCGGCGCAATGACCTGCGGTCTAGCTTCTCACTCTGCGGGATCAGGTGCCTGAGCTCGC
ACACAACGACAAGGCAGCAAAGGTGGTATCCTAAAGAAGGCCACTGATTACGTCAGCTCCCTGGAGGCTCAGGA
GTTCCGACTCCAGCAGGAGAAAGACAGATTGCAAGCCAAACGACAACAGCTCCTCCGAGACTTGAGCAGGCCAG
GACTCGTAATACAGAACTATAGTGAGTCGTATTACTCGACCGATCCTGAGAACTTAC

PCR II *nrgn* var. 1

GTGCTAATGGGAGGTCTATATAAGCAATGCTCGTTT_{AGGGA}ACCGCCATTCTGCCTGGGGACGTCGGAGCAA
GCTTGATTTAGGTGACACTATAGAATACAAGCTACTTGTCTTTTTGCAGGATCCCATCGATTCCAATTTCGCCGCCA
CCATGCCAGTAAAACCATGAGCTCAGATCTGGAGTTTACTCCTTGCAGCCGTGTTTCTACCCGGACGAGGATGA
CTTCTACTTCTGCAGACCAGACGCCGCACCCTGGTGAGGACATCTGGAAGAAATTCGAGCTGCTGCCGCTCCT
CCTCTGGCCCCGAGCCGGGACGCTTCCAGGGGACCCGGGGAGCTGGGCGCGGTGGCTGGGGATTGCTCGCTG
ATGGGCTTGGATTAACCGACCCGTTGGACTGGGCTTCCGAGCTTCTGCTTTTACCGGGAGACGACATTTGGGGGG
CGTCGGACGGGGACCTCTTTGGCTCCGTTTTGGATACTACGGACAATTCCATCATCATTGAGGACTGCATGTGGAG
CGGCTTCTCGGCGGAGAGAACTGGAGCGGGTTGTGAATGAGAACTCGGCAAAGTCGTTCTACTCCAACCTG
TACTGAAGCCGTAAGACACGACAGTCAAAGCGCCCGAAGTGAGCCACTCTATAACCGGAGTGTGTGGACCCTAC
CTGGTTTTCCGTTATCCAGTCAACAAAAGAAACGGGAGCAGCAGCAGCAAAGTGTGACACAACCTGAGGAGCCA
ACAATTGCCTCAAGTCAGTGCAGGCGAGACTCCGAGCGACTCTGATGATGATGATGAGGATGATGAAGATGAGGA
TGATGAGGAAGATGATGAAGAAGAGGAAGAAGATGAAGAAGAGGAAGAGATTGATGTCGTCACGGTGGAGAAG
AGGCGTCCATCACCAGCAGGACAACCAGCACTGGACTGTCTGCTGTCTCCAACCTCTCAGGCAGGAGGGCGACTG
GGCTCAGGGGTGAGCAAAGCTCCGAGGAACTCATTTTAAAGAGGACAGCAGCAGCCTCCATCCACCAGCAGCAA
CATAACTACGCAGCCCCATCCCCTTACTCCGAACAGCAAGACGTTCCAGCGCTCCTCCAAGCAAGAAAACCTCAGG
ATCGACAGCAGCACTATAACTCTACGCACTGGCAGGAACCAGAGCTCTTCTCCAACCTCCCCTACCAACAGCGTAC
CAAGTCAGCGCTTGAGGAAGAGCGACTCCAGCAGCCCCAGATGCTCCGACTCGGAGGACAGCGAACGCAGACGC
AACCACAACATCTTGAGCGYACGCGGCGCAATGACCTGCGGTCTAGCTTCTCACTCTGCGGGATCAGGTGCCTG
AGCTCGCACACAACGACAAGGCAGCAAAGGTGGTATCCTAAAGAAGGCCACTGATTACGTCAGCTCCCTGGAGG
CTCAGGAGTTCCGACTCCAGCAGGAGAAAGACAGATTGCAAGCCAAACGACAACAGCTCCTCCGAGACTTGAGC
AGGCCAGGACTCGTAATACAGAACTATAGTGAGTCGTATTACTCGACCGATCCTGAGAACTTAC

PCR II *nrgn* var. 2

GTGCTAATGGGAGGTCTATATAAGCAATGCTCGTTT_{AGGGA}ACCGCCATTCTGCCTGGGGACGTCGGAGCAA
GCTTGATTTAGGTGACACTATAGAATACAAGCTACTTGTCTTTTTGCAGGATCCCATCGATTCCAATTTCGCCGCCA
CCATGCCAGTAAAACCATGAGCTCAGATCTGGAGTTTACTCCTTGCAGCCGTGTTTCTACCCGGACGAGGATGA
CTTCTACTTCTGCAGACCAGACGCCGCACCCTGGTGAGGACATCTGGAAGAAATTCGAGCTGCTGCCGCTCCT
CCTCTGGCCCCGAGCCGGGACGCTTCCAGGGGACCCGGGGAGCTGGGCGCGGTGGCTGGGGATTGCTCGCTG
ATGGGCTTGGATTAACCGACCCGTTGGACTGGGCTTCCGAGCTTCTGCTTTTACCGGGAGACGACATTTGGGGGG

CGTCGGACGGGGACCTCTTTGGCTCCGTTTTGGATACTACGGACAATTCCATCATCATTTCAGGACTGCATGTGGAG
CGGTTCTCGGGCGAGAGAACTGGAGCGGGTTGTGAATGAGAACTCGGCAAAGTCGTTCTACTCCAACCTG
TACTGAAGCCGGTAAAGACACGACAGTCAAAGCGCCGAAAGTGAGCCACTTATACCGGAGTGTGTGGACCCTAC
CGTGGTTTTCCCTTATCCAGTCAACAAAAGAAAACGGGAGCAGCAGCAGCCAAAAGTGTGACACAACCTGAGGAGCCA
ACAATTGCCTCAAGTCAGTGCAGGCGAGACTCCGAGCGACTCTGATGATGATGATGAGGATGATGAAGATGAGGA
TGATGAGGAAGATGATGAAGAAGAGGAAGAAGATGAAGAAGAGGAAGAGATTGATGTCGTCACGGTGGAGAAG
AGGCGTTCCATCACCAGCAGGACAACCAGCACTGGACTGTCTGCTGTCTCCAACCTCAGGCAGGAGGGCGACTG
GGCTCAGGGGTGAGCAAAGCTCCGCAGGAATCATTTTAAAGAGGACAGCAGCAGCCTCCATCCACCAGCAGCAA
CATAACTACGCAGCCCCATCCCTTACTCCGAACAGCAAGACGTTCCAGCGCTCCTCCAAGCAAGAACTCAGG
ATCGACAGCAGCACTATAACTCTACGCACTGGCAGGAACCAGAGCTTCTTCCAACTCCCCTACCAACAGCGTAC
CAAGTCAGCGCTTGAGGAAGAGCGACTCCAGCAGCCCCAGATGCTCCGACTCGGAGGACAGCGAACGCAGACGC
AACCACAACATCTTGGAGCGYACGCGGCAATGACCTGCGGTCTAGCTTCTCACTCTGCGGGATCAGGTGCTG
AGCTCGCACACAACGACAAGGCAGCAAAGGTGGTATCCTAAAGAAGGCCACTGATTACGTCAGCTCCCTGGAGG
CTCAGGAGTCCGACTCCAGCAGGAGAAAGACAGATTGCAAGCCAAACGACAACAGCTCCTCCGACAGACTTGAGC
AGGCCAGGACTCGCTAATACAGAACTATAGTGAGTCGTATTACTCGACCGATCCTAGA

PCR II zf *calb1*

GTGCCTAATGGGAGGTCTATATAAGCAATGCTCGTTAGGGAACCGCCATTCTGCCTGGGGACGTCGGAGCAA
GCTTGATTTAGGTGACACTATAGAATACAAGCTACTTGTCTTTTTGCAGGATCCCATCGATTGAAATTCGCCGCCA
CCATGCCAGCTAAAACCATGAGCTCAGATCTGGAGTTTACTCCTTGCAGCCGTGTTTCTACCCGGACGAGGATGA
CTTCTACTTCTGCAGACCAGACGCCGCACCGCCTGGTGAGGACATCTGGAAGAAATTCGAGCTGCTGCCCGCTCCT
CCTTGGCCCCGAGCCGGGACGCGCTTCCAGGGGACCCGGGGGAGCTGGGCGCGGTGGCTGGGGATTGCTCGCTG
ATGGGCTTTGGATTAACCGACCCGTTGGACTGGGCTTCCGAGCTTCTGCTTTTACCGGGAGACGACATTTGGGGGG
CGTCGGACGGGGACCTCTTTGGCTCCGTTTTGGATACTACGGACAATTCCATCATCATTTCAGGACTGCATGTGGAG
CGGCTTCTCGGGCGAGAGAACTGGAGCGGGTTGTGAATGAGAACTCGGCAAAGTCGTTCTACTCCAACCTG
TACTGAAGCCGGTAAAGACACGACAGTCAAAGCGCCGAAAGTGAGCCACTTATACCGGAGTGTGTGGACCCTAC
CGTGGTTTTCCCTTATCCAGTCAACAAAAGAAAACGGGAGCAGCAGCAGCCAAAAGTGTGACACAACCTGAGGAGCCA
ACAATTGCCTCAAGTCAGTGCAGGCGAGACTCCGAGCGACTCTGATGATGATGATGAGGATGATGAAGATGAGGA
TGATGAGGAAGATGATGAAGAAGAGGAAGAAGATGAAGAAGAGGAAGAGATTGATGTCGTCACGGTGGAGAAG
AGGCGTTCCATCACCAGCAGGACAACCAGCACTGGACTGTCTGCTGTCTCCAACCTCAGGCAGGAGGGCGACTG
GGCTCAGGGGTGAGCAAAGCTCCGCAGGAATCATTTTAAAGAGGACAGCAGCAGCCTCCATCCACCAGCAGCAA
CATAACTACGCAGCCCCATCCCTTACTCCGAACAGCAAGACGTTCCAGCGCTCCTCCAAGCAAGAACTCAGG
ATCGACAGCAGCACTATAACTCTACGCACTGGCAGGAACCAGAGCTTCTTCCAACTCCCCTACCAACAGCGTAC
CAAGTCAGCGCTTGAGGAAGAGCGACTCCAGCAGCCCCAGATGCTCCGACTCGGAGGACAGCGAACGCAGACGC
AACCACAACATCTTGGAGCGYACGCGGCAATGACCTGCGGTCTAGCTTCTCACTCTGCGGGATCAGGTGCTG
AGCTCGCACACAACGACAAGGCAGCAAAGGTGGTATCCTAAAGAAGGCCACTGATTACGTCAGCTCCCTGGAGG
CTCAGGAGTTCGACTCCAGCAGGAGAAAGACAGATTGCAAGCCAAACGACAACAGCTCCTCCGACAGACTTGAGC
AGGCCAGGACTCGCTAATACAGAACTATAGTGAGTCGTATTACTCGACCGATCCTAGA

Eidesstattliche Erklärung

Ich erkläre hiermit an Eides statt, dass ich die vorliegende Arbeit selbständig ohne unzulässige fremde Hilfe angefertigt habe. Die verwendeten Literaturquellen sind im Literaturverzeichnis vollständig zitiert.

München, 29. 12. 2008

(Andreas Babaryka)

Danksagung

Mein erster und vorzüglichster Dank gilt Dr. Reinhard Köster für sein vorbildliches Engagement als mein Lehrer und Gruppenleiter. Seine fortdauernde Unterstützung, sein beständiges Interesse und sein kritischer, hilfreicher Kommentar waren für das Zustandekommen dieser Arbeit unerlässlich.

Prof. Dr. Wolfgang Wurst danke ich für seine Unterstützung und die Gelegenheit, diese Arbeit an seinem Institut anfertigen zu können.

Ein großes Dankeschön allen Kollegen der RKG für die schöne, von Teamgeist und Hilfsbereitschaft gekennzeichnete Zeit im Lab. Mein besonderer Dank gilt hier Dr. Jen Hocking für Korrekturlesen und Anmerkungen. Enrico Kühn danke ich seine Großzügigkeit, die er mir in vielen Emails versichert hat. Martin Distel sei gedankt für schwer zu lesende Paper und Anträge. Niklas „Uwe“ Senghaas danke ich für die erfolgreiche Stimmabgabe bei der Wahl der Mitarbeitervertretung. Nicht vergessen möchte ich die beiden Ehemaligen Dr. Sandra Rieger und Katrin „rain woman“ Volkmann ($\text{CO}_2(\text{f}) \xrightarrow{RT} \text{CO}_2(\text{g}) + \text{Peng!!}$) sowie die Neueren (Al Kerner, Dr. Kazuhiko „Karsten“ Namikawa) und die Neuen. Und natürlich danke ich Petra Hammerl und den Mädels aus der Fischanlage.

Weiterhin danke ich Annerose Kurz-Drechsler, Ulrike Buchholz, Dr. Ruth Klafke und Dr. Thorsten Naserke für Hilfe beim Schnippeln, IHCs und ISHs. Den Kollegen der ZEN-Gruppe sei gedankt für gute Nachbarschaft, ABs und vieles mehr.

Mr. Pete Saunders danke ich herzlich für wiederholtes Korrekturlesen.

Schließlich danke ich meiner Familie, deren Hilfe einfach unentbehrlich war. So wäre ohne Konstantins kompetente Hilfe eine Übersetzung dieser Arbeit ins „Afrikanische“ nicht möglich gewesen (KOSTllöööllllkkiiiiuuuuuzzz). Ich danke Kristina ihre Geduld und jedwede Unterstützung, die sie mir gewährt hat. Zulezt und ganz besonders danke ich meinen Eltern Dr. Igor und Barbara Babaryka, weil sie mich immer gefördert und in jeder Hinsicht unterstützt haben.

München, im Juni 2009